THE
PHYSICAL REVIEW
A journal of experimental and theoretical physics established by E. L. Nichols in 1893

SECOND SERIES, VOL. 71, No. 6 MARCH 15, 1947

Long Range Alpha-Particles Emitted in Connection with Fission. Preliminary Report†

G. FARWELL,* E. SEGRÈ,** AND C. WIEGAND**
Los Alamos Scientific Laboratories, Los Alamos, New Mexico
(Received December 12, 1946)

Alpha-particles are emitted in coincidence (i.e., within 5×10^{-6} sec.) with fission by U^{235} and Pu^{239}. The maximum range observed corresponds to an energy of 16 Mev. About one alpha per 250 fissions is emitted by U^{235} and one alpha per 500 fissions by Pu^{239}. The investigation is being continued.

INTRODUCTION

L. W. ALVAREZ reported (verbal communication) that a foil of U^{235} irradiated with slow neutrons emits charged particles which are probably alpha-particles with a range of about 20 cm of air.

An experiment has been performed to determine the nature, energy, and abundance of particles other than fission fragments and neutrons which are occasionally emitted in connection with the fission process. We have found that these particles are emitted in coincidence (within 5×10^{-6} sec.) with fission in U^{235} and Pu^{239}, that they are alpha-particles, and that their maximum energy is about 16 Mev. About one alpha per 250 fissions has been detected for U^{235}, and one alpha per 500 fissions for Pu^{239}.

EXPERIMENTAL ARRANGEMENT AND RESULTS

A double chamber connected to twin linear amplifiers and counting circuits was used as a detector. The chamber was filled with argon and electrons were collected. A coincidence circuit registered events occurring simultaneously on each side of the chamber. The resolving time of the circuits was measured experimentally from the formula: $N_c=2N_AN_Bt$. N_c is the rate of accidental coincidence counts; N_A the counting rate of A side; N_B the counting rate of B side; t the resolving time.

With various single counting rates the resolving time was found to be from six to ten microseconds.

The chamber is shown in Fig. 1. It was so constructed that the sample foil acted as a high voltage electrode between two collecting electrodes which were connected to first amplifier tube grids. Thus the sample mounted on a thin metallic foil could emit particles into either side

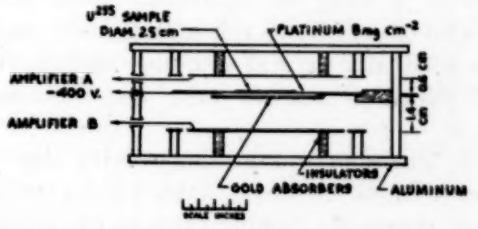

FIG. 1. Schematic diagram of ionization chamber.

† This report was filed on May 18, 1944; the press of other work prevented the continuation of this investigation at Los Alamos.

* Present address: Institute of Nuclear Studies, University of Chicago, Chicago, Illinois.
** Present address: Department of Physics, Radiation Laboratory, University of California, Berkeley, California.

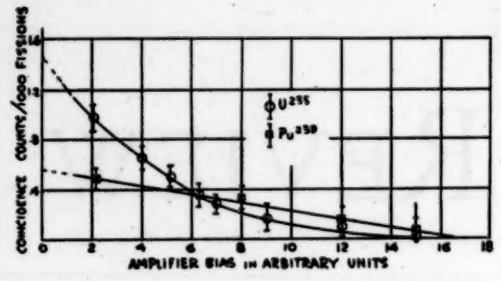

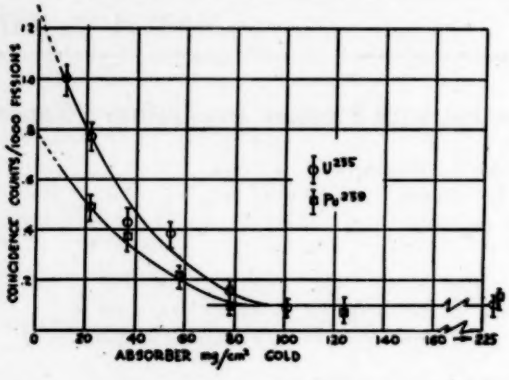

FIG. 2. (upper) Number of coincidences per 1000 fissions *versus* bias of the *B* chamber amplifier. Pressure in chambers 4 atmos. argon. Absorber between *A* and *B* chambers 8 mg/cm² Pt+5 mg/cm² Au for the U^{235} curve; 8 mg/cm² Pt +15 mg/cm² Au for the Pu^{239} curve.

FIG. 3. (lower) Number of coincidences per 1000 fissions *versus* absorber thickness between chambers *A* and *B*. Pressure in chambers 4 atmos. argon. Bias of the *B* amplifier 2.2 of the units used in Fig. 3.

or both sides. In our experiment the actual sample of uranium faced the chamber side which we will call *A*. The back of the foil faced into side *B*. The physical depth of side *A* was 0.6 cm and the physical depth of side *B* was 1.4 cm. A pressure of 4 atmospheres of argon was used, making an effective depth of 5.7 cm air equivalent on side *B* and of 2.3 cm air equivalent on side *A*.

The enriched sample used consisted of 0.220 mg of U^{235} electrodeposited on a thin platinum foil weighing 8 mg/cm². This foil was also backed with an additional layer of gold weighing 5 mg/cm² making an equivalent total of 12.2 mg/cm² of gold. With this arrangement, and the bias used, the natural uranium alpha-particles and fission fragments were not detected in side *B*.

The chamber was irradiated with slow neutrons from the cyclotron. Table I gives the ratios of the observed counting rates in the chambers as functions of the bias voltage. The fission rate on side *A* was maintained at about 4000 counts/min. The non-coincident counts on side *B* may perhaps be caused by an (n, p) reaction on a nitrogen impurity in the argon (tank argon was used); considerably less than 1 percent of nitrogen would account for the effect.

The data of the last column are shown graphically in Fig. 2. When the curve is extrapolated to zero bias, it indicates approximately 1.5 coincidence counts per 1000 fissions.

The next part of the experiment was the making of an absorption curve for the particles in coincidence with the fission counts. Various thicknesses of gold foils were used as absorbers. The bias of side *B* was maintained constant at 2.1 units; and the fission rate in side *A* was maintained at about 3500 counts/min. Table II gives the observed data on the counting rates as functions of the absorber thickness.

The data of the last column are shown graphically in Fig. 3.

We are now able to determine the number of penetrating particles emitted per fission. The extrapolated bias curve gives a coincidence rate of 1.5 per 1000 fissions. To this we apply a correction factor of 1.3, representing an extrapolation of the absorption curve from 12.2 mg/cm² of gold (the absorber thickness at which the bias curve was run) to zero absorber thickness. In addition we allow for the fact that chamber side *B* subtends a solid angle 2π seen from the fissionable material, hence half the particles are lost to possible observation. We have finally:

Number per 1000 fissions $= 1.5 \times 1.3 \times 2 = 4$ per 1000 fissions.

Having bias and absorption curves for the particle, we are able to calculate its range and

TABLE I. Ratios of counts in amplifiers *A* and *B*. *A* and *B* represent the single counting rates in chambers *A* and *B*. *C* is the coincidence counting rate.

Amplifier bias in arbitrary units	*B/A*	*C/A*
2.1	0.022	0.0010
4.0	0.0029	0.00066
5.2	0.0024	0.00045
6.3	0.0028	0.00035
7.0	0.0011	0.00029
9.0	0.0006	0.000163
12.0	0.00069	0.000103
14.7	0.0001	0.000025

specific ionization, which in turn identify the particle and its energy.

The range is obtained from Fig. 3, which shows that the particle of maximum range is stopped by 90 to 100 mg/cm² of gold. Using 3.9 mg/cm² of gold as the equivalent in stopping power of 1 cm of air, we estimate the maximum range of the particle in air to be about 23 cm. The range determination allows us to use the bias curve for the particle to show that its specific ionization is that of an alpha-particle.

The considerations leading to the conclusion that we are dealing with an alpha-particle are as follows: When collecting electrons in an ionization chamber of our type the pulse output of the chamber is determined by the product of the ionization charge and its displacement. Practically speaking the maximum pulse output from a particle of given energy is produced when the ionization track arises from a sample mounted on a negative electrode and when the track is parallel to that electrode. The total charge is then displaced the entire depth of the chamber. Referring to the bias curve of the alpha-particles of polonium of Fig. 4, we see that these particles of range 3.84 cm, energy 5.3 Mev, are able to produce a maximum pulse output corresponding to 14.5 of our units. This occurs when the electrons move through the whole depth of the chamber, which is 5.7 cm.

As a check we used the datum given above to calculate also the minimum output from the polonium alphas. This is obtained for a particle emitted perpendicularly to the electrode; the center of gravity of the ionization is taken to be at $\frac{3}{4}$ of the range of the particle. The chamber depth is 5.7 cm so the average charge is displaced 3.4 cm.

The minimum output should then have the ratio 3.4/5.7 to the maximum output, i.e., be $14.5(3.4/5.7)=8.7$ of our units. This is in agreement with the bias curve which breaks at a value between 8 and 9.

TABLE II. Absorption curves of particles.

Absorber gold mg/cm²	B/A	C/A
12.2	0.032	0.0010
22.2	0.019	0.00077
37.2	0.0421	0.00043
53.2	0.039	0.00038
78.2	0.0365	0.00016
99.2	0.035	0.00009
124.2	0.055	0.000075
225	0.051	0.00010

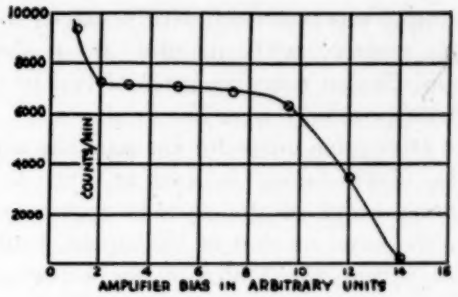

FIG. 4. Bias curve for alpha-particles from a Po sample facing downwards from the high voltage electrode in chamber *B*. Pressure in the chamber 4 atmospheres of argon.

We have calculated the geometrical path in our chamber which would cause maximum pulse output from an alpha-particle whose range in air is 23 cm. Taking into account the part of the range spent in the absorber by such a particle, we find that the residual energy available for ionization in the gas is 11 Mev. Its trajectory is such that the average charge displacement is 2.8 cm. The largest pulses of polonium alphas should then be in a ratio $(5.3\times5.7)/(11\times2.8)=0.98$ to the maximum pulses of the other particles.

Thus the assumption that the particle under observation is an alpha leads to the conclusion that the maximum pulse heights of Po alphas and the unknown particle are about the same.

From the bias curves of Po alphas and long range particles of Figs. 2 and 4 it is seen that both produced about the same maximum ionization pulse. It can, therefore, be concluded that the particle emitted in coincidence with fission of U^{235} (within a few micro-seconds) is an alpha of 23 cm of air range. From curves of Livingston and Bethe[1] this corresponds to an energy of about 16 Mev.

Long range alpha-particles were also observed in coincidence with Pu^{239} fission. A sample of about 2 mg of Pu^{239} was used for the experiment. A collimating screen, necessary to reduce the alpha-background on the fission side *A*, reduced the effective mass of the Pu^{239} to about 0.200 mg.

[1] M. S. Livingston and H. A. Bethe, Rev. Mod. Phys. 9, 266 (1937).

The sample was irradiated with neutrons from a Ra+Be source, with paraffin as a slowing medium. Fission counting rates of two to three hundred per minute were observed.

The absorption curve for the particles accompanying Pu^{239} fission is seen in Fig. 3. The maximum range of the particle appears to be about the same as that of the alphas from U^{235} fission, within the limits of the experimental error. The curves relevant to the Pu^{239} experiments are also reported in Figs. 2 and 3, together with the curves for U^{235}.

The difference in shape of the curves for U^{235} and Pu^{239} in Fig. 3 may be accounted for by the additional absorber used for Pu^{239}, which has the effect of eliminating the particles which made very small pulses on the U^{235} run. The same arguments used for U^{235} establish also that the ionizing particles emitted by Pu^{239} in coincidence with fission are α-particles.

The number of alpha-particles emitted in coincidence with Pu^{239} fission is computed from the data exactly as before. The result obtained is about 2 alphas per 1000 fissions.

This investigation will be followed up with the purpose of finding for both U^{235} and Pu^{239}:

(1) The energy distribution of the alphas.
(2) The possible presence of protons.
(3) The time relation of the emission of the charged particles to the fission.

ACKNOWLEDGMENT

This document is based on work performed under Contract W-7405-Eng-36 for the Manhattan Project at the Los Alamos Scientific Laboratories of the University of California.

The information covered in this document will appear in Division V of the Manhattan Project Technical Series as part of the contribution of the Los Alamos Scientific Laboratories.

PHYSICAL REVIEW VOLUME 71, NUMBER 6 MARCH 15, 1947

The Probability of K Ionization of Nickel by Electrons as a Function of Their Energy

LEONARD T. POCKMAN, DAVID L. WEBSTER, PAUL KIRKPATRICK, AND KEITH HARWORTH
Stanford University, California

(Received July 22, 1946)

Thin targets of Ni were bombarded with electrons at 12 to 183 kv and intensities of the $K\alpha$ doublet were measured in arbitrary units. The results were converted to absolute cross sections for ionization by comparison with Smick and Kirkpatrick's absolute measurements at 70 kv. At any voltage $V=UV_K$, where V_K is the K ionization voltage, the cross section is well represented empirically as

$$\Phi_K=7.3(e/V_K)^2U^{-0.837}\log_{10}U,$$

with e and V_K both in electrostatic units. Burhop's theory is confirmed with accuracy probably well within the limits of error imposed on it by the Born approximation and neglect of relativity, exchange and other minor factors. The effect of relativity is found by comparison of the cross sections for Ni with ones for Ag, previously measured in this laboratory. Relativity increases the cross sections by moderate percentages, which increase with voltage. Deduction of these percentages yields data for a hypothetical non-relativistic element; and Burhop's non-relativistic theory fits this element best. Smith's cross sections for helium are compared with these non-relativistic cross sections and with those for real nickel. At low U's the cross sections for helium are notably less than would be predicted by simple analogy with the other elements, presumably because of unusually great effects in helium, due to movement of the electron which remains in the atom.

I. INTRODUCTION

BECAUSE of the mathematical complexity of wave mechanics and the physical complexity of most real atoms, atomic hydrogen would be the best element for a test of theories of K ionization by electron impact. Experiments with atomic hydrogen are difficult; but silver, which has been studied both experimentally and theo-

retically,[1–5] provides an approximately hydrogenic field of force for the K electron. At the same time, however, silver involves serious relativistic effects. The K ionization probability of helium has been measured by Smith.[6] With helium, relativistic effects are negligible; but because its nuclear charge is not large compared to the mutual screening of the K electrons, the effective nuclear field is far from hydrogenic.

Nickel avoids to an appreciable extent the relativistic complications associated with silver and the nonhydrogenic character of helium. For this reason along with many others of experimental practicability, nickel was chosen for the tests to be reported here.

II. SURVEY OF EXPERIMENTAL TECHNIQUE

On the experimental side of the test, the ionization cross section was calculated from the intensity of the $K\alpha$ x-ray doublet; so the experiments consisted primarily of measurements of this intensity as a function of the energy of electron impact. The general plan was the same as for silver.[3,4] That is, the measurements were all on intensities of x-rays from extremely thin targets, and they were divided into two parts: one, a series of measurements with a crystal spectrometer, giving only relative intensities, i.e., in arbitrary units, but covering a wide range of tube voltage; the other, a set of absolute intensity measurements with Ross filters, at the voltage best suited to their use. These absolute measurements were made and described by Smick and Kirkpatrick.[7] In this paper the relative measurements will be described and standardized by use of the absolute measurements, and then compared with the theory. Finally, the measurements on silver and helium will be compared with these on nickel, for evidence on the effects of relativity and the other K electron.

III. DETAILS OF APPARATUS

Most parts of the apparatus used in this research had been used already in the later relative measurements on thin targets of silver.[3–8] Naturally there were improvements, especially as the apparatus was used for two researches on thick targets, of silver[9] and nickel,[10] before starting the work for this paper. This work, however, followed immediately after the thick-target researches, and was finished by 1938.

Many of the improvements need no detailed description. Among these are several in the vacuum pumping system. Another was the introduction of an indirectly heated cathode, with a flat emitting surface of columbium, to distribute the cathode rays smoothly over the focal spot and reduce the danger of burning holes in the target. Still another improvement, more specifically related to the change from silver to nickel, was the elimination of most of the air from the path of the x-rays, to reduce absorption. This was done partly by adding to the x-ray tube an 18″ neck of metal and glass, projecting toward the spectrometer, and partly by inserting a 12″ tube full of hydrogen between the spectrometer crystal and the ionization chamber. Finally, the gas in this chamber was changed from CH_3Br to SO_2, to prevent too much concentration of ionization at one end in using such soft rays, and yet absorb about 90 percent of them.

Even with all these changes, the Ni $K\alpha$-rays were very weak. So the electrometer was thoroughly overhauled and studied by Pockman[11] and its sensitivity was increased fivefold.

The preparation of nickel targets, thin enough for this work, required a special technique, described elsewhere by Pockman and Webster.[12]

IV. EXPERIMENTAL PROCEDURE

As in the work on thin silver, the experiments consisted primarily of relative measurements of

[1] D. L. Webster, H. Clark, R. M. Yeatman, and W. W. Hansen, Proc. Nat. Acad. Sci. **14**, 679 (1928).
[2] D. L. Webster, H. Clark, and W. W. Hansen, Phys. Rev. **37**, 115 (1931).
[3] D. L. Webster, W. W. Hansen, and F. B. Duveneck, Phys. Rev. **43**, 839 (1933).
[4] J. C. Clark, Phys. Rev. **48**, 30 (1935).
[5] H. S. W. Massey and E. H. S. Burhop, Phys. Rev. **48**, 468 (1935).
[6] P. T. Smith, Phys. Rev. **36**, 1293 (1930).
[7] A. E. Smick and Paul Kirkpatrick, Phys. Rev. **67**, 153 (1945).
[8] D. L. Webster, W. W. Hansen, and F. B. Duveneck, Rev. Sci. Inst. **3**, 729 (1932).
[9] D. L. Webster, W. W. Hansen, and F. B. Duveneck, Phys. Rev. **44**, 258 (1933).
[10] L. T. Pockman, Paul Kirkpatrick, and D. L. Webster, Phys. Rev. **45**, 131A (1934). The data reported in this abstract need to be combined with the thin-nickel data of the present paper, as for silver in reference 9, to get the most out of them; so the abstract referred to will be replaced soon by a more complete paper.
[11] L. T. Pockman, Rev. Sci. Inst. **7**, 238 (1936).
[12] L. T. Pockman and D. L. Webster, Rev. Sci. Inst. **12**, 389 (1941).

the intensities of the $K\alpha$-doublet at different tube voltages, an ionization chamber filled with sulfur dioxide being used as the detecting device. It was essential, therefore, that of the total line-spectrum radiation produced in the target, the fraction which went to the ionization chamber should be the same at all voltages. A further essential requirement was that auxiliary measurements should be taken, so that the continuous-spectrum rays accompanying the line rays could be eliminated by subtraction. Except for minor differences, the spectrometric procedure was all as described for silver.[3]

For outgassing the tube and measuring tube voltages and currents also, the procedure was almost the same as for silver.[3–8] Since the preparation of the thin nickel targets was very costly in time and effort, however, they were protected against gas bursts by a non-inductive resistor (made of xylene and alcohol) between the anode and the high voltage system. This required the subtraction of its IR drop (not often over 1 or 2 kv) from the measured voltage; and since it was convenient to work at standard points on the voltmeter scale, the tube voltages differed slightly from day to day.

A more important innovation relative to the targets was in the procedure for guarding against possible errors due to changes in the target during its use. One possible change of this sort would be the formation of holes by burning or tearing. With both silver and nickel, this was guarded against by careful visual inspection of each target after the conclusion of work with it. Another possibility for trouble was contraction of the target, especially of the cellulose acetate which backed the nickel. This would pull more nickel into the focal spot and increase the intensity of the rays. This possibility was suggested by the disappearance of shallow wrinkles, observed in the inspections. As a further check, therefore, a statistical test was introduced. This consisted of adding the intensities measured at 7 or 8 well-distributed voltages in each "run" (or sequence of measurements at decreasing voltages) and comparing the sums found for all the different runs with the same target. This test is open to the objection that there might be a compensation of holes by contraction; but such a coincidence would be improbable, and if it did occur, the holes would show on inspection.

An important question is, how to know how small a change in the sum to consider significant. A quantitative measure of the statistical significance of the deviations of these sums from their mean was developed. As an example of the application of this method, if Target 22 had undergone a 3 percent change of thickness just before its last run, the deviations would have been such as would occur by chance only about once in 50 such sets of data. Other possible cases, of course, would give different probabilities, so it seems difficult to formulate an exact general rule; but the existence of systematic errors of more than a few percent seems unlikely.

For the first four targets (21, 22, 25, 26) used without tearing them, this statistical test indicated that if there was any appreciable increase of thickness by contraction it must have occurred during outgassing, before measurements began.

These four targets were used by Pockman and Webster.[13] Then in 1937 they turned the apparatus over to Kirkpatrick and Harworth, who made a new target holder and some other improvements and used it with three more targets, Nos. 29, 30, and 34. Since the essential parts of the apparatus were the same, or equivalent, the results of both sets of measurements agreed within their limits of erratic error. Therefore they are averaged here as products of a single research.

Because the ionization measurements were in arbitrary units, no effort was made to measure the thickness of the targets with more accuracy than was needed for computing the corrections to be described in the next section.

V. CORRECTIONS

For comparing intensities from different targets, each value of the intensity was normalized in terms of a standard for its target. Letting $i(V)$ stand for the measured intensity (in arbitrary units) at voltage V, and $i_0(V)$ for the corrected intensity, to be described, the normalization consists in dividing each $i(V)$ or $i_0(V)$ by the average of the $i_0(V)$'s at 70, 80, 90, and 100 kv.

[13] If necessary, many further details about them and the rest of the apparatus can be found in L. T. Pockman's Ph.D. thesis, "The Probability of K Ionization of Nickel by Cathode Rays as a Function of Cathode Ray Energy," in the Stanford University Library.

TABLE I. Correction factors, c_s, for single and multiple scattering as calculated for four targets.

V	No. 21(670A)	No. 22(960A)	No. 25(150A)	No. 26(100A)
15			0.932	0.956
25			0.974	0.982
35	0.940		0.986	0.991
45	0.960	0.939		0.995
55	0.972	0.956	0.994	0.996
75	0.983	0.974	0.996	0.998
95	0.989	0.982	0.997	0.998
125	0.993	0.989	0.999	0.999
155	0.995	0.992		
180	0.996	0.994		

TABLE II. Correction c_r, for rediffusion of cathode rays from cellulose acetate.

V	Target 25	Target 26
15	0.993	0.992
20		0.995
25	0.996	
30		0.997
35	0.998	
40		0.999
55	0.999	1.000 at $V>40$ kv
>55	1.000	

This division cancels the arbitrary unit, giving a pure number, either the "reduced intensity" $j(V)$, or the "reduced corrected intensity" $j_0(V)$. $j_0(V)$ is the quantity which should be, and is found to be, the same within limits of erratic error for all targets.

The end product of the experiments reported here, therefore, will be a table of values of $j_0(V)$, obtained by averaging at each V the values from different runs. Going on then from these experiments, $j_0(V)$ will be converted back to $i_0(V)$, but this time in absolute units, not arbitrary, by the use of the absolute measurement of i_0 (70 kv) by Smick and Kirkpatrick.[7] This $i_0(V)$ will then be compared with theories and with values for helium and silver, as outlined in Section I.

In principle the corrections required by the finite target thickness and the proximity of supporting structures are like those for silver[3,4,8] but on account of the lower speeds of impact with nickel the corrections are more important, so the theory used with silver has been developed further.

Four corrections for the target thickness have been considered: (1) retardation of the bombarding electrons; (2) screened nuclear scattering (both multiple and single); (3) absorption of the Ni $K\alpha$-radiation by the nickel target itself; (4) fluorescent radiation due to production and absorption of the continuous spectrum within the target. Corrections (3) and (4) turn out to be negligible for all targets and all voltages, and the correction for retardation is very small. Thus the only important correction for target thickness is (2).

Impacts beyond the nickel film require consideration of the following corrections: (5) fluorescence of the nickel under the rays from the thin backing film of cellulose acetate; (6) fluorescence under the rays from the bottom of the supporting aluminum structure, several centimeters behind the target; (7) rediffusion of electrons from cellulose acetate; (8) rediffusion of electrons from the aluminum structure. Of these corrections only (7) is appreciable. What little rediffusion there is, is primarily by large-angle single scattering. Thus it will be noticed that of the seven corrections considered only three are found to be appreciable.

The increase in path length of fast β-rays through thick films was calculated in good approximation by Bothe[14] as due exclusively to multiple scattering. With the thinner nickel targets at the lower voltages, the assumptions on which Bothe's approximation is based are not valid and it becomes necessary to consider both multiple and single scattering. However, with the 150A target at 15 kv, if the impact parameter chosen to divide multiple from single scattering is changed from 0.008A, where Bothe chose it, to 0.15A, the calculated path length is changed only from 1.073 times the target thickness to 1.081 times the thickness. Of course, the distribution between the parts calculated as single and multiple scattering is radically changed. The remarkable feature is that it makes so little difference in the final result where the dividing line is drawn.

To be sure, the division into single and multiple scattering is an approximation. In between, around 10° in this target at 15 kv, there is a range of plural scattering. This range is somewhat indefinite but calculations indicate it is probably short enough to permit the division into multiple and single scattering.

[14] W. Bothe, *Handbuch der Physik*, Vol. 24, Chap. I (1927).

TABLE III. Reduced corrected intensities from the first four usable targets.

V in kv	Reduced corrected intensity Target 21 (670A)	Target 22 (960A)	Target 25 (150A)	Target 26 (100A)	Wtd. av.	Wtd. percent av. dev.
183.3	0.749	0.709			0.725	2.6
153.1	0.812	0.757			0.780	3.4
124.5	0.864	0.831	0.864	0.922	0.850	2.0
95.1	0.964	0.960	0.970	0.914	0.961	0.6
75.3	1.030	1.035	1.020	1.096	1.034	0.6
55.6	1.170	1.172	1.180	1.048	1.167	1.0
46.2	1.255	1.272		1.138	1.258	1.2
35.7	1.335		1.338	1.236	1.327	1.2
24.8			1.385	1.226	1.353	3.8
14.8			1.125	1.002	1.101	3.5

TABLE IV. Intensities from last three usable targets.

Target 29 2150A			Target 30 1320A			Target 34 110A		
V	$i(V)$	$j_0(V)$	V	$i(V)$	$j_0(V)$	V	$i(V)$	$j_0(V)$
179.3	114.2	0.707	175.0	171.8	0.728	100	87.9	0.952
169.5	120.1	0.743				80	93.0	1.005
159.5	121.7	0.751	155.4	181.1	0.767	60	106.1	1.145
149.5	126.2	0.779	125.5	200.9	0.845	40	122.2	1.311
139.5	127.7	0.785	95.4	226.7	0.944	30	130.3	1.386
129.5	137.0	0.841	75.4	254.0	1.047	25	130.2	1.378
119.5	142.3	0.870	57.73	294.1	1.192	20	126.6	1.330
109.6	145.4	0.885				15	108.3	1.116
99.6	151.8	0.920						
89.6	161.2	0.969						
79.6	173.3	1.031						
69.6	185.6	1.084						

For practical application of the scattering correction a factor c_s has been calculated by which each measured x-ray intensity has to be multiplied to reduce it to the intensity which would have been found if all electrons had gone straight through the target. The factor c_s as computed for the first four usable targets is shown in Table I.

The correction for scattering from the backing film of cellulose acetate depends on those electrons scattered by more than 90°. Therefore it is very small. The correction factor c_r derived from it is shown in Table II.

Finally the correction for retardation of electrons in the target in the distance x gives a correction factor c_x. This correction is very small at the voltages for which scattering can be calculated well enough. For targets 25 and 26 it is negligible at all voltages. For 21 and 22 it is negligible above 75 kv; from these down as far as Table I goes, $c_x = 0.999$.

VI. RESULTS OF EXPERIMENTS

The reduced corrected intensities for the first four usable targets are listed in Table III. To save printing, uncorrected intensities have been omitted, but may be found if needed by "uncorrecting" the figures in this table with the corrections listed above. The exact meanings of the headings in this table are as follows:

The column for each target shows averages of the reduced corrected intensities for all runs with that target, with the data from each run weighted in proportion to the tube current for that run. The thickness of each target is shown in angstroms.

The column headed "Wtd. av." shows weighted averages of the averages in the preceding columns. In preparing this column the weight to be given to the data from each target was determined by two independent objective methods which gave essentially the same results.

For Targets 29, 30, and 34 the procedure was similar except that, as only one run was made with each of these targets there was no problem of weighting the data from different runs. Moreover the voltages used for different targets were too different for easy reduction to a common list by interpolation. In Table IV, therefore, there are three columns for each target: voltage in kv, measured intensity in arbitrary units, and corrected reduced intensity.

To combine the results of the two sets of measurements, a first step is to get the measurements from the last three usable targets expressed in terms of the voltages used with the first four. To do this, use is made of an empirical reduced intensity, taken from the work on silver,[3]

$$j_2(V) = \text{constant}\ (U^{-m_2} \log U), \qquad (1)$$

where $U = V/V_K$ and V_K is the K ionization voltage. For silver m_2 was 0.783; and for nickel, as will be shown below, $m_2 = 0.837$. Finally, a weighted average between the data from the two

TABLE V. Comparison and averaging of values of $j_0(V)$ from the two groups of targets.

V in kv	First group $j_0(V)$	Weight	Second group $j_0(V)$	Weight	Final Wtd. av. $j_0(V)$
183.3	0.725	(7)	0.707	(2)	0.721
153.1	0.780	(7)	0.771	(2)	0.778
124.5	0.850	(16)	0.852	(2)	0.850
95.1	0.960	(16)	0.952	(3)	0.959
75.3	1.034	(16)	1.048	(3)	1.036
55.6	1.167	(16)	1.213	(2.3)	1.173
46.2	1.258	(10)	1.289	(1.85)	1.263
35.7	1.327	(12)	1.363	(1.4)	1.331
24.8	1.353	(9)	1.380	(1)	1.356
14.8	1.101	(9)	1.107	(1)	1.102

groups of targets was computed, weighting the data of each group at any one voltage in proportion to the number of runs made in that group at that voltage. The result of this averaging is the "Final wtd. av." recorded in Table V.

This final weighted average $j_0(V)$ is now ready for standardization by means of the absolute cross section for ionization at $V=70$ kv, namely $(3.38\pm0.2)\times10^{-22}$ cm², measured by Smick and Kirkpatrick.[7] For this standardization, $\log\{j_0(V)/\log U\}$ was plotted against $\log U$ as shown in Fig. 1, and the straight line which seems to fit the data near 70 kv best was drawn there. This line gives three valuable pieces of information, namely: (1) the reliability of the empirical function $j_2(V)$ as shown by the accuracy with which the data are fitted by the straight line; (2) the value of m_2 for Eq. (1); and (3) the best value of $\log\{j_0(V)/\log(U)\}$ at 70 kv, and from it the best value of j_0 (70 kv), namely 1.096. The ratio of Smick and Kirkpatrick's absolute ionization cross section to this value of j_0 (70 kv), is 3.08×10^{-22} cm². The product of this area by $j_0(V)$ at any other V is therefore the absolute ionization cross section $\Phi_K(V)$, so it is tabulated in Table VI.

Theories, both classical and wave mechanical, predict values for this cross section as products of a characteristic area $A_K=e^2/V_K^2$ and a dimensionless function of U which changes relatively little from one element to another. To facilitate

TABLE VI. Final results of experiments.

V in kv	Φ_K in (10^{-22} cm²)	U	Φ_K/A_K
183.3	2.22	22.00	0.746
153.1	2.40	18.37	0.805
124.5	2.62	14.94	0.879
95.1	2.96	11.41	0.993
75.3	3.20	9.04	1.073
55.6	3.62	6.67	1.213
46.2	3.90	5.54	1.309
35.7	4.11	4.28	1.380
24.8	4.18	2.98	1.401
14.8	3.40	1.78	1.140

TABLE VII. Parameters of empirical functions.

Element	Z	m_1	C_1	m_2	C_2
Helium	2	10.8	20.2	Inapplicable	
Nickel	28	4.3	15.4	0.837	7.27
Silver	47	5.25	17.8	0.783	7.06

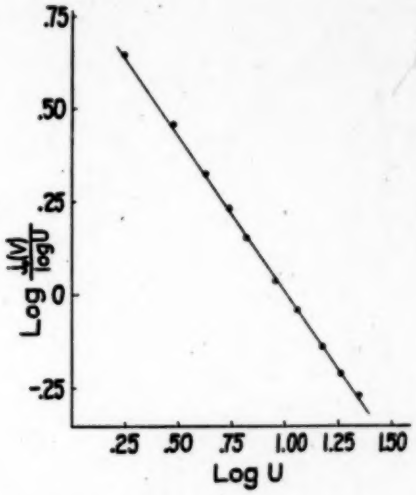

FIG. 1. Graph of $\log_{10}\{j_0(V)/\log_{10}U\}$ against $\log_{10}U$, for finding the value of the parameter m_2 of Eq. (1).

comparisons between different elements, e.g., nickel, silver, and helium, therefore, the dimensionless ratios Φ_K/A_K and U are also tabulated in Table VI. For nickel, $V_K=8.336$ kv $=27.81$ e.s.u., and $A_K=2.98\times10^{-22}$ cm².

Empirical formulas for these cross sections, and probably those of other elements not too far from nickel and silver, may be found by standardizing the $j_2(V)$ of Eq. (1) and another function, $j_1(V)$, also taken from reference 3. Thus we find

$$\Phi_2(V)=C_2A_KU^{-m_2}\log_{10}U \qquad (2)$$

and

$$\Phi_1(V)=C_1A_K(U-1)/(U^2+m_1U). \qquad (3)$$

Of these functions Φ_2 is the more accurate but Φ_1 is clearly more convenient for any calculations involving integration. Their parameters for Ni and for Ag (references 3 and 4) are listed in Table VII. Evidently in the range of Z covered here, the relative change in any one of these parameters is considerably less than that in Z. This fact encourages interpolation. So two other facts must be noted with it: (1) Φ_2 will not fit Smith's[6] data on helium well with any value of m_2, and the value of m_1 for helium seems out of line; and (2) relativity must be much more important at any given U in very heavy elements than in nickel and silver. Therefore extrapolation very far outside the range of Z between nickel and silver is unreliable; but interpolation in this range seems reasonable.

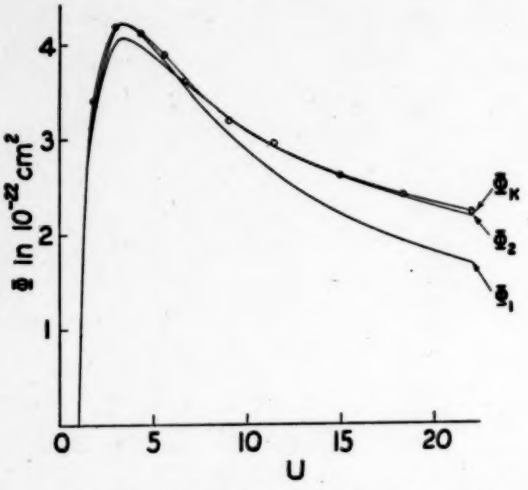

FIG. 2. Graph and points for experimentally determined K-ionization cross sections of nickel atoms (not single K electrons) and graphs of the empirical functions defined in Eqs. (2) and (3).

Graphs of Φ_K, Φ_1, and Φ_2 for nickel are shown in Fig. 2.

VII. COMPARISON WITH THEORIES

That classical mechanics, with some quantizing assumptions, does not work well for K ionization was proved conclusively for silver in reference 3; and if any further proof were needed, it could be found in a similar form with the present measurements on nickel.

Turning to wave mechanics, it seems that most of the theoretical work to date has been done by means of Born's first approximation. This work was started by Ochiai[15] and Bethe,[16] the latter arriving at an equation for the cross section, but only by using approximate methods of integration, which limit its applicability to higher values of U than would be required by Born's approximation alone. For these U's Liska[17] found Bethe's equation very good, but for the range of our data on nickel the approximations additional to Born's must be replaced by more accurate calculations.

This requires very tedious arithmetical integrations. Therefore it was not done at once, but only after intermediate approximations by Massey and Mohr,[18] Wetzel,[19] and Soden.[20] Finally a calculation without any of these intermediate approximations, but with Born's and those inherent in arithmetical integration of a double integral with a highly variable integrand, was made for the K electrons of silver by Massey and Burhop.[5] Comparing their results with Clark's[4] experimental cross sections they found a much better agreement than that of any preceding theory. Therefore Burhop[21] made similar calculations for the K electrons of nickel, silver and mercury and the L electrons of silver and mercury, also with very good results. For the K of nickel his comparison with experiment was with such data as we could give him by letter at that time, i.e., cross sections in arbitrary units. Now, therefore, we must extend the comparison by using absolute units.

In the theoretical calculations a major source of uncertainty is the difference between ordinary atoms, with their full quotas of electrons, and the hydrogenic atoms (either with the true Z and only one electron or with $Z_K=Z-0.30$ to allow for the other one) which are amenable to calculation. This difference becomes especially serious as the voltage gets low. For nickel, at the voltage where the ionization cross section of a "screened hydrogenic" atom ($Z_K=27.7$) would drop to zero, that of an ordinary nickel atom is still greater than $\frac{1}{3}$ of its maximum value. The correction from hydrogenic atoms to ordinary ones is evidently a serious matter.

To make it worse, the difference is due to more than one cause. The ratio of V_K to the screened-hydrogenic ionization potential V_H is 0.800 for nickel, 0.861 for silver, 0.962 for mercury, and 1.006 for uranium. The difference from unity, which is so notable in nickel, is caused primarily by the screening of the nuclear electrostatic field by the outer electrons. But for heavier elements, the lack of so much difference is not primarily caused by any lack of so much screening. Rather, it is caused by relativity, which affects V_K in the direction opposite to the effect of screening, and is more important in heavier elements because the K electrons move faster. Altogether, the transition from hydrogenic atoms to ordinary ones is even more difficult than it looks.

[15] K. Ochiai, Proc. Phys. Math. Soc. Japan 11, 43 (1929).
[16] H. Bethe, Ann. d. Physik 5, 325 (1930).
[17] J. Liska, Phys. Rev. 46, 169 (1934).
[18] H. S. W. Massey and C. B. O. Mohr, Proc. Roy. Soc. A140, 613 (1933).
[19] W. W. Wetzel, Phys. Rev. 44, 25 (1933).
[20] D. Graf Soden, Ann. d. Physik 19, 409 (1934).
[21] E. H. S. Burhop, Proc. Camb. Phil. Soc. 36, 43 (1940).

For hydrogenic atoms, the double integral which Burhop[21] had to evaluate arithmetically can be expressed as a product of a dimensional constant by an integral in which all variables are dimensionless ratios. Those in the integrand are ratios of momenta of other electrons to that of a hydrogenic K electron; and those in the limits of integration are functions of such ratios and the ratio $U_H = V/V_H$. On integration, all these ratios but U_H disappear. Consequently, the cross sections for hydrogenic atoms take the form

$$\Phi_H = A_H f(U_H), \qquad (4)$$

with $A_H \equiv e^2/V_H^2$ and f independent of V_H.

For ordinary atoms, such a complete separation into a shape factor f and a scale factor A seems almost too much to hope for; but these questions arise: how near we can come to it, and whether possibly the differences may be within the limits of error imposed on any arithmetic integration by the character of the integrand in the double integral which has to be computed. In answer to these questions, Burhop, in a recent letter, says he would expect the greatest effect of the transition from hydrogenic to ordinary atoms to be in the scale factor. On the shape factor, taking everything now known about it into consideration, he favors using the same function of U to cover nickel, silver, and mercury. Therefore we are following this plan; and to compute this function we are averaging, for each U, the three almost-equal values of $\Phi(U)/\Phi(3)$ tabulated for these three elements in his paper. For the scale factor for each element we are using his absolute $\Phi(3)$ for that element. The resulting theoretical curve for nickel is compared with our experimental points in Fig. 3.

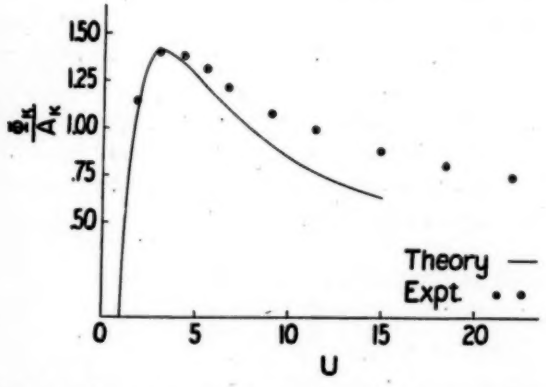

FIG. 3. Comparison of Burhop's theory with experimental cross sections for K ionization of nickel atoms.

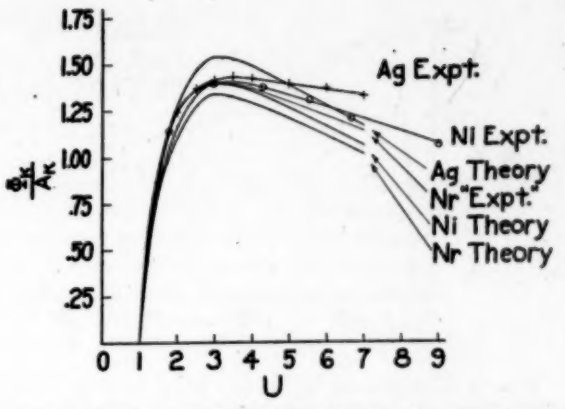

FIG. 4. Comparison of Ag with Ni, showing the effect of relativity; and graphs obtained by extrapolation for a hypothetical non-relativistic element Nr, showing how Burhop's non-relativistic theory fits this element best.

As will be seen there, the agreement is remarkably good, and especially good near the maxima of these functions.

VIII. THE EFFECT OF RELATIVITY

Only at high U's is there any serious disagreement in Fig. 3 between theory and experiment; and it is at these U's that we must expect the greatest effect of relativity, which did not enter into the theory. These facts raise two questions: (1) what is the effect of relativity; and (2) how well would the theory agree with experiment if we could find a strictly non-relativistic element with which to test it?

To answer these questions, in Fig. 4 we are comparing nickel with silver, for which an electron at any given U has almost exactly 3 times as much kinetic energy. At kinetic energies small in comparison with mc^2, most quantities which are changed by relativity in ways independent of the direction of motion are changed from their non-relativistic values by fractions thereof, which are roughly proportional to the kinetic energy. Consequently we may expect the K ionization cross sections Φ_K at any given U to follow this rule; and so will the characteristic areas A_K, and the ratios $F = \Phi_K/A_K$. Moreover the non-relativistic F, like $f(U_H)$ in the preceding section, should be practically the same, at any given U, for both elements. Therefore, at the same U, F_{Ag} should be about 3 times as far from this non-relativistic F

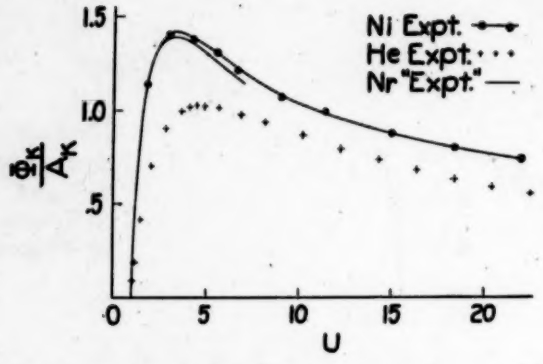

FIG. 5. Comparison of Smith's cross sections for He with those of Ni and the hypothetical non-relativistic element Nr, showing how something, presumably the electron which remains in the He atom, gives He abnormally small ionization cross sections at low U's.

as F_{Ni}. Half the difference $(F_{Ag}-F_{Ni})$, then, should be a fair measure of the effect of relativity in nickel. Roughly, this answers Question (1).

Moreover, it furnishes a basis for answering Question (2). If this measure of the relativity effect is deducted from the observed F for nickel, the result should be the F for the hypothetical non-relativistic element which we should like to use for testing the theory. We shall denote this element by Nr, for non-relativistic, and call the graph for it, derived in this way from the data on silver and nickel, its experimental graph. This graph and the corresponding one from Burhop's theory are shown along with those of the real elements in Fig. 4.

Here it should be noted again that the scale factors are more uncertain than the shape factors, both in experiment and in theory. In experiment the scale factors come from the absolute cross sections. Clark estimated the probable error of his absolute cross section for silver at 70 kv as 9 percent, and we have recomputed his cross section here by using more recent data on the fluorescence yield of silver[22] which we take to be 0.81 instead of 0.72, and on the ratio of the total number of K quanta to the number of $K\alpha$-quanta[23] (1.21 instead of 1.16), thus reducing all absolute cross sections by nearly 8 percent. Smick and Kirkpatrick estimated their probable error for the absolute cross section for nickel at 6 percent. The probable errors in *relative* cross sections are considerably smaller. On the theoretical side also, the scale factor is uncertain, because of the adjustment for the fact that $V_K \neq V_H$; and the extent of this inequality, as noted in Section VII, depends on both relativity and outer electrons. Altogether, the scale factor in Nr seems rather uncertain.

Regarding it therefore as somewhat arbitrary, it is evident that with a change of only a few percent in scale factor the theoretical non-relativistic curve would fit the experimental Nr points extremely well.

IX. THE OTHER K ELECTRON

In elements as heavy as nickel the use of the screening constant 0.30 is probably satisfactory, while the theory is in its present stage of approximation, as an allowance for the effect of the K electron which remains in the atom. This rule holds so long as $0.30 \ll Z$; but in helium the forces exerted on the electrons by the nucleus are so weak that the motion of the remaining electron cannot be neglected, and an allowance for it as a static $0.30e$ is no longer satisfactory. To see what effect it has, therefore, in Fig. 5 we are comparing our data on nickel with those of Smith's[6] data on helium which are within our range of U; and we are replotting also the "experimental" graph for our hypothetical non-relativistic element.

Evidently the helium cross sections, when expressed in the unit A_K, differ notably from those of nickel. Moreover, they show no signs of approaching agreement at U's above our range. With the hypothetical non-relativistic element, on the other hand, helium differs notably at low U's, but their graphs in Fig. 5 look likely to come into agreement at high U's.

[22] E. Arends, Ann. d. Physik **22**, 281 (1935), value 0.795±0.024; R. J. Stephenson, Phys. Rev. **51**, 637 (1937), value 0.81; I. Backhurst, Phil. Mag. **22**, 737 (1936), value 0.838.

[23] J. H. Williams, Phys. Rev. **44**, 146 (1933).

Proton-Proton Scattering at 8 Mev

ROBERT R. WILSON* AND EDWARD C. CREUTZ**
Princeton University, Princeton, New Jersey

(Received December 14, 1946)

A coincidence method of studying the scattering of protons by protons has been developed and applied to the 8-Mev protons obtained from the Princeton cyclotron. Relative measurements of the scattering cross section as a function of the angle of scattering are most consistent with theoretical cross sections calculated, assuming S wave scattering only. However, the accuracy of the experiment is not great enough definitely to exclude P wave scattering effects, positive or negative. An absolute measurement of the scattering cross section has been made and the experimental value $1.7\pm.1\times10^{-25}$ cm² agrees with the theoretical value 1.80×10^{-25} cm to within the experimental uncertainty.

1. INTRODUCTION

ONE of the immediate problems of nuclear physics is the determination of the nature of the short range forces between elementary particles of the nucleus. The study of the anomalous scattering of protons by protons has given much information on this subject. The first work was done by Wells,[1] and White.[2] Tuve, Heydenburg, and Hafstad[3] have examined proton-proton scattering in the energy range from 200 kev to 1.6 Mev, and Herb[4] and others have extended the measurements to proton energies of 2.4 Mev. Breit, Condon, and Present,[5] and Breit, Thaxton, and Eisenbud[6] have shown that all of the measurements can be adequately fitted by a theory which assumes only the effects of Mott type scattering, plus an anomaly obtained from the solution of the Schroedinger wave equation corresponding to the partial wave of zero angular momentum. The best fit of the data was obtained when a square potential hole 10.5 Mev deep and of electronic radius, (e^2/mc^2), was used. However, other shapes required by the various nuclear force theories fit nearly as well. The present experiment on proton-proton scattering was carried out with 8 Mev protons, since the differences in the scattering predicted by various theories at this energy are much larger than those which obtain in the region already investigated.

Unfortunately, this work was interrupted by the war at a time when consistent results were just beginning to be obtained. The data are presented, even though the accuracy is not high, because in arriving at this stage a number of difficulties were met and overcome, and it is thought worth while to point out some of these difficulties to future workers in this field.

2. METHOD

To eliminate to a large extent background counts, a coincident counting method first tried out by one of us at Berkeley was used. In the collision of like particles, one of which is initially at rest, the angle between the two velocity vectors after collision is 90°.[7] By use of a narrow proton beam and a thin cellophane foil as scatterer, the point of scattering was well defined so that two counters fixed on rotating arms at 90°, with the scattering foil at the center of rotation, could be used to count the scattered and the recoiling particle in coincidence. This prevented counting particles scattered from the oxygen and carbon of the foil or from gas in the vacuum chamber. The apparatus is shown schematically in Fig. 1.

3. COUNTERS

Although good results have been obtained by others in counting protons with an ionization chamber and linear high gain amplifier, and indeed this system was tried out in early work by

* Now at Harvard University.
** Now at Carnegie Institute of Technology.
[1] W. H. Wells, Phys. Rev. **47**, 591 (1935).
[2] M. G. White, Phys. Rev. **47**, 573 (1935).
[3] M. A. Tuve, N. P. Heydenburg, and L. R. Hafstad, Phys. Rev. **50**, 806 (1936).
[4] R. G. Herb, D. W. Kerst, D. B. Parkinson, and G. J. Plain, Phys. Rev. **55**, 998 (1939).
[5] G. Breit, E. U. Condon, and R. D. Present, Phys. Rev. **50**, 825 (1936).
[6] G. Breit, H. M. Thaxton, and L. Eisenbud, Phys. Rev. **55**, 1018 (1939).

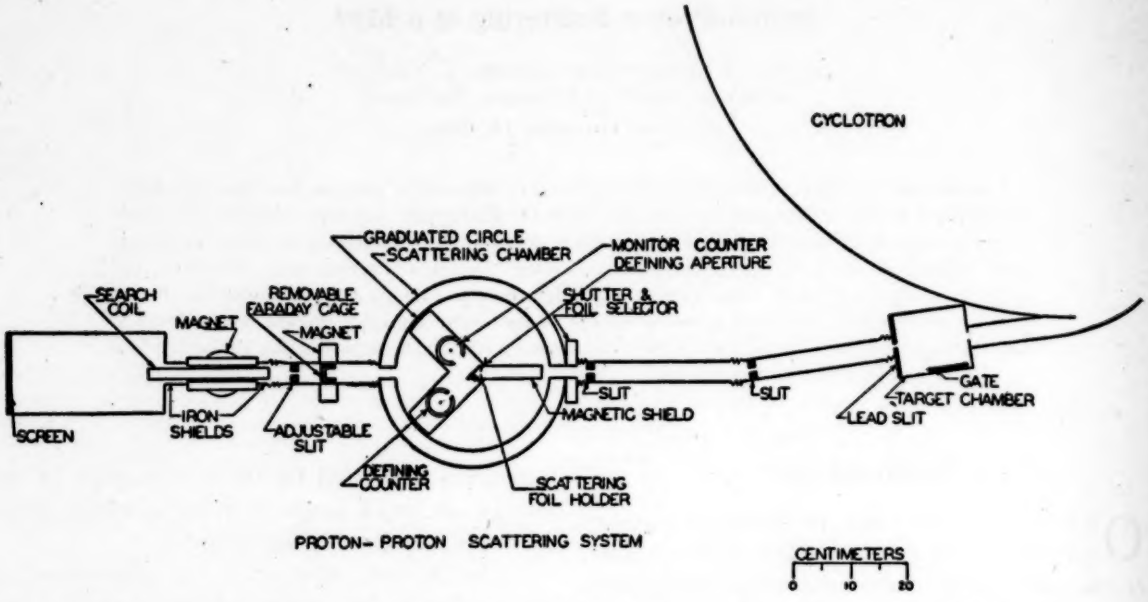

FIG. 1. Schematic drawing showing three slit energy-selecting system, scattering chamber, and the energy measuring device.

one of us at Berkeley, it was decided to use proportional counters for the following two reasons. First, owing to the small amount of ionization produced by several million volt protons passing through a few centimeters of low pressure gas, considerable amplification is required, so the large gas-amplification obtained in this type of counter is very desirable. Second, it is quite difficult completely to eliminate radio-frequency pick-up from the cyclotron oscillator in the a.c. lines and amplifier circuits, making the extremely high electrical amplification required with the non-multiplying chamber less convenient to use.

Because of the neutron field which always surrounds an operating cyclotron, it was necessary to design the counters so that no hydrogenous material was exposed to their sensitive regions, thus eliminating proton recoils. The counters used are illustrated in Fig. 2. It was necessary to use various sized apertures in the counters, as is explained in Section 9. Interchangeable diaphragms with circular openings could be placed over the elongated windows. This shape of window was chosen for the monitoring counter (and hence for both, to keep them internally identical) because the area determined by drawing all possible "conjugate" proton paths corresponding to protons being scattered from any part of the finite scattering area and into any part of the circular aperture of the defining counter, is oval in shape. Thus, considerable height to the maximum useful oval was obtained, without needlessly increasing the background count as would have been done by using a large circular opening.

In order to maintain a sufficiently uniform field (and hence to secure uniform pulses) the long axis of the hole had to be parallel to the axis of the counter, and not perpendicular to it, as was found by trial. The length was limited by the depth of the scattering chamber, and as the length must also be greater than a certain minimum to obtain a uniform field, a compact design of the counter ends was essential. The counters were completely assembled with neoprene gaskets. The wire used was 0.005″ steel. The windows were 0.0001″–0.0005″ Cellophane made gas tight with lead gaskets punched out of foil about 0.002″ thick by means of a simple concentric punch.

For scattering at small angles, it was found desirable to put about 0.006″ of aluminum over the defining counter window to slow the protons down somewhat and increase their specific ionization, thus improving the voltage plateau. The counter at large angles, which received lower

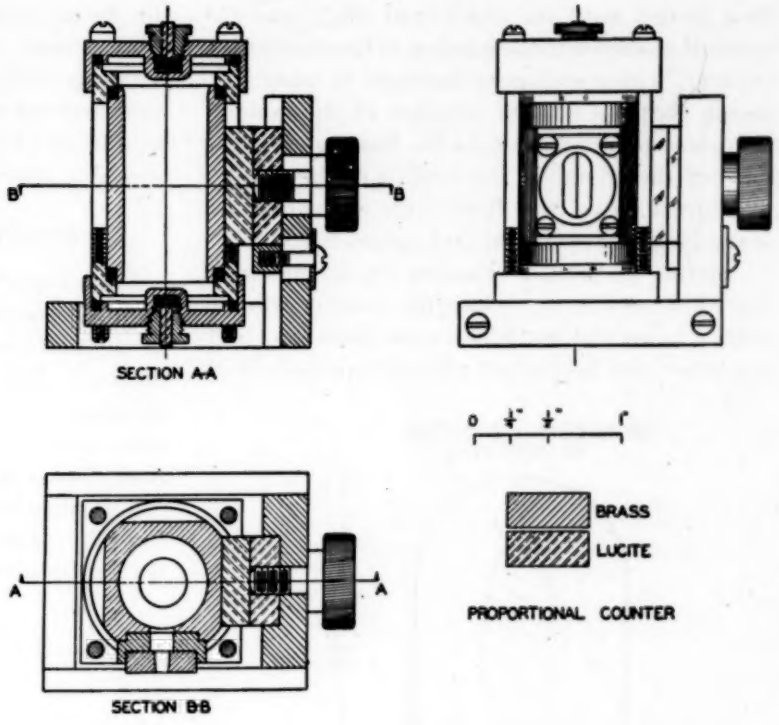

FIG. 2. The proportional counter.

energy protons, always had a 0.0001″ Cellophane window. The counters were filled with dry air at about 7 cm pressure, measured with a mercury manometer and kept constant to ½ mm during a run.

The efficiency of this type of counter was measured by sending alpha-particles through two in series, the front one having a hole in back. First the pulses in the rear chamber were counted, and next the coincidences between the two. The efficiency was thus found to be better than 99 percent. The over-all resolving time of the counters and electrical circuits was measured by placing separate alpha-particle sources in front of two separate counters and counting, first the pulses in the individual counters, and then the accidental coincidences. The resolving time was 5×10^{-6} second computed from the usual formula

$$N=2n_1n_2\tau, \qquad (1)$$

where N=accidental coincidence counting rate; n_1, n_2=counting rates in the two counters, respectively; and τ=resolving time. This fairly long resolving time arose from the slowness of the high gain amplifiers available at that time (1940).

4. ALIGNMENT

After having determined that the proton beam was horizontal, the scattering foil holder and iron magnetic shield (see Fig. 1) were leveled and the iron shield centered in the chamber. A rectangular block of brass was machined flat on one end, and a scratch made on its side, perpendicular to the flat end. This scratched face was then sprayed with fluorescent material. When the block was placed on the floor of the chamber with the scratch vertical and intersecting the center line of the chamber, the proton beam was turned on. The chamber was then rotated slightly about a vertical axis until the fluorescent spot caused by the beam was split by the scratch. Thus the beam was accurately parallel to the center line of the chamber. A steel mandril was made to fit snugly into the magnetic shield when the defining aperture was removed. With the other end of the mandril slipped into the window of the defining counter, the counter was fastened in place on the rotating arm, and the index was set on the zero of the graduated circle. The rotating arm was

then turned until the index read 89½°,[7] and the mandril pushed into the window of the monitoring counter, which was next fastened in place. To assure that the axis of rotation of the counter arms was perpendicular to the beam and to the floor of the chamber, the heights of the counter apertures above the floor were measured for several angular positions, and agreed to 0.001".

Another method of checking the alignment of the counters was to replace the counter window with a brass disk on which cross lines had been scratched and fluorescent material sprayed. With the beam coming through the chamber the counter was turned into the beam, and the centering of the fluorescent spot on the cross lines was observed with the index of the angular scale set a 0° and 89½° for the defining and monitoring counters, respectively.

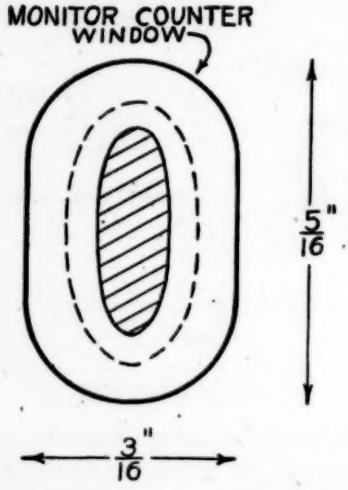

FIG. 3. The thick outside line indicates the area of the monitor counter aperture. The shaded area indicates where the recoils of protons scattered into the defining counter can enter the monitor counter when the defining counter is at 15°. The dotted curve indicates the magnitude of the effect of multiple scattering in diffusing the shaded area.

[7] Actually this angle ϕ between the two proton velocity vectors is given by the expression

$$\tan\phi = 2c^2(1-V^2/c^2)^{\frac{1}{2}}/V^2\sin\theta^*,$$

where θ^* is the angle of scattering in the center of gravity system; c is the velocity of light; and V is the velocity of the protons relative to the center of gravity. For the relativistic case V is given by

$$V = v/[1+(1-v^2/c^2)^{\frac{1}{2}}],$$

where v is the velocity of the incident proton in the laboratory system. When the scattering angle in the laboratory system is between 45° and 15°, 89½° is a satisfactory value for ϕ since the angular aperture of the monitoring counter is several degrees. The exact value of ϕ for various proton energies is given below; for $\theta^* = 90°$

Proton Energy (Mev)	ϕ
0	90°
8	89° 52′ 40″
16	89° 44′ 40″
25	89° 36′ 34″
50	89° 14′ 20″
100	88° 30′ 50″
1000	77° 51′ 30″

5. EFFECT OF MULTIPLE SCATTERING

In an early attempt to increase the ionization of the proton by slowing it down with foils placed in the scattered beam, the yield was found to decrease. This was found to be caused by the diffusion of the beam by small angle scattering and showed the necessity of using very thin scatterers. The multiple scattering of the protons can be calculated by the application of Williams'[8] formula. According to it, the mean square deflection[9] is given by:

$$\langle\theta^2\rangle = \frac{\pi}{2}\left(\frac{Ze^2}{E}\right)^2 Nt\log\frac{Z^{4/3}Nth^2}{2m^2v^2}, \qquad (2)$$

where Z is the atomic number of the scattering foil, e the electronic change, E the energy, N the number of nuclei per cm³, t the thickness of foil, h Planck's constant, m the electronic mass, and v the proton velocity.

Let us assume the Cellophane in the foil has the molecular formula $C_6H_{10}O_5$ and has a density of 1.15 g/cm³. Then the root mean square deflection becomes

$$\langle\theta^2\rangle^{\frac{1}{2}} = 0.5t^{\frac{1}{2}}/E_{\text{Mev}} \text{ radian}. \qquad (3)$$

The log term was evaluated for a one Mev proton, then its variation with E neglected. A factor of $\frac{2}{3}$ has been included in Eq. (3) because the protons are as likely to be scattered near the back of the foil as near the front of the foil, and the average value of $(X)^{\frac{1}{2}} = \frac{2}{3}(X_{\max})^{\frac{1}{2}}$.

In Fig. 3 the heavy oval line represents the opening of the monitor counter which is 4 cm from the scatterer. Let us consider protons scattered at 15° from a parallel beam 2 mm in diameter into the monitor counter whose aperture is $\frac{1}{16}$" in diameter and which is 7.6 cm from the

[8] E. J. Williams, Proc. Roy. Soc. 169, 531 (1939).

[9] This is defined by

$$n(\theta)d\theta = [2/\pi\langle\theta^2\rangle]^{\frac{1}{2}}\cdot\exp(-\theta^2/2\langle\theta^2\rangle)\cdot d\theta$$

where $\langle\theta^2\rangle$ is the mean square deflection.

TABLE I. Collected scattering data.*

Date	Holder	Scattering angle $=\theta$	$C=\frac{\text{counts}}{8}$	Mean square error (%)	Total galv. defl. $=D$	$\frac{C}{D}$	Window	$\frac{C}{D\cos\theta}$	Angles for which ratio of yields is taken	Ratio of yields	M.s.e. of ratio (%)
1/21/41	90°	45°	903	1.2	17.27	52.3	1/8″	74.0	48–45	1.04	2.2
1/21/41	90°	48°	258	2.0	5.00	51.6	1/8″	77.1	48–45		
3/24/41	90°	50°	634	1.5	18.6	34.1	1/8″	53.2	50–45	0.97	2.0
3/24/41	90°	45°	813	1.2	20.9	38.9	1/8″	55.0	50–45		
3/25/41	90°	45°	302	2	7.76	38.91	1/8″	55.0	35–45	1.02	2.4
3/25/41	90°	35°	598	1.4	13.00	46.1	1/8″	56.2	35–45		
3/25/41	90°	45°	441	1.8	46.07	9.58	1/16″	13.5	35–45	1.03	1.8
3/25/41	90°	35°	235	2.5	20.67	11.4	1/16″	13.9	35–45		
3/30/41	90°	30°	693	1.3	24.70	28.1	1/8″	32.4	30–45	1.02	1.8
3/30/41	90°	45°	686	1.3	30.57	22.5	1/8″	31.8	30–45		
3/30/41	90°	40°	508	1.6	20.00	25.4	1/8″	33.2	40–45	1.01	2.0
3/30/41	90°	35°	481	1.6	18.00	26.7	1/8″	32.6	35–45	1.02	2.2
4/12/41	90°	45°	905	1.2	147.31	6.15	1/16″	8.70	30–45	1.01	1.7
4/12/41	90°	30°	815	1.2	107.40	7.58	1/16″	8.76	30–45		
4/14/41	90°	45°	493	1.6	86.44	5.71	1/16″	8.08	30–45	1.01	2.0
4/14/41	90°	30°	869	1.2	122.40	7.09	1/16″	8.18	30–45		
4/19/41	90°	45°	2135	0.8	30.07	71.0	1/8″	100.3	35–45	1.01	1.2
4/19/41	90°	35°	1862	0.8	22.58	82.6	1/8″	101.0	35–45		
6/20/41	40°	30°	2243	0.8	52.21	43.1	1/8″	49.7	25–30	0.96	1.2
6/20/41	40°	25°	1972	0.8	45.49	43.3	1/8″	47.8	25–30		
7/3/41	40°	30°	797	1.2	30.85	25.8	3/32″	29.8	25–30	0.99	2.0
7/3/41	40°	25°	523	1.6	19.56	26.8	3/32″	29.6	25–30		
7/9/41	30°	25°	2062	0.8	68.87	29.9	3/32″	33.0	20–25	0.97	1.2
7/9/41	30°	20°	1951	0.8	64.95	30.1	3/32″	32.0	20–25		
7/12/41	30°	25°	2063	0.8	181.84	11.35	1/16″	12.52	20–25	0.94	1.2
7/12/41	30°	20°	2012	0.8	181.95	11.05	1/16″	11.75	20–25		
7/12/41	30°	15°	1297	1.0	116.17	11.15	1/16″	11.55	15–25	0.92	1.3

Summary of Table I:

Angles for which ratio of yields is taken	Weighted average of yield ratio	M.s.e. of ratio (%)
50–45	0.97	2.0
48–45	1.04	2.2
40–45	1.01	2.0
35–45	1.01[7]	0.9
30–45	1.01[3]	1.1
25–30	0.96[9]	1.0
20–25	0.95[5]	0.9
15–25	0.92	1.3

Angles for which ratio of yields is calculated from Table I	Weighted average of yield ratio	M.s.e. of ratio (%)
25–45	0.98[6]	1.5
20–45	0.93[7]	1.7
15–45	0.90	2.1

scatterer which is placed at 30° with respect to the direction of the beam. Then all the "conjugate" protons (i.e., the recoil protons at 90° to the scattered protons) would fall into the shaded area in the monitor opening, if there were no multiple scattering. This area was found by a simple geometrical construction. The distribution of the conjugate protons within the shaded area was not found; it would obviously not be uniform. However, as long as the limits of the area fall within the opening of the monitor counter, then no counts should be lost. In some of our earlier work, larger apertures were used on the defining counter so that the shaded area overlapped the opening of the monitor counter and hence some counts were lost.

Now let us consider the effect of multiple scattering due to a Cellophane foil 0.1 mil thick. The 8 Mev protons scattered at 15° will have their energy reduced by the collision to 7.5 Mev ($=E_0\cos^2\theta$). The thickness of the foil (at 30° to direction of beam) (see Table I) for protons passing through at 15° is $0.1/\sin\theta=0.4$ mil. Hence the root mean square deflection according to Eq. (3) is 0.21×10^{-2} radians or 0.12°. The recoil or conjugate protons at 75° have their energy reduced to 0.54 Mev, and the foil thickness in that direction is 0.1 mil. The root mean square deflection for the recoil protons, then, is 1.5×10^{-2} radian or 0.85°. Thus the total root mean square deviation from 90° between recoil and scattered protons is $(0.85^2+0.12^2)^{\frac{1}{2}}=0.86°$. This causes the limits of the shaded area of Fig. 3 to become diffuse. If all the protons were concentrated on the limiting edge of the shaded area without multiple scattering, then the dotted line repre-

sents the root mean square deflection outside the shaded area with multiple scattering. The extreme loss is then given by

$$1-\left(\frac{2}{\pi^{\frac{1}{2}}}\right)\int_0^{X_{\max}} \exp(-X^2)dX$$

where

$$X_{\max}=\theta_{\max}/2^{\frac{1}{2}}\langle\theta^2\rangle^{\frac{1}{2}},$$

and θ is the angle between the edge of the shaded area and the edge of the aperture. For our geometry shown in Fig. 3, $\theta_{\max}/\langle\theta^2\rangle^{\frac{1}{2}}$ is about 2.5 so not over 1.3 percent would be scattered outside the monitor counter window. Actually the loss should be far less as the density of protons will be greatest at the center of the shaded area rather than at the edges as we have assumed.

We have considered the worst case at 15°. At larger scattering angles the energy of the proton scattered into the monitor counter rapidly increases and the multiple scattering then decreases rapidly. At some of the larger angles a $\frac{1}{8}''$ diameter aperture could be used in addition to the $\frac{1}{16}''$ diameter aperture.

The effect was studied experimentally by measuring the yield of scattered protons per unit solid angle as a function of the solid angle (defining counter) and as a function of the thickness of the scattering foil. Effects could be produced using very thick foils or very large solid angles, but for the conditions used in taking the final data no multiple scattering effects were observed. To minimize any possible effects of multiple scattering, the scattering foil was not always placed normally to the incident proton beam but was placed at such an angle that the low energy protons scattered into the monitor counter would pass through a minimum of scattering foil, i.e., come out of the scattering foil normally. This was done by making several holders which fit snugly into the magnetic shield, and which were cut off at various angles on the end to which the foil was cemented. Thus for comparing the yields at 15°, 20°, and 25°, a holder cut off at an angle of 30° was used. For scattering at 25°, 30°, and 35°, one cut off at 40° was used, while for measuring at 30°, 35°, 40°, and 45°, one cut at 60° was used. For the absolute yield determination at 45° the foil was held normally to the incident beam, and not cemented, but supported in a removable cap so it could be weighed before and after use.

6. CHARGE MEASUREMENT

The incident proton current was collected in a faraday cup, which could be removed by means of an insulated sliding seal when it was desired to allow the beam to pass into the energy measuring system. Various magnetic fields and voltages were applied to the cup to study the effect of secondary electrons. That no effect on the yield was observed for fields up to 1000 gauss is probably because of the fact that the stray cyclotron field was about 100 gauss which kept secondaries from getting out. From the faraday cup a concentric evacuated cable led to a switching arrangement and thence to a specially constructed evacuated condenser. The concentric cable consisted of 1″ brass tubing soldered into standard stream-lined copper elbows. At each elbow (3 in all) were placed two thin lucite wafers fitting snugly inside and held in place by the inserted brass tubing. The wafers were perforated with several holes to decrease their conduction and to increase pumping speed through the cable, while through the center hole was inserted a piece of $\frac{1}{8}''$ copper tubing, extending around the bend. The conductor in the cable was 0.006″ steel wire passed through the $\frac{1}{8}''$ tubing around the elbows and held firmly at the ends of the cable by low electrical leakage lucite fittings. This construction served the following purposes: (a) the brass tubing provided a shield against radio-frequency pick-up which might have been rectified in the switch or elsewhere to produce spurious charges, and (b) the evacuated region around the wire prevented loss of charge due to ionization from the cyclotron radiation.

The condenser on which the charge was accumulated, and which was later discharged through a ballistic galvanometer, was designed to be as free from leakage as possible. It consisted of two interlaced stacks of copper plates 3″×4″ in area and $\frac{1}{16}''$ thick piled up with brass spacers $\frac{1}{8}''$ thick at the ends of each plate so that the two consecutive plates of one stack, placed crosswise to the intervening ones of the other stack, were separated from it by $\frac{1}{32}''$. One stack was supported by lucite pillars at the bottom, which provided the only leakage path between it and the other (grounded) set, except for the lucite insulated lead-in which passed through the

vacuum jacket. This jacket consisted of a piece of brass tubing sealed by neoprene gaskets into the end plates, and clamped by bolts extending from end to end. A pump-out valve and vacuum-pressure gauge were provided, so that if desired, the condenser could be used for a pressure ionization chamber. The capacity was measured as 0.00937 μf. Extensive leakage tests were made with the cyclotron running, so a small correction could be made in determining the absolute number of protons incident on the scattering foil. For the relative angular distribution measurements this correction was not made, since all runs in a given set were made for the same length of time, with a nearly constant beam intensity. A great advantage of the vacuum condenser was the total absence of soakage of charge into the dielectric. This soakage effect was found troublesome with several standard mica condensers tried out. Two or three minutes after these condensers were discharged, a second discharge showed that a percent or so of the original charge was left. The almost complete elimination of dielectric material in the vacuum cable and condenser system prevented this difficulty.

The absolute charge sensitivity of the galvanometer was determined in two independent ways; namely, by the current-time method, and by the potential-capacity method. In the first case a small current obtained from a stabilized 2000 volt supply and S. S. White resistors was fed into the condenser for various measured times. The current was measured with a sensitive galvanometer. The charged condenser was then discharged through the ballistic galvanometer. The system was found to be linear within 0.5 percent for throws from 2 to 25 centimeters. This calibration was made frequently, and always immediately before and after an absolute yield run. For the second method of calibration of the charge measuring system, the capacity of the condenser was measured with two different bridges. Both bridges gave the value 0.00937 $\pm$0.00003 μf, the second one showing the capacity to be independent of frequency from 60 to 1000 cycles per second. A dry cell, reserved for this purpose, was then connected across the condenser through a high resistance, its potential difference measured, and the condenser then disconnected and discharged.

Typical values for the first method are:

Current	Time	Charge	Ballistic throw	Coulomb/mm
2.87×10^{-9} amp	30 sec	8.61×10^{-8} coulomb	12.23 cm	6.54×10^{-10}

And for the second method:

Cell e.m.f.	Capacity of condenser	Charge	Ballistic throw	Coulomb/mm
1.365 v	0.00937 μf	1.279×10^{-8} coulomb	1.95 cm	6.55×10^{-10}

Agreement of the two methods was always better than one-half percent. Both methods ultimately depend on the e.m.f. of a standard cell, since the calibration of the current galvanometer in the first, and the measurement of the dry cell in the second, each made use of it.

7. ENERGY MEASUREMENT

The energy of the protons emerging from the 3 slits was measured by means of an auxiliary magnetic field deflecting system.[10] This device was capable of measuring the energy to within about 1 percent, and showed that the selected beam was homogeneous to this degree. The energy of the protons used in these experiments was 8.0$\pm$0.1 Mev. Accuracy in this value is of no theoretical importance, inasmuch as other duties prevented the carrying out of the experiments over a range of energies, which would be useful for an accurate determination of the range of nuclear forces.

8. CELLOPHANE

It was early decided that Cellophane would be a useful material for the scattering foil because it is tough, contains a relatively large percentage of hydrogen by weight (6.22 percent) and presumably has a known empirical formula—$X(C_6H_{10}O_5)$. Commercial Cellophane contains a small amount of glycerine to keep it from becoming brittle, but since it was desired to determine the number of hydrogen atoms per square centimeter of the foil by weighing, a pure chemical compound was required. The usefulness of Cellophane in these experiments is owing to the cooperation of Dr. Nelson Allen of the Cellophane Analytical Research Division of E. I. du Pont de Nemours and Co. From him were obtained several batches of very pure Cellophane, cast in special thin sheets, down to 0.00008". These thin foils were necessary to minimize the multiple scattering effect discussed above.

[10] E. Creutz and R. Wilson, Rev. Sci. Inst. **17**, 385 (1946).

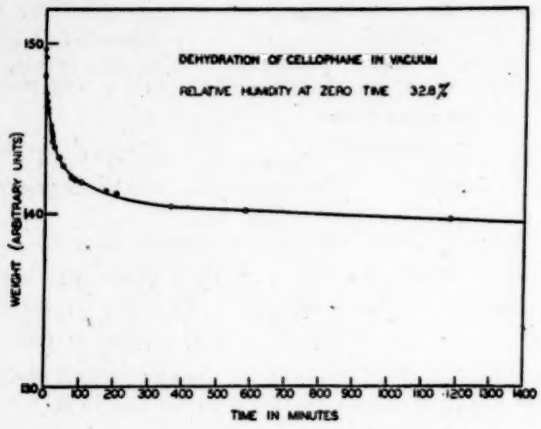
DEHYDRATION OF CELLOPHANE IN VACUUM
RELATIVE HUMIDITY AT ZERO TIME 32.8%
WEIGHT (ARBITRARY UNITS)
150
140
130
0 100 200 300 400 500 600 700 800 900 1000 1100 1200 1300 1400
TIME IN MINUTES

FIG. 4. Weight of 0.005 inch thick Cellophane foil ½" in diameter as a function of time in vacuum. The decrease in weight is because of dehydration. Relative humidity of the air with which the foil was originally in equilibrium was 32.8 percent.

The foils used were punched out of sheet as discs ⅜" in diameter. The punch used was made of drill rod, hardened and ground, and its diameter was measured before and after punching out a foil. The diameter of aluminum disks punched out by it were also measured as a check. The Cellophane disks were then weighed on a quartz fiber torsion microbalance which follows the same general design as given in Strong,[11] except that it was built into a chamber which could be evacuated. The weight of the foil was observed as a function of the time after evacuation, while a large part of the absorbed water was removed. It was observed[12] that the dehydration proceeded rapidly at first (probably corresponding to loss of water absorbed on the surface), and then much more slowly, presumably as water diffused out of the interior of the cellophane and then evaporated. This effect is shown in Fig. 4. With the 0.0005" foil about 20 hours were required for the weight to arrive within 0.5 percent of its final equilibrium value. With 0.0001" foil the "volume effect" was much less pronounced, and the weight became essentially stationary in about four hours. The same effect was noticed by the variation of the yield of scattered protons from a foil freshly put into the scattering chamber. After about a day the yield settled down and remained constant, showing that there was no appreciable deterioration of the Cellophane due to the beam's passing through it.

Since it was not known if all of the absorbed water had left the foil even after the weight had become constant, it was desirable to have an analysis of the material made under as nearly as possible the conditions obtained in the scattering chamber. Mr. E. L. Stanley, of the Department of Chemistry at Princeton University, kindly made some micro-analyses of the Cellophane. In foils which had been in vacuum for several days he found (6.6±0.3) percent hydrogen. Later the National Bureau of Standards made some analyses, obtaining (6.45±0.1) percent. Further analyses by a modified technique were made by Dr. Yensen, of Westinghouse Research Laboratories, whose results did not conflict with these. Considering the theoretical value of 6.22 percent, one sees an unpleasant uncertainty in the hydrogen content of the scatterer used for the absolute yield determination, which would need to be cleared up before an accuracy better than a few percent could be hoped for by this method. This difficulty, however, does not affect the relative angular distribution measurements of scattered protons.

9. METHOD OF TAKING THE DATA

Although the counters were constructed to be rather insensitive to neutrons, more or less background in each single counter was always found even with the proton beam kept out of the scattering chamber by means of a shutter. This was in a large part probably owing to the fact that the gas used in the counters was air, providing a source of alpha-particles from the reaction $N^{14}(n, \alpha)B^{11}$. However, since the resolving time of the coincidence system was measured to be sufficiently small, it was not difficult to keep the individual counting rates (including the protons scattered from the oxygen and carbon of the foil) down so that the accidental coincidence rate was low. In all runs, repeated checks were made on this background rate, and in the worst cases (where very small proton admitting apertures were used on the defining counter, so that a rather large beam was required, which not only increased the neutron intensity but also the spurious proton rate in the monitor

[11] J. Strong and others, *Procedures in experimental physics* (McGraw-Hill Book Company, Inc. 1942).
[12] E. Creutz and R. Wilson, J. Chem. Phys. 14, 725 (1946).

counter) it amounted to 3 or 4 percent. At angles from 45° to 30° where larger apertures could be used, so that the total beam required to obtain data in a reasonable time was smaller, the background coincidence rate was negligible, amounting to less than 0.5 percent. In all cases it was found advisable to keep the pressure in the cyclotron low to decrease the number of neutrons produced inside the dees.

The runs made, the foil holder and aperture used, the number of counts with the mean square percentage error, the ballistic galvanometer deflection, the number of counts divided by this deflection, this quotient divided by the cosine of the angle of scattering, and the yield ratios obtained are listed in Table I. The fact that different yields are obtained for the same angle in some cases, means that the foil was changed between runs. The parenthesis indicates runs for which the same foil was used.

In Fig. 5 are plotted the ratios of the scattering yields per unit solid angle in the center of gravity system, measured at the laboratory angle θ, to that at 45°. The vertical lines indicate the uncertainty corresponding to the mean square counting error. The mean square errors are computed from the square root of the number of counts and increase at smaller angles because in calculating the relative cross section for, say 20°, several ratios must be taken, namely 20° to 25°, 25° to 30°, and 30° to 45°, each one of which adds to the error. Any errors in alignment of the apparatus would be larger at smaller angles than at 45°, so all points would be raised by the elimination of such errors.

The point at 15° is least certain because possible effects due to misalignment and multiple scattering are greatest at small angles. Both effects tend to lower the experimental result. Another source of error at 15° can arise because the protons entering the monitor counter have an energy of only 0.54 Mev. Hence they barely penetrate the thin (about 0.1 mil) Cellophane scattering foil and window of the counter. Because of the straggling of range, it is possible that all protons will not penetrate the two foils. This effect will also tend to lower the experimental result. Thus the cross section at 15° can be regarded as a lower limit as the arrow in Fig. 5 indicates. All the above effects should become much smaller at 20° where the protons entering the monitor counter now have an energy of about one Mev. Since the cross section at 15° has a reasonable value, we can regard the value at 20° as being quite reliable.

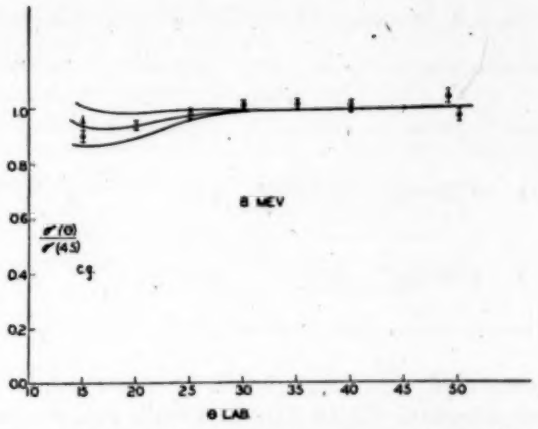

FIG. 5. Ratio of the proton-proton scattering yield at various angles to the yield at 45° in the laboratory system. The vertical lines are drawn to correspond to the mean square counting error. However, as explained in the text, the point at 15° is a definite lower limit, the upper limit is uncertain. The solid curves are calculated from a square potential well 10.5 Mev deep and of radius e^2/mc^2. Middle curve is calculated on the assumption of S scattering only. Upper and lower curves include the effect of P scattering for repulsive and attractive potential respectively.

10. ABSOLUTE YIELD

The absolute yield determinations were made at 45°. The results of two such runs are shown in Table II.

The cross section per unit solid angle for the scattering process is defined in the following way:

$$\sigma = (N_s/N_i)(1/\rho\Omega),$$

where N_s is the number of protons scattered into the solid angle Ω out of an incident group N_i by a stationary group of areal density ρ. The measurement of N_s, N_i, and ρ have been discussed. The solid angle Ω was determined by measuring four diameters of the nearly circular defining aperture by means of a traveling microscope. Typical values are 0.3230, 0.3231, 0.3229, 0.3240 centimeters. The average value was used to compute the area. The distance of the aperture to the scattering foil was measured with calipers to be 7.60 ± 0.01 centimeters. The angle Ω is thus determined as $1.40 \times 10^{-3} \pm 0.01 \times 10^{-3}$ sterad. The scattering foil was weighed before and after the

TABLE II. Absolute yield determinations of proton-proton scattering. σ is the laboratory cross section for 8 Mev protons scattered at 90° in the C. G. System (45° in laboratory system).

Run	Foil wt.	Foil area	Foil density	Fraction by wgt. of hyd.	ρ	N_s	N_i	σ
1	0.785 mg.	2.053 cm²	$3.82\times10^{-4}\ \frac{\text{gms}}{\text{cm}^2}$	0.0645	$1.48\times10^{19}\ \frac{\text{proton}}{\text{cm}^2}$	5520	1.45×10^{12}	1.8×10^{-25} cm²
2	0.785 mg.	2.053 cm²	$3.82\times10^{-4}\ \frac{\text{gms}}{\text{cm}^2}$	0.0645	$1.48\times10^{19}\ \frac{\text{proton}}{\text{cm}^2}$	2480	0.746×10^{12}	1.6×10^{-25} cm²

runs and no change could be observed. More significant is the fact that during a run the yield did not change. The microbalance was calibrated by weighing small lengths of platinum wire which had been weighed previously together on an analytical balance. The area of the foil was assumed to be the same as the area of the punch, whose diameter was measured as 1.6152 ± 0.0005 centimeters.

11. COMPARISON WITH THEORY

The expected value of the cross section for proton-proton scattering has been calculated by L. B. Eisenbud on the assumption of a square well of depth 10.5 Mev and width (e^2/mc^2), both for S wave scattering alone and for $S+P$ wave scattering with the potential for the P wave both attractive and repulsive. These calculations were made at 7 Mev and 10 Mev proton energy. Since the experiment was at 8 Mev, a linear interpolation of the calculated values was carried out for comparison. The relative angular distribution values for the three cases, S wave only, S wave plus P wave scattered by attractive potential, and S wave plus P wave scattered by repulsive potential, are plotted with the experimental data in Fig. 5. It is seen that the data are most consistent with the curve calculated for S wave scattering only but that the accuracy of the experiment is not great enough to exclude definitely P wave scattering effects positive or negative.

The absolute value of the cross section at 45° in the laboratory system (90° in the center of gravity C. G. system at which angle there is no P scattering) is calculated from the above well to be 1.80×10^{-25} cm², if the forces are central in character. The experimental value $1.7\pm0.1\times10^{-25}$ cm² agrees with this to within the uncertainty in the hydrogen concentration in the Cellophane.

It should be emphasized that the work was terminated before all the desired checks for systematic errors could be made, hence statistical errors indicated in Fig. 5 should be regarded as lower limits for the actual errors.

The Infra-Red Spectrum of Methyl Fluoride

KENNETH P. YATES AND HARALD H. NIELSEN
Mendenhall Laboratory of Physics, The Ohio State University, Columbus, Ohio

(Received December 13, 1946)

All of the important bands in the spectrum of methyl fluoride except the 8μ (1200 cm^{-1}) band, have been remeasured under considerably higher resolution than that available to Bennett and Meyer. In this work the parallel bands as well as the perpendicular bands have been resolved. The approximate average spacing between lines in the P and R branches of the parallel type bands was found to be about 1.7 cm^{-1}. New and more precise determinations of band centers and molecular constants have been achieved.

I. INTRODUCTION

THE spectrum of methyl fluoride was investigated by Bennett and Meyer[1] who were able to resolve the Q branches in the perpendicular type bands and to separate rather incompletely the lines in one of the parallel type bands. In the time that has elapsed since this investigation was made infra-red spectroscopy has been much improved. Moreover, the theory of the infra-red bands of polyatomic molecules has been carefully studied and suggests many new and interesting details to look for in the spectra of symmetric molecules. This has given impetus to the remeasurement of the bands in the infra-red spectrum of methyl fluoride, particularly since the measurements of Bennett and Meyer already gave evidence of anomalies in the rotational structure which could not be explained readily. In this investigation all the bands except the 8.0μ perpendicular type band observed by Bennett and Meyer have been re-examined and quite completely resolved. The improvement in the resolution is particularly noticeable in the parallel type bands.

II. EXPERIMENTAL WORK

The methyl fluoride gas was produced by heating dimethyl sulphate, $(CH_3)_2SO_4$, with potassium fluoride, KF, to about 160°C. The gas was purified by partial distillation and stored in glass flasks from which it could be drawn when desired.

The absorption cell was of a conventional type, made of 2″ glass tubing fitted at the ends with windows of polished rocksalt. The absorption cell was 10 cm long and had a stopcock for admitting the gas. For the more intense bands a gas pressure of about 5 cm Hg was sufficient, but for the less intense bands it was found necessary to fill the cell with gas to about 20 cm Hg.

The spectrometer is a prism-grating instrument used in previous measurements and is operated manually. In this investigation three gratings were employed; two replica gratings produced by R. W. Wood with 7200 lines per inch and 3600 lines per inch to scan the spectrum from 3 microns (μ) to 8μ, and a grating ruled by Wood with 800 lines per inch for the 9μ to 10μ region. In every case, it was possible to operate the spectrograph so that the slits subtended a wave-length interval of not more than 0.3 cm^{-1}. Observations were made on the spectrum at intervals on the spectrometer circle of 5 seconds of arc or about every 0.15 cm^{-1}. The grating was calibrated using a strong infra-red line in the emission spectrum of mercury near 1.0μ.

III. EXPERIMENTAL RESULTS

There are four principal regions of absorption in the spectrum of methyl fluoride. These regions lie, respectively, near 3.5μ, 7.0μ, 8μ, and 9.6μ and embrace the six fundamental bands in the spectrum and two weaker bands of the parallel type. In the following sections will be given a description of the characteristics of these absorption regions together with the frequency positions of the most important lines.

A. The 3.5μ Region

Figure 1 shows the data recorded on the less intense portion of the absorption region near 3.5μ.

[1] W. H. Bennett and C. F. Meyer, Phys. Rev. 32, 888 (1928).

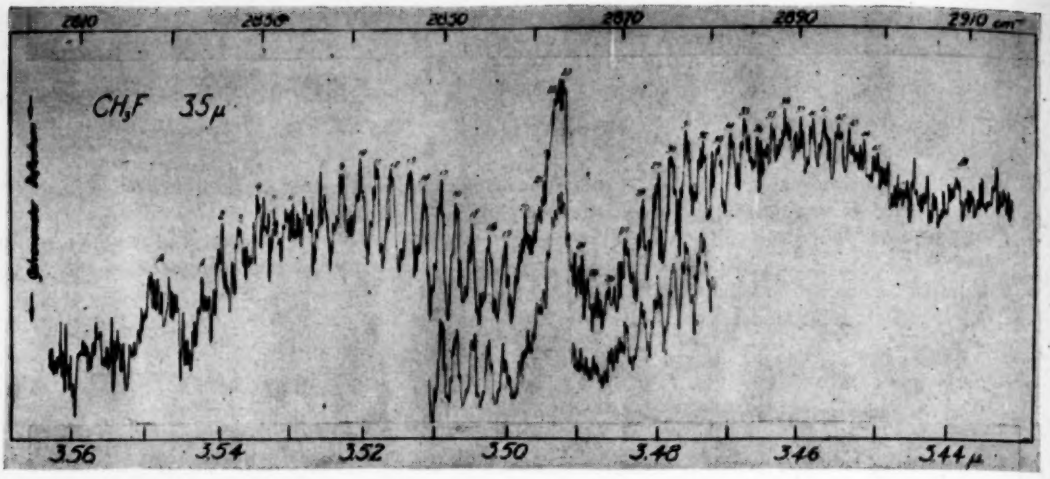

FIG. 1. The 3.5μ absorption region of CH_3F.

The curve given is a composite curve of several sets of data and is representative of the details which repeat from run to run. A scale of frequencies and wave-lengths has been substituted for the actual circle settings. The band is evidently of the parallel type. The high frequency end overlaps to a degree with the more intense bands which lie in this general neighborhood. This accounts for the fact that it is very complex in appearance and does not fall off in intensity in the usual manner. The low frequency end of the band is also complex. This is caused by the overlapping of this band with another weaker band of the parallel type, the Q branch of which lies at 2818 cm^{-1}.[2] The frequency positions of the most significant lines corrected to vacuum are given in Table I.

Figure 2 depicts the more intense portion of this absorption region. Measurements were here made with less gas in the cell than in the former case, and the curve is again a composite of all the data taken. In this region there is some absorption caused by water vapor and to eliminate this effect it was necessary to take readings at each setting of the circle, with the cell in the light beam and the cell out of the beam. Compensation for the diminution of the energy due to the windows has been made. The region is evidently made up of a band of the parallel type at the low frequency end, and a band of the perpendicular type at the high frequency end. The frequency positions, corrected to vacuum, of the most important lines are given in Table II.

[2] This band has just been observed by Robert Noble in scanning the 3.5μ region with the Ohio State University self-recording grating spectrometer.

B. The 7.0μ Region

There are strong atmospheric water vapor lines throughout this region. For this reason the spectrometer was sealed and carefully dried with

TABLE I. Frequency positions and identification of lines in the 3.5μ parallel band.

Line No.	Identification	Frequency	Line No.	Identification	Frequency
1	$P(22)$	2821.5	25	$R(1)$	2864.7
2	$P(21)$	2823.5	26	$R(2)$	2866.8
3	$P(20)$	2825.5	27	$R(3)$	2868.7
4	$P(19)$	2827.3	28	$R(4)$	2870.5
5	$P(18)$	2829.2	29	$R(5)$	2872.3
6	$P(17)$	2830.8	30	$R(6)$	2874.0
7	$P(16)$	2832.8	31	$R(7)$	2875.7
8	$P(15)$	2834.8	32	$R(8)$	2877.3
9	$P(14)$	2836.9	33	$R(9)$	2879.1
10	$P(13)$	2838.9	34	$R(10)$	2880.7
11	$P(12)$	2840.7	35	$R(11)$	2882.3
12	$P(11)$	2842.5	36	$R(12)$	2883.9
13	$P(10)$	2844.4	37	$R(13)$	2885.5
14	$P(9)$	2846.1	38	$R(14)$	2887.1
15	$P(8)$	2848.0	39	$R(15)$	2888.6
16	$P(7)$	2849.7	40	$R(16)$	2890.2
17	$P(6)$	2851.5	41	$R(17)$	2891.6
18	$P(5)$	2853.4	42	$R(18)$	2893.1
19	$P(4)$	2855.3	43	$R(19)$	2894.6
20	$P(3)$	2857.2	44	$R(20)$	2895.9
21	$P(2)$	2859.1	45	$R(21)$	2897.3
22	$P(1)$	2860.9	46	$R(22)$	2898.7
23	Q	2861.9	47	$R(23)$	2900.1
24	$R(0)$	2863.0	48	$R(24)$	2901.7
			49	$R(25)$	2903.3

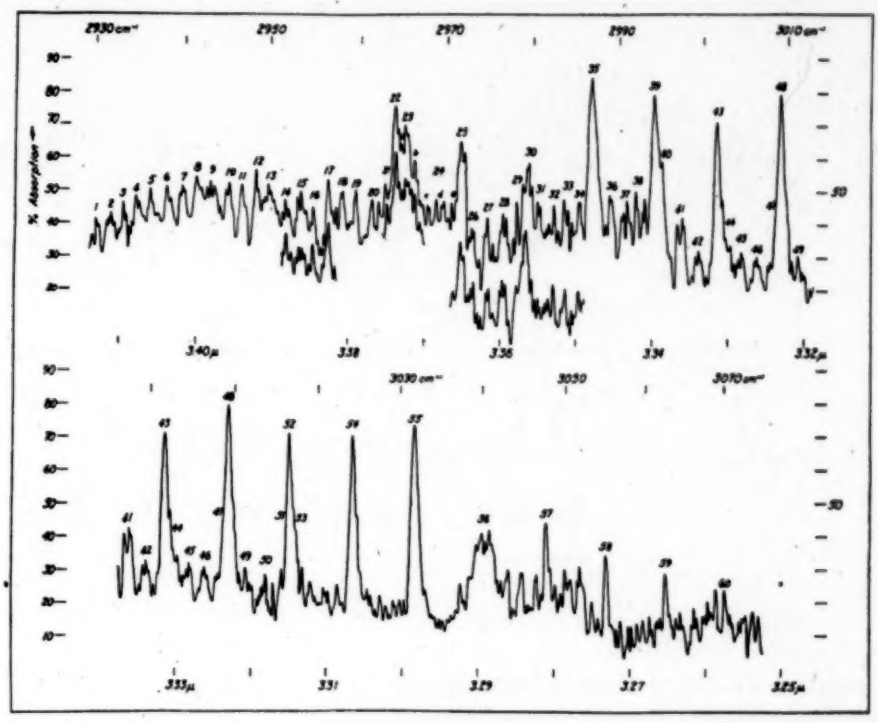

FIG. 2. The 3.35μ and 3.37μ bands of CH_3F.

P_2O_5. In spite of this, some falsification of the absorption pattern due to methyl fluoride is apparent in Fig. 3 where a composite picture of the data is given. The reason for the falsification is discussed in a footnote by Cameron, Sears, and Nielsen[3] and need not be repeated here, This region consists of two almost coincident bands, one of the parallel type and another of the perpendicular type and in Table III the frequencies of many of the most intense maxima are given.

TABLE II. Frequency positions and identifications of lines in the 3.4μ bands.

Line No.	Identification	Frequency	Line No.	Identification	Frequency
1	$P(22)$	2929.8	26		2972.8
2	$P(21)$	2931.6	27		2974.5
3	$P(20)$	2933.1	28		2976.5
4	$P(19)$	2934.7	29		2978.4
5	$P(18)$	2936.3	30	$^pQ(4)$	2979.3
6	$P(17)$	2938.0	31		2980.3
7	$P(16)$	2939.7	32		2982.0
8	$P(15)$	2941.6	33		2983.7
9	$P(14)$	2943.2	34		2985.5
10	$P(13)$	2945.0	35-*a*	$^pQ(3)$	2986.7
11	$P(12)$	2946.5	35-*b*		2987.2
12	$P(11)$	2948.2	36		2989.0
13	$P(10)$	2949.6	37		2990.8
14	$P(9)$	2951.3	38		2992.5
15	$P(8)$	2953.0	39-*a*	$^pQ(2)$	2994.0
16	$P(7)$	2954.5	39-*b*		2994.3
17	$P(6)^pQ(7)$	2956.1	40		2995.8
18	$P(5)$	2957.8	41		2997.5
19	$P(4)$	2959.3	42		2999.4
20	$P(3)$	2961.1	43	$^pQ(1)$	3001.6
21	$P(2)$	2962.7	48	$^RQ(0)$	3009.1
22	$^pQ(6)$	2963.9	52	$^RQ(1)$	3016.5
a	$P(1)$	2964.4	54	$^RQ(2)$	3024.1
b	Q	2965.2	55	$^RQ(3)$	3031.6
c		2967.7	56	$^RQ(4)$	3039.4
d		2969.3	57	$^RQ(5)$	3044.6
e		2971.0	58	$^RQ(6)$	3055.0
25	$^pQ(5)$	2971.5	59	$^RQ(7)$	3062.4
			60	$^RQ(8)$	3069.8

C. The 8.0μ Region

This band was quite well resolved in the earlier work of Bennett and Meyer and it was not deemed necessary to remeasure this band in the present investigation.

D. The 9.5μ Region

The 9.5μ band is a parallel type band and was partially resolved by Bennett and Meyer.[1] Their data on this band gave indications that the structure of the band was not simple as indicated by the simple theory. On re-examination this effect is confirmed, although much greater detail than that observed by Bennett and Meyer was

[3] D. C. Cameron, W. C. Sears, and H. H. Nielsen, J. Chem, Phys. **7**, 994 (1939).

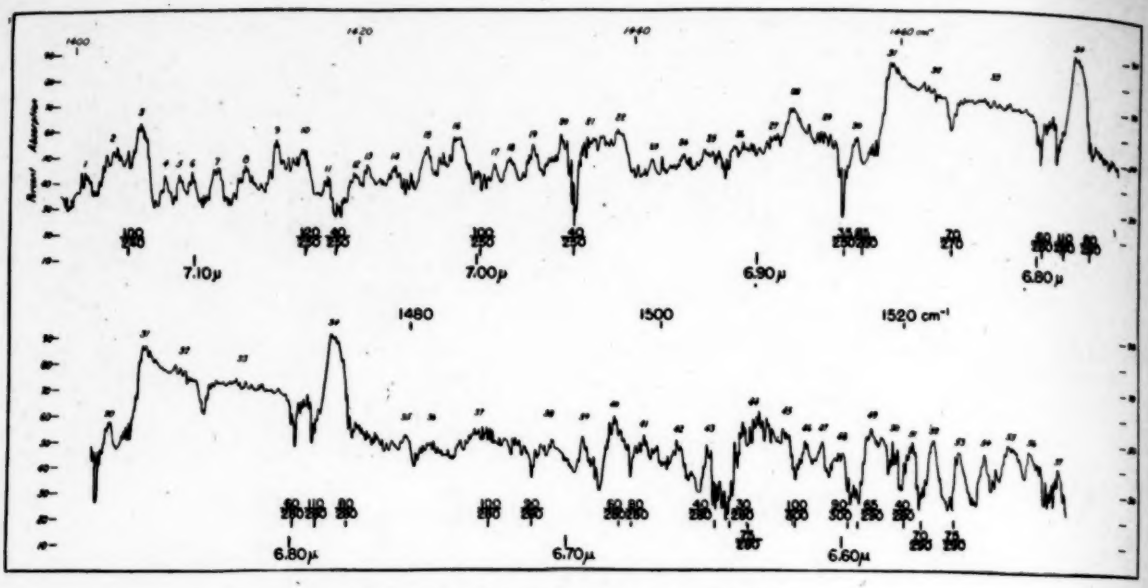

FIG. 3. The 7.0μ absorption region of CH_3F.

recorded. In Fig. 4 is shown a composite curve of the data taken in several runs across this band where circle settings have been replaced by a scale of frequencies. In Table IV are given the frequency positions of the lines in the band, where by a line is meant the most intense of a group of closely lying line components. Certain of the details in the structure lie just on the threshold of the practical resolving power of the instrument and are difficult to distinguish from the background. Much of the detail, however, can be repeated from time to time.

IV. DISCUSSION OF THE RESULTS

The lines in a vibration-rotation band arise from quantum transitions between two vibration-rotation levels. The energy of a vibration-rotation level for a symmetric polyatomic molecule is given to a good approximation by the relation:

$$(E/hc)=(E_v/hc)+J(J+1)B_v-K^2(B_v-C_v)$$
$$\mp 2\sum_t \zeta_t \nu_t K c_v - J^2(J+1)^2 D_J$$
$$-J(J+1)K^2 D_{JK}-K^4 D_K. \quad (1)$$

In Eq. (1), (E_v/hc) is the vibration energy; ζ_t is the Coriolis coupling factor which is different from zero only for the twofold degenerate frequencies and depends in an involved manner upon the normal coordinates; and

$$B_v=B_e-\sum_s \alpha_s(v_s+g_s/2)$$

where

$$B_e=(h/8\pi^2 c I_{zz}^{(e)}); \quad C_v=C_e-\sum_s \gamma_s(v_s+g_s/2)$$

TABLE III. Frequency positions of the principal absorption lines at 6.8μ.

Line No.	Frequency	Line No.	Frequency
1	1402.3 cm^{-1}	30	1458.2 cm^{-1}
2	1404.4	31	1461.0
3	1406.2	32	1464.0
4	1407.9	33	1468.8
5	1408.9	34	1477.1
6	1409.8	35	1481.4
7	1411.5	36	1483.4
8	1413.5	37	1487.5
9	1415.7	38	1493.0
10	1417.6	39	1495.5
11	1419.4	40	1498.2
12	1421.3	41	1500.5
13	1422.3	42	1503.2
14	1424.2	43	1505.7
15	1426.4	44	1509.6
16	1428.7	45	1512.0
17	1431.5	46	1513.8
18	1432.5	47	1515.1
19	1434.2	48	1516.5
20	1436.3	49	1519.6
21	1438.5	50	1521.0
22	1440.5	51	1521.6
23	1443.1	52	1524.4
24	1445.4	53	1526.6
25	1447.0	54	1528.7
26	1449.6	55	1531.0
27	1452.1	56	1532.6
28	1453.4	57	1535.1
29	1456.0		

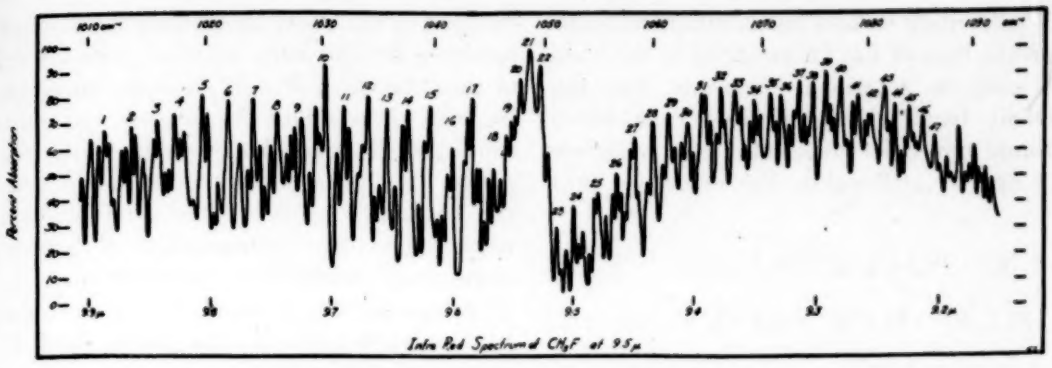

FIG. 4. Infra-red spectrum of CH_3F at 9.5μ.

and

$$c_v = C_e - \sum_t \Gamma_t(v_t+1)$$

where[4]

$$C_e = (h/8\pi^2 c I_{zz}^{(e)});$$

D_J, D_{JK}, and D_K are centrifugal distortion constants. α_s, γ_s, and Γ_t in the above are correction terms to the reciprocals of inertia arising out of the non-rigidity of the rotator, and g_s is a constant which is equal to 1 or 2 depending upon whether the oscillation is non-degenerate or twofold degenerate. l_t is a quantum number which has values only for the twofold degenerate frequencies ω_t. For a quantum number v_t where ω_s is twofold degenerate, l_t may take the values $v_t, v_t-2, \cdots 1$ or 0.

There occur two types of bands in the spectra of molecules like CH_3F, namely the parallel type and the perpendicular type. The first of these arises from an electric moment induced parallel to the axis of symmetry and occurs when the selection rules $\Delta J = \pm 1, 0$; $\Delta K = 0$ prevails. The second type arises from an electric moment induced normal to the axis of symmetry, and occurs when the selection rule $\Delta J = \pm 1, 0$; $\Delta K = \pm 1$ prevails. The perpendicular bands are twofold degenerate.

TABLE IV. Frequency positions and identification of lines in the 9.5μ parallel band.

Line No.	Identification	Frequency	Line No.	Identification	Frequency
1	$P(20)$	1010.4	25	$R(2)$	1054.2
2	$P(19)$	1012.7	26	$R(3)$	1056.1
3	$P(18)$	1014.9	27	$R(4)$	1057.7
4	$P(17)$	1017.0	28	$R(5)$	1059.3
5	$P(16)$	1019.1	29	$R(6)$	1060.7
6	$P(15)$	1021.1	30	$R(7)$	1062.5
7	$P(14)$	1023.1	31	$R(8)$	1064.0
8	$P(13)$	1025.3	32	$R(9)$	1065.6
9	$P(12)$	1027.5	33	$R(10)$	1067.2
10	$P(11)$	1029.3	34	$R(11)$	1068.8
11	$P(10)$	1031.1	35	$R(12)$	1070.3
12	$P(9)$	1033.1	36	$R(13)$	1071.5
13	$P(8)$	1034.9	37	$R(14)$	1072.8
14	$P(7)$	1036.8	38	$R(15)$	1074.3
15	$P(6)$	1038.6	39	$R(16)$	1075.6
16	$P(5)$	1040.5	40	$R(17)$	1077.1
17	$P(4)$	1042.3	41	$R(18)$	1078.4
18	$P(3)$	1044.2	42	$R(19)$	1079.7
19	$P(2)$	1046.1	43	$R(20)$	1081.3
20			44	$R(21)$	1082.1
21	$P(1)$	1047.6	45	$R(22)$	1083.4
22	Q	1048.9	46	$R(23)$	1084.8
23	$R(0)$	1050.5	47	$R(24)$	1086.1
24	$R(1)$	1052.4			

[4] H. H. Nielsen, Phys. Rev. **70**, 184 (1946).

A. The Parallel Type Band

When the selection rules $\Delta J = \pm 1, 0$; $\Delta K = 0$; $\Delta l = 0$ are applied to two sets of energy states of the form (1) a series of overlapping bands, one component band for each value of K, is obtained.[5] The band center of these component bands is in each case the same. The $P(J)$ and $R(J-1)$ lines for a component band, the number in the parenthesis being the value of J in the normal state, will be found to be the following:

$$\left.\begin{matrix} P(J) \\ R(J-1) \end{matrix}\right\} = \nu_0 \mp J(B'+B'') + J^2(B'-B'') + K^2[C'-C''+B''-B'], \quad (2)$$

B'', B' and C'', C' being, respectively, the B_v and C_v values in the normal and final states. In the case of the diatomic molecule where K takes some single value, say $K=0$, it has been

[5] See for example G. Herzberg, *Infrared and Raman Spectra of Polyatomic Molecules* (D. Van Nostrand Company, Inc., New York, 1945), p. 418.

fruitful to employ certain combination relations between the lines of Eq. (2) to arrive at the band centers and the rotational constants. For any component band of the parallel type for a polyatomic molecule the combination relations are, of course, still valid. For these we may write

$$R(J-1, K)-P(J+1, K)=4(J+\tfrac{1}{2})B'', \quad (3a)$$

$$R(J, K)-P(J, K)=4(J+\tfrac{1}{2})B', \quad (3b)$$

$$R(J-1, K)+P(J, K) = 2[\nu_0+J^2(B'-B'')]. \quad (3c)$$

The resolution is in general not sufficient to separate completely a parallel band into its component bands and hence the above relations cannot be applied directly. Some progress may be made, nevertheless, if one takes as the Jth line in the P and R branches the most intense of the Jth lines in the P and R branches of the K component bands. Neglecting symmetry considerations this will be associated with the value $K=0$. One may now again use the combination principles.

The entire parallel band at 9.6μ and at least the central portion of the parallel band at 3.5μ do not overlap with other bands. In these two instances it has been possible to identify the $P(J)$ and $R(J)$ lines on both sides of the center to a considerable distance. The parallel band at 3.4μ overlaps badly on the high frequency side, but it is possible to identify a considerable number of the $P(J)$ lines. The identifications of the lines are set down in the second columns of the tables.

When the combination principle (3a) is applied to the lines in Tables I and IV, i.e., when the differences $R(J-1)-P(J+1)$ are plotted against $4(J+\frac{1}{2})$ for the two bands, it is seen that the points in both cases lie along the same straight line. This indicates that the initial state from which the molecule makes its transition is in each case the same. Since the 9.6μ band is unquestionably a fundamental band B'' is the B_γ value for the normal state. The value of B'' as read from the graph shown in Fig. 5 is $B''=0.8688$ cm^{-1}.

If now the combination principle (3c) is applied and the sum $R(J-1)+P(J)$ is plotted against J^2 for each of the above two bands, the slope of the resulting straight lines will give twice the values of the differences $B'-B''$, and the intercept will be twice the value of the frequency of the band center, ν_0, B' being the Bv values in the excited states. The values of ν_0 obtained for the 9.6μ and the 3.5μ bands are 1049.5 cm^{-1} and 2862.9 cm^{-1}, respectively. The corresponding B' values are, respectively, 0.8606 cm^{-1} and 0.8635 cm^{-1}. The B' values derived in this manner may be verified by the application to the above data of the combination rule (3b).

In the 3.4μ band the $R(J)$ lines cannot be identified with any certainty although the $P(J)$ lines are quite clearly discernible. The combination rules (3), therefore, cannot be used. If, however, one takes the differences between the two P lines $P(J)-P(J-1)$ one obtains

$$P(J)-P(J-1) = -(B'+B'')+(2J-1)(B'-B''). \quad (4)$$

When the differences $P(J)-P(J-1)$ for the above band are plotted against $2J$ as ordinates the slope of the resulting straight line gives the difference $(B'-B'')$ and the intercept will be $-(B'+B'')$. The value obtained for B'' in this manner agrees well with the value B'' obtained for the two other parallel bands referred to before. This indicates that this band is caused by a vibrational transition originating in the normal vibration state. The value of B' determined in this manner is found to be $B'=0.872$ cm^{-1}.

To arrive at a value for the frequency of the band center the sum $P(J)+P(J-1)$ is taken. It gives

$$P(J)+P(J-1)-2J^2(B'-B'') = 2[\nu_0-(2J-1)B']. \quad (5)$$

If the left-hand side of Eq. (5) is plotted against $2(2J-1)$ the slope will give an independent value for B', and $2\nu_0$ may be arrived at by reading the intercept from the graph. The value of ν_0 is found to be 2966.5 cm^{-1}.

The information derived from these three bands is summarized in Table V.

In the 7.0μ region there is found still another parallel type band. The Q branch of this band coincides almost exactly with the center of the perpendicular band which is found here. The

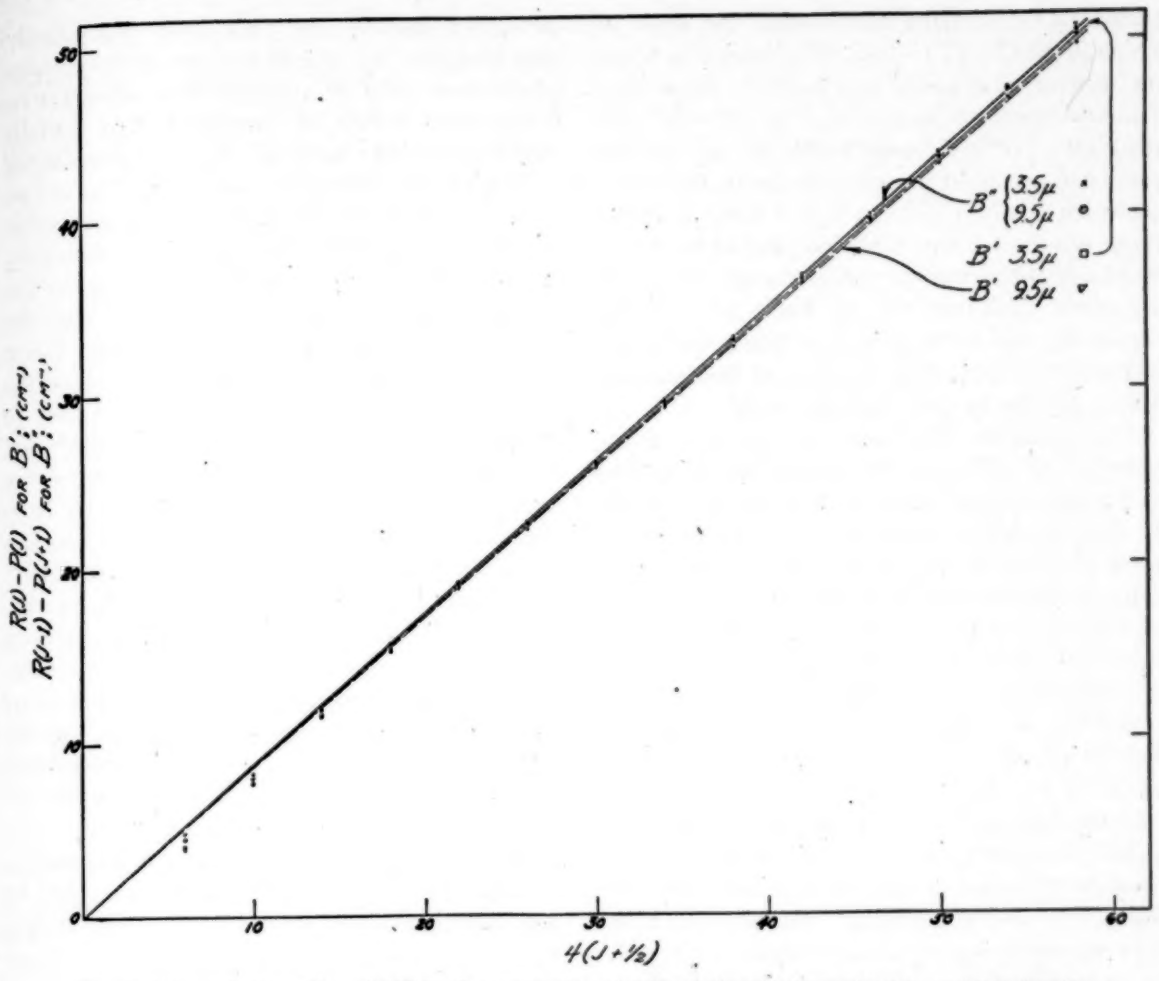

FIG. 5. Infra-red absorption of CH_3F. Determination of B'' and the B''s from the 3.5μ and 9.5μ bands.

discussion of the 7.0μ parallel band is deferred for Section V which concerns itself with this region quite in general.

B. The Perpendicular Bands

When the selection rules $\Delta J=\pm 1, 0$; $\Delta K=\pm 1$, $\Delta l=\pm 1$ are applied to two sets of energy levels like those described in (1), one of which is the normal state, a series of overlapping component bands, each of which has the general appearance of a parallel type band, is obtained.[6] If it were possible to resolve such a band completely, a set of combination relations of the form (3) could be applied to the lines in each of the component bands. This is not possible, at least in the case of molecules like CH_3F. The prominent lines present in perpendicular bands like those observed here are Q lines. Those on the high frequency side are known as ${}^RQ$ branches and those on the low frequency side as ${}^PQ$ branches. With the aid of the selection rule $\Delta K=\Delta l=\pm 1$ one obtains as the frequency positions of these

$$\left.\begin{matrix}{}^RQ_K\\ {}^PQ_K\end{matrix}\right\}=\nu_0+[C'-2c'\zeta_t-B'] \pm 2[C'-c'\zeta_t-B']K+[(C'-C'')-(B'-B'')]K^2+J(J+1)(B'-B''). \quad (6)$$

The effect of the last term in Eq. (6) is to cause the Q branches to spread out and it may be neglected at this point. If, as suggested by Herzberg,[5] the sum of ${}^RQ_K+{}^PQ_K$ is plotted

[6] D. M. Dennison, Rev. Mod. Phys. 3, 280 (1931).

against K^2 a straight line results, the slope of which is $2[(C'-C'')-(B'-B'')]$ and which has the intercept $2[\nu_0+C'-2c'\zeta_t-B']$. Moreover, if the quantities ${}^RQ_K-[(C'-C'')-(B'-B'')]K^2$ and ${}^PQ_K-[(C'-C'')-(B'-B'')]K^2$ are plotted against K, straight lines are obtained, the slopes of which are $2[C'-c'\zeta_t-B']$. Figure 6 shows these graphs for the 3.36μ perpendicular band. Values of the constants obtained from the above are given in Table VI. In Table VI are also stated the constants arrived at when the above procedure is applied to the data of Bennett and Meyer for the 8μ perpendicular band.

It is possible to obtain an estimate of the value of $B'-B''$ from the breadth of the Q lines in a perpendicular band when it is well resolved. It was suggested earlier that the effect of the term $J(J+1)(B-B'')$ in Eq. (6) is to split the Q branches into component lines. These components cannot be resolved spectroscopically, but produce the effect of broadening the Q branches. By measuring the breadth of these lines, and observing that the components have begun to fall off rapidly in intensity by the time J has assumed the value $J=20$, a value for $B'-B''$ may be obtained by setting the average line equal to 20×21 $(B'-B'')$. This value, which must be regarded as not very accurate, takes the value $(B'-B'')=0.003$ cm^{-1} for the 3.33μ band. The algebraic sign to be attached to $(B'-B'')$ is determined by observing whether the Q branches taper off toward lower frequencies or toward higher frequencies. If the Q branches taper off toward lower frequencies $B'<B''$; if they taper off in the opposite direction $B'>B''$. It appears that $B'-B''$ is positive for the 3.33μ perpendicular band. No estimate of the value $B'-B''$ for the 8μ perpendicular band was attempted.

C. The 6.8μ Parallel-Perpendicular Band

Two bands, almost exactly coincident, occupy the 6.8μ region of the spectrum. Both bands are extremely intense and they have accordingly been identified by several authors as the parallel vibration ν_3, and the perpendicular vibration ν_4. It has been shown by Shaffer[7] that a Coriolis interaction exists between the two frequencies ν_3 and ν_4, the effect manifesting itself as a correction term to the moment of inertia effective for these frequencies. This correction term contains the resonance denominator $\omega_3-\omega_4$. In the case which here is considered $\omega_3\approx\omega_4$ so that the correction term becomes indefinitely large. When this condition prevails the usual methods of the perturbation theory fail, and it is necessary to compute the interaction in the manner discussed by Nielsen[8] where the frequencies ν_3 and ν_4 are regarded as degenerate. As may be seen from that discussion the computation of the energies is no simple matter. Certain generalities may, nevertheless, be stated. Because of the perturbation there results a mixing of the wave functions which characterize these states. For this reason, it is better to designate the two states by $(\nu_3:\nu_4)$ and $(\nu_4:\nu_3)$, respectively, where the frequency which occurs first within the parentheses is the frequency to which the state would degenerate if the resonance were removed.

Normally the selection rules for a perpendicular vibration are $\Delta J=\pm1,0$ and $\Delta K=\pm1$, and for a parallel band they are $\Delta J=\pm1$, 0 and $\Delta K=0$. Because of the resonance both types of transitions may take place in each band, i.e., the band which normally would be perpendicular will have some parallel type transitions and *vice versa*. It may be seen in Fig. 3 that many of the Q lines of the band appear double; for example lines 2 and 3; 9 and 10, etc. It is suggested that the high frequency component in each case is caused by the transitions $\Delta K=\pm1$, $\Delta J=0$ in the band $(\nu_4:\nu_3)$, while the low frequency components are caused by the transition $\Delta K=\pm1$; $\Delta J=0$ in the

TABLE V. Rotational constants and frequencies obtained from parallel bands.

Band center in μ	Band center in cm^{-1}	Value of B''	Value of B'
3.4	2966.5 cm^{-1}	0.869	0.872
3.5	2862.9	0.8688	0.8635
9.6	1049.5	0.8688	0.8606

TABLE VI. Rotational constants and frequencies obtained from perpendicular bands.

Band center in μ	$[\nu_0+C'-2c'\zeta_t-B']$ cm^{-1}	$[C'-c'\zeta_t-B']$ cm^{-1}	$[(C'-C'')-(B'-B'')]$ cm^{-1}	$(B'-B'')$ cm^{-1}
3.36μ	3009.08	3.81	0.023	0.003
8.0μ	1200.03	2.85	0.011	—

[7] W. H. Shaffer, J. Chem. Phys. 10, 1 (1942).
[8] H. H. Nielsen, Phys. Rev. 68, 181 (1945).

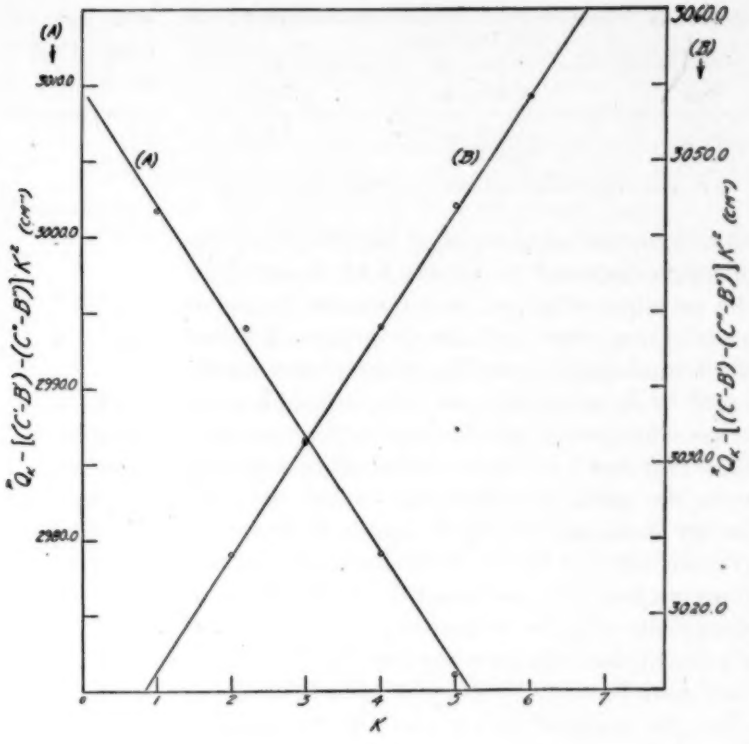

FIG. 6. Infra-red absorption of CH_3F. Determination of $(C'-\zeta C-B')$ 3.35μ ($\perp$) band.

band ($\nu_3:\nu_4$). The separations between the components will be seen to be roughly $\Delta\nu=2.0$ cm^{-1}. It does not seem practicable to attempt to analyze the lines in this absorption region further than this owing to the extreme complexity of the pattern. An estimate may nevertheless be made of the band centers. We take the following as the values for ($\nu_3:\nu_4$) and ($\nu_4:\nu_3$), respectively, 1467.9 cm^{-1} and 1469.7 cm^{-1}. The separation between ($\nu_3:\nu_4$) and ($\nu_4:\nu_3$) is not inconsistent with the value $\Delta\nu=2.0$ cm^{-1} between the components of the Q lines.

It appears, moreover, that the effect of the perturbations upon the energy levels, and consequently on the spectrum as well, decreases with increasing values of K. An estimate of the value $[C'-\zeta'\zeta_t-B']$ may be made by noting the spacing between K lines near the extremity of the band. Our estimate for $[C'-\zeta'\zeta_t-B']$ is 5.6 cm^{-1}. We restate these results in Table VII.

V. IDENTIFICATION OF THE OBSERVED BANDS

The information gained from the preceding paragraphs indicates that a review of the identification of the bands in the spectrum of CH_3F might be desirable. We follow other authors and identify the bands at 9.6μ and 8μ (i.e., 1049.5 cm^{-1} and 1200 cm^{-1}) as ν_5 and ν_6, respectively. The two bands in the 7.0μ region we identify as ($\nu_3:\nu_4$) and ($\nu_4:\nu_3$) as has been suggested in the preceding section.

In the 3.5μ region there are found three bands of the parallel type with centers near 2818 cm^{-1}, 2862.9 cm^{-1}, and 2966.5 cm^{-1}. These we identify in the following manner $(\nu_1:2\nu_3:2\nu_4)=2862.9$ cm^{-1}, $(2\nu_3:2\nu_4:\nu_1)=2966.5$, and $(2\nu_4:2\nu_3:\nu_1)=2818$ cm^{-1}, where $(\nu_1:2\nu_3:2\nu_4)$ etc. indicates that the levels ν_1, $2\nu_3$, and $2\nu_4$ are three mutually resonating levels. The level $(\nu_1:2\nu_3:2\nu_4)$ is the one which would degenerate to ν_1, the level $(2\nu_3:2\nu_4:\nu_1)$ would reduce to $2\nu_3$, etc., if the perturbation between the levels were reduced to zero. The identification of the last three frequencies must be regarded as somewhat uncertain, but seems plausible and consistent with the conclusions arrived at by others.

The resonance which occurs here is of a rather complicated nature. The energy matrix for the CH_3F molecule contains elements along the principal diagonal which are of the form of the

TABLE VII. Vibration rotation constants estimated from the 7.0μ band.

Band	Band center	$[C'-C'\zeta_4-B']$
$(\nu_3:\nu_4)$	1467.9 cm^{-1}	5.6 cm^{-1}
$(\nu_4:\nu_3)$	1469.7 cm^{-1}	—

vibration-rotation energies of the XY_3Z type of molecule discussed by Shaffer.[9] All elements off the principal diagonal are of second or higher order of magnitude and may be neglected. When the frequencies $2\nu_3$ and $2\nu_4$ become very nearly equal to ν_1, as is the case here, a complication arises since the energies contain the denominators $(\omega_1-2\omega_3)$ and $(\omega_1-2\omega_4)$.[9] These terms originate with the cubic contributions to the potential energy $hck_{133}q_1q_3^2$ and $hck_{144}q_1q_4^2$. It has been pointed out by Fermi and Dennison[10] that it becomes necessary to regard the frequency ω_1 as degenerate with the frequencies $2\omega_3$ and $2\omega_4$. The result obtained has been discussed by Dennison[11] and more recently by Nielsen[8] who have shown that the diagonal terms are still the same as before except that the terms containing the denominators $2\omega_3-\omega_1$, etc., are absent. In addition, the terms $hck_{133}q_1q_3^2$, etc., now give rise to elements lying off the principal diagonal which are of first-order importance. These elements are the following:

$$\begin{aligned}&(v_1-1, v_3+2, v_4, l_4\cdots|v_1, v_3, v_4, l_4\cdots)\\&\quad=(v_1, v_3, v_4, l_4\cdots|v_1-1, v_3+2, v_4, l_4\cdots)\\&\quad=(hck_{133}/2)[v_1/2]^{\frac{1}{2}}[(v_3+1)(v_3+2)]^{\frac{1}{2}},\\&(v_1-1, v_3, v_4+2, l_4\cdots|v_1, v_3, v_4, l_4\cdots)\\&\quad=(v_1, v_3, v_4, l_4\cdots|v_1-1, v_3, v_4+2, l_4\cdots)\\&\quad=(-hck_{144}/2)[v_1/2]^{\frac{1}{2}}[(v_4+2)^2-l_4^2]^{\frac{1}{2}}.\end{aligned}\quad(7)$$

Moreover, when the frequencies $2\omega_3$ and $2\omega_4$ become very nearly equal to each other, as they do in the CH_3F molecule, a type of resonance described by Darling and Dennison[12] in connection with the water vapor spectrum may occur because of the terms $hck_{3344}q_3^2\rho_4^2$ in the quadratic part of the potential energy function and certain other terms in the cubic portion of the potential energy. In such cases it is necessary to treat $2\omega_3$ and $2\omega_4$ as degenerate frequencies with the result that certain new elements which do not lie on the principal diagonal will arise. In this case these may be shown to be:

$$\begin{aligned}&(v_3, v_4\cdots|v_3-2, v_4+2, \cdots)\\&\quad=(v_3-2, v_4+2, \cdots|v_3, v_4\cdots)\\&\quad=hc\{(k_{3344}/4)-(k_{344}^2/2\omega_4)\\&\quad+(k_{333}k_{344}/4\omega_3)\\&\quad-(k_{441}k_{133}/8\omega_1)[\omega_1/(2\omega_4+\omega_1)]\\&\quad+(k_{445}k_{533}/4\omega_5)[\omega_5^2/(4\omega_4^2-\omega_5^2)]\}\\&\quad\times\{[v_3(v_3-1)]^{\frac{1}{2}}[(v_4+2)^2-l_4^2]^{\frac{1}{2}}\}.\end{aligned}\quad(8)$$

The matrix elements described above will be grouped together about the principal diagonal in a little box. This sub-matrix can then be diagonalized by itself. For the case where $(v_1=1, v_3=v_4=0)$, $(v_1=0, v_3=2, v_4=0)$ and $(v_1=0, v_3=0, v_4=2, l_4=0)$ the sub-matrix takes the form

	$v_1=1$, $v_3=v_4=0$	$v_1=v_4=0$, $v_3=2$	$v_1=v_3=0$, $v_4=2$, $l_4=0$
$v_1=1$, $v_3=v_4=0$	$W-\epsilon$	$(hck_{133}/2)$	$(-hck_{144}/\sqrt{2})$
$v_1=v_4=0$, $v_3=2$	$(hck_{133}/2)$	$W'-\epsilon$	$(hc\gamma/\sqrt{2})$
$v_1=v_3=0$, $v_4=2$, $l_4=0$	$(-hck_{144}/\sqrt{2})$	$(hc\gamma/\sqrt{2})$	$W''-\epsilon$

(9)

where W, W', and W'' are the diagonal elements of the matrix corresponding, respectively, to $(v_1=1, v_3=v_4=0)$, etc., and γ is the value of the term inside the first set of braces in Eq. (8). The energy values determined from (9) will be seen to be given by the roots of the cubic equation:

$$\begin{aligned}&\epsilon^3-(W+W+W'')\epsilon^2\\&\quad+(WW'+W'W''+W''W\\&\quad-(h^2c^2/2)(k_{144}+k_{133}/2)\\&\quad-[WW'W''-h^3c^3k_{133}k_{144}\gamma-2h^2c^2\gamma^2]=0.\end{aligned}\quad(10)$$

The effect of the latter perturbation, if the first kind were absent, would be to separate the levels $(2\nu_3:2\nu_4)$ and $(2\nu_4:2\nu_3)$ abnormally away from each other, while the level ν_1 would remain unaltered. The presence of the elements in the energy sub-matrix corresponding to the former type of interaction would further alter the positions of the levels, but it does nevertheless seem reasonable to assume that the bands at 2818 cm^{-1} and 2966.5 cm^{-1} are caused by transi-

[9] In this discussion ω_i is taken to be the value of the normal frequency and ν_i is the value of the band center.
[10] E. Fermi, Zeits. f. Physik. 71, 250 (1931).
[11] D. M. Dennison, Rev. Mod. Phys. 12, 175 (1940).
[12] B. T. Darling and D. M. Dennison, Phys. Rev. 57, 129 (1940).

TABLE VIII. Identification of the observed bands in the CH_3F spectrum.

Band center in cm^{-1}	Identification	Character
1049.5	ν_5	parallel
1200.0	ν_6	perpendicular
1467.9	$(\nu_3:\nu_4)$	parallel-perpendicular
1469.7	$(\nu_4:\nu_3)$	perpendicular-parallel
2818.0	$(2\nu_4:2\nu_3:\nu_1)$	parallel
2862.9	$(\nu_1:2\nu_3:2\nu_4)$	parallel
2966.5	$(2\nu_3:2\nu_4:\nu_1)$	parallel
3009.1	ν_2	perpendicular

tions to the levels $(2\nu_4:2\nu_3:\nu_1)$ and $(2\nu_3:2\nu_4:\nu_1)$, respectively, hence fixing the band at 2862.9 cm^{-1} as $(\nu_1:2\nu_4:2\nu_3)$. The band at 2818 cm^{-1} is assigned as $(2\nu_4:2\nu_3:\nu_1)$ because it has the lesser intensity of the two. A further argument for identifying the band at 2862.9 cm^{-1} as $(\nu_1:2\nu_3:2\nu_4)$ is the following. There exists a Coriolis interaction between the frequency ν_1 and ν_2 as has been shown by Shaffer.[7] The effect is to cause the Q branches in the higher frequency perpendicular band ν_2 to converge toward higher frequencies (i.e., the low frequency side is sharp), while the Q branch of the lower frequency band ν_1 will converge toward lower frequencies. The band 2862.9 cm^{-1} has this characteristic while the band at 2966.5 converges in the opposite sense. It should be pointed out that this last argument is not entirely rigorous since each of these three bands is a mixture of the frequencies ν_1, $2\nu_3$, and $2\nu_4$ but it seems reasonable to suppose the band $(\nu_1:2\nu_3:2\nu_4)$ to resemble ν_1 more than the other two, $(2\nu_3:2\nu_4:\nu_1)$ to resemble $2\nu_3$ most, etc. The identifications of the observed bands as we have proposed them are given in Table VIII.

Two Notes on Phase-Integral Methods

W. H. FURRY
Research Laboratory of Physics, Harvard University, Cambridge, Massachusetts*
(Received October 24, 1946)

I. The connection formulas are derived by a new method. The general approach is that of Zwaan's discussion of Stokes' phenomenon, but no use is made of any assumptions about the reality of the coefficients of the differential equation. Instead of this, the proof is based only on the fact that actual solutions of the differential equation must be single-valued. Both this manner of proof and the form in which the results are obtained are suited to the discussion of certain problems in which a boundary condition consists in the requirement that the field at a great distance contain an out-going wave only. The results serve to establish the validity of Eckersley's phase-integral method for the treatment of problems of wave propagation. **II.** General arguments used to establish phase-integral methods are asymptotic in nature, and lead to the expectation that the methods will be valid only in a certain limit; in the language of quantum mechanics this is the limit of large quantum numbers. Much of the methods' usefulness, however, comes from the fact that they give in practice surprisingly accurate results even for small quantum numbers. In the case of the energy levels of the anharmonic oscillator, special arguments have been devised by Kemble and by Birkhoff to establish the usual phase-integral formula without assuming large quantum numbers. In this note a special argument is given for calculating normalization factors for the approximate wave functions of the oscillator. It is shown that the usual asymptotic formula for the normalization factor holds for the lowest quantum states, with about the accuracy with which the phase-integral solution approximates the shape of the exact wave function at the point at which the potential energy function has its minimum.

I. A NEW DERIVATION OF THE CONNECTION FORMULAS

Introduction

THE phase-integral method for solving ordinary differential equations was first clearly formulated by Jeffreys,[1] and was applied to quantum-mechanical problems by Brillouin,[2] Wentzel,[3] and Kramers.[4] It is usually referred to among physicists as the B.W.K. method or the W.K.B. method.

The differential equation

$$d^2u/dz^2+k^2(y(z)+\lambda)u=0 \qquad (1)$$

is solved approximately, on the assumption that $k|\Delta z|$ is large if Δz is a distance in which $y(z)$ changes significantly. Any point z_0 for which

$$y(z_0)+\lambda=0 \qquad (2)$$

is called a turning point. In the neighborhood of such a point the coefficient $y(z)+\lambda$ changes significantly for arbitrarily small Δz, so that the approximate solutions to be obtained cannot be valid near such points. They must have the character of asymptotic solutions, providing good approximations to actual solutions in regions sufficiently far from all turning points. In the usual applications of the method it is assumed that the turning points are all simple zeros of $y+\lambda$, and that any two of them are so far apart that the asymptotic solutions provide good approximations to actual solutions throughout the greater part of the region between them. It is also assumed that the function $y(z)$ has no singularities in the finite region of the z plane.

The general approximate solution of Eq. (1) on these assumptions is

$$u\cong(y+\lambda)^{-\frac{1}{4}}\{Ae^{ikw}+Be^{-ikw}\}, \qquad (3)$$

where

$$w=\int_{z_0}^{z}(y+\lambda)^{\frac{1}{2}}dz. \qquad (4)$$

The derivation has been published a great many times. The two arbitrary constants in the solution are A and B; the constant lower limit of the integral in Eq. (4) is of course not an independent arbitrary constant, and has been chosen for convenience to be a turning point, z_0.

A given solution u can be approximated closely in a certain region of the z plane by choosing

* This paper is based in part on work done for the Office of Scientific Research and Development under contract OEMsr-262 with the Massachusetts Institute of Technology.

[1] H. Jeffreys, Proc. London Math. Soc. [2] **23**, 428 (1923).
[2] L. Brillouin, Comptes rendus **183**, 24 (1926).
[3] G. Wentzel, Zeits. f. Physik **38**, 518 (1926).
[4] H. A. Kramers, Zeits. f. Physik **39**, 828 (1926).

suitable values of the constants A and B. Since the differential equation (1) has no finite singularities, the solution $u(z)$ is a single-valued function;[5] on the other hand, the right-hand member of Eq. (3) is multiple-valued. Accordingly, it is not possible for the same choice of values of A and B to give a good approximation to a given solution u throughout the whole of the part of the plane, remote from turning points, where an approximation in the form of Eq. (3) is possible. Different values of A and B must be used in different regions in order to approximate the same solution u. This phenomenon, which is of general occurrence in the study of common types of asymptotic approximations,[6] was first noted and explained by Stokes.[7]

Connection formulas relating the different expressions of the type of Eq. (3) which approximate the same solution u were given by Jeffreys.[8] The use of such formulas in understanding clearly the approximate solution of quantum-mechanical problems was stressed by Kramers.[4] Kramers first obtained the formulas by approximating $y(z)$ by a linear function in the neighborhood of z_0, and studying the exact solutions of the resulting differential equation. A simpler derivation was given by Zwaan,[9] who used the basic idea by means of which Stokes had explained the phenomenon: In certain regions of the z plane one of the exponential factors in Eq. (3) is very large and the other is very small. Because the relation between the right-hand member of Eq. (3) and the actual solution u is only approximate, there is no meaning to the assignment of any particular value to the coefficient of the small exponential factor, for points in such a region. Thus this coefficient can have different values for two regions adjacent to such a "Stokes region" on opposite sides, but the other coefficient must keep the same value.

More elaborate discussions have been given by Langer[10] and by Kemble.[11] Langer's treatment is a generalization of that of Kramers; Kemble's is a critical discussion of Zwaan's method, with applications to certain further situations not covered by the usual connection formulas.[12]

The present treatment uses Stokes' fundamental idea in the same simple way as did Zwaan. In his treatment Zwaan assumed that the coefficient $k^2(y+\lambda)$ is real for real values of z. This assumption is unnecessarily restrictive, and is untrue in some cases of interest; for example, in problems of wave propagation it often happens that the imaginary part of λ is not small. The derivation given here involves no assumption about reality; instead we use the fact that the true solution $u(z)$ does not have a branch-point at z_0.

Derivation of the Formulas

The only assumption we shall make about the analytic function $y(z)$, is that $y(z)+\lambda$ has a simple zero at z_0, and that there are no singularities or other zeros near enough to z_0 to prevent our going out from this turning point in an arbitrary direction far enough to make the asymptotic expression (3) a good approximation.

Very near to z_0 we can represent $y(z)+\lambda$ by the first term of Taylor's expansion, and get

$$w=\int_{z_0}^{z}(y+\lambda)^{\frac{1}{2}}dz\cong(y'(z_0))^{\frac{1}{2}}\int_0^{z-z_0}\zeta^{\frac{1}{2}}d\zeta$$
$$=\tfrac{2}{3}(y'(z_0))^{\frac{1}{2}}(z-z_0)^{\frac{3}{2}}. \quad (5)$$

There are three directions, making angles of 120° with each other, along which we can move z away from z_0 in such a way that the expression (5) is purely real. Once we have started out in any one of these three directions we can choose

[5] The assumption that $y(z)$ is an integral function, made here for convenience, is unnecessarily restrictive. It suffices to assume that any singularities of $y(z)$ are well removed from z_0. The true solution u, unlike the functions in the right-hand member of Eq. (3), does not have z_0 as a branch point.

[6] For example, in many of the asymptotic formulas for Bessel functions: cf. G. N. Watson, *Treatise on the Theory of Bessel Functions* (The Macmillan Company, New York, 1922 and 1944), pp. 201–202, and further mention on pp. 203, 238, 336.

[7] G. G. Stokes, *Mathematical and Physical Papers* (Cambridge University Press, Cambridge), Vol. IV, pp. 77–109 and pp. 283–298; *ibid* Vol. V, pp. 221–225.

[8] Reference 1. There is a misprint in one of Jeffreys' formulas.

[9] A. Zwaan, Thesis, "Intensitäten im Ca-Funkenspektrum," Utrecht, 1929.

[10] R. E. Langer, Trans. Am. Math. Soc. **33**, 23 (1931); *ibid.* **34**, 447 (1932); Phys. Rev. **51**, 669 (1937).

[11] E. C. Kemble, Phys. Rev. **48**, 549 (1935); *Fundamental Principles of Quantum Mechanics* (McGraw-Hill Book Company, Inc., New York, 1937), pp. 90–112, 572–578.

[12] Kemble discusses the radial equation of the Kepler problem by his method, and also the low quantum states of the oscillator, as mentioned in the second of these notes.

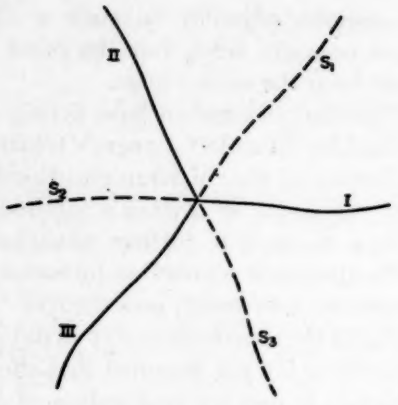

FIG. 1. Loci extending from a turning point.

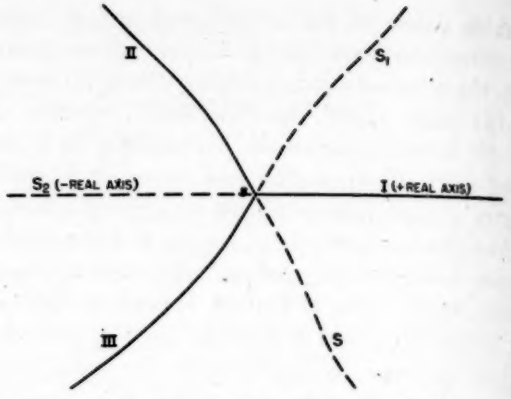

FIG. 2. Loci for case in which $y(z)$ is real for real z, and λ and z_0 are real.

each successive increment dz such that $(y+\lambda)^{\frac{1}{2}}dz$ is real, and thus define a locus, which in general is a curved line. We accordingly get three curves, shown as I, II, III in Fig. 1, such that

$$w(z)=\int_{z_0}^{z}(y+\lambda)^{\frac{1}{2}}dz \text{ is pure real on I, II, III.} \quad (6)$$

We define a branch of $(y+\lambda)^{\frac{1}{2}}$ by requiring this expression to be positive on I and then continuing counterclockwise from I. Then

$$w(z)=\int_{z_0}^{z}(y+\lambda)^{\frac{1}{2}}dz \text{ is } \begin{cases} +\text{on I,} \\ -\text{on II,} \\ +\text{on III,} \\ \text{and} -\text{on } \textit{return} \text{ to I.} \end{cases} \quad (7)$$

Along each of these three loci the two functions which appear in Eq. (3) are equal in magnitude, and if we are to take Eq. (3) as an approximate expression for u we must know both A and B. We set ourselves the problem of determining the coefficients A_{II} and B_{II} which must be used on II to approximate a function which is approximated on I by Eq. (3) with given coefficients A_I and B_I. Since the problem is linear and admits of superposition of solutions, there must be a relation in the form

$$\begin{aligned} A_{II}&=aA_I+bB_I \\ B_{II}&=cA_I+dB_I, \end{aligned} \quad (8)$$

with coefficients a, b, c, d independent of the A's and B's.

We can also construct three loci running out from z_0, on each of which $w(z)$ is purely imaginary. These are shown in Fig. 1 as S_1, S_2, S_3. With the choice of branch, and of direction of continuation used in writing (7) we then have

$$\begin{aligned} &w(z) \text{ is } + \text{ imaginary on } S_1\text{; far out on } S_1, && e^{-ikw}\gg e^{ikw}, \\ &w(z) \text{ is } - \text{ imaginary on } S_2\text{; far out on } S_2, && e^{ikw}\gg e^{-ikw}, \\ &w(z) \text{ is } + \text{ imaginary on } S_3\text{; far out on } S_3, && e^{-ikw}\gg e^{ikw}. \end{aligned} \quad (9)$$

These loci are commonly called "Stokes lines." On or near such a locus only one coefficient in (3) needs, in general, to be given in order to specify the expression which approximates a given function u asymptotically. This is, of course, the coefficient of the exponential which is large on the locus in question. The coefficient of the other exponential has no meaning on or near the locus, except in the special case where the coefficient of the large exponential vanishes. The Stokes phenomenon consists in the fact that if a coefficient becomes meaningless on a Stokes line, its value in the region on one side of the line can differ from that in the region on the other side.

Applying this conception of the Stokes phenomenon to the continuation from I to II across S_1, we see that B_{II} must equal B_I, but A_{II} need not equal A_I unless $B_I=0$. Thus (8) becomes

$$\begin{aligned} A_{II}&=A_I+\alpha B_I, \\ B_{II}&=B_I. \end{aligned} \quad (10)$$

All now that remains of our problem is to evaluate the constant α.

Similarly, we get for the continuation from II

to III across S_2:

$$A_{III}=A_{II},$$
$$B_{III}=\beta A_{II}+B_{II}; \tag{11}$$

and for the continuation from III back to I across S_3:

$$A_I'=A_{III}+\gamma B_{III},$$
$$B_I'=B_{III}. \tag{12}$$

Then from (10)–(12) we get

$$A_I'=(1+\gamma\beta)A_I+(\alpha+\gamma+\alpha\beta\gamma)B_I,$$
$$B_I'=\beta A_I+(1+\alpha\beta)B_I. \tag{13}$$

On the other hand we can obtain directly a relation between A_I' and B_I', the coefficients to be used in (3) after continuation through one revolution counterclockwise, and the original coefficients A_I and B_I. We simply use the fact that, since u is single valued, both expressions (3) must give the same value. Since, by Eq. (7), the two functions e^{ikw} and e^{-ikw} interchange values by this continuation, and since the factor $(y+\Lambda)^{-\frac{1}{4}}$ acquires a factor $e^{-\frac{1}{4}\cdot 2\pi i}=-i$, we must accordingly require

$$A_I'=iB_I; \quad B_I'=iA_I. \tag{14}$$

The necessary and sufficient condition for Eqs. (13) and (14) to be consistent is $\alpha=\beta=\gamma=i$. Then (10) becomes

$$A_{II}=A_I+iB_I; \quad B_{II}=B_I. \tag{15}$$

This is the fundamental connection formula, from which the various formulas required for specific applications can readily be obtained.

The traditional statement of the connection formulas is based on the assumptions that λ is real; that $y(z)$ is real for real z; and that the turning-point under consideration, z_0, is real. In this case the lines I and S_2 are straight and coincide with portions of the real axis. We write the connection from I to S_2 by using that from I to II and neglecting the term e^{-ikw} on S_2 unless A_{II} is zero. By using $A_I=e^{-i\pi/4}$, $B_I=e^{i\pi/4}$, we get from Eqs. (15) and (3)

$$|y+\lambda|^{-\frac{1}{4}}\exp\left(-k\int_z^{z_0}|y+\lambda|^{\frac{1}{2}}dz\right)\rightarrow 2(y+\lambda)^{-\frac{1}{4}}\cos\left\{k\int_{z_0}^{z}(y+\lambda)^{\frac{1}{2}}dz-\frac{\pi}{4}\right\}. \tag{16}$$

(on S_2) (on I)

Since we are interested only in values *on* the axis, we have used absolute values in the left member so as to express it in terms of real positive quantities only.

The meaning of Eq. (16) is that if a function u is approximated on S_2 by the left member, then it is approximated on I by the right member. The arrow points to the right only, because a small error in phase in fitting the right member to u would correspond to the appearance of the positive real exponential with a non-vanishing coefficient on the left, and this would completely ruin the agreement on S_2.

If we use $A_I=e^{i(\pi/4-\theta)}$, $B_I=e^{-i(\pi/4-\theta)}$, we get

$$\cos\theta\cdot|y+\lambda|^{-\frac{1}{4}}\exp\left(k\int_z^{z_0}|y+\lambda|^{\frac{1}{2}}dz\right)\leftarrow(y+\lambda)^{-\frac{1}{4}}\cos\left\{k\int_{z_0}^{z}(y+\lambda)^{\frac{1}{2}}dz+\frac{\pi}{4}-\theta\right\}. \tag{17}$$

(on S_2) (on I)

This result is reliable when $|\theta|$ is not too near $\pi/2$. Since any constant multiple of u is a solution as well as u, the value of θ cannot be found by examining u on S_2, so that the arrow must point to the left only. This rule is often written with $\theta=0$, which gives

$$|y+\lambda|^{-\frac{1}{4}}\exp\left(k\int_z^{z_0}|y+\lambda|^{\frac{1}{2}}dz\right)\leftarrow(y+\lambda)^{-\frac{1}{4}}\cos\left\{k\int_{z_0}^{z}(y+\lambda)^{\frac{1}{2}}dz+\frac{\pi}{4}\right\}. \tag{18}$$

(on S_2) (on I)

These formulas (16)–(18) are written in such a way that they can be applied to the situation shown in Fig. 2 if we simply take all quantities as positive unless the minus sign is written explicitly.

To get formulas which hold when I extends to the left and S_2 to the right, we have only to interchange the limits on the integrals so that dz will continue to point from left to right.

Equations (16) and (18) are usually called the first and second connection formulas. From the fundamental result (15) we can readily derive a formula of somewhat similar appearance, which is valid independently of any assumptions about the reality of λ, $y(z)$, or z_0. For $A_I=0$, $B_I=1$, Eqs. (15) and (3) give the result

$$2e^{i\pi/4}(y+\lambda)^{-\frac{1}{4}}\cos\left\{k\int_{z_0}^{z}(y+\lambda)^{\frac{1}{2}}dz+\frac{\pi}{4}\right\}\leftarrow(y+\lambda)^{-\frac{1}{4}}\exp\left\{-ik\int_{z_0}^{z}(y+\lambda)^{\frac{1}{2}}dz\right\}. \tag{19}$$

(on and near II) (on and near I)

In application of this formula it must be remembered that the choice of branch is as indicated in (7), so that the term kw in the argument of the cosine is almost or quite purely negative.

The meaning of (19) is that if a given function u is closely approximated by the right member on and near I, then it is closely approximated by the left member on and near II. The converse is not true: if we fit the asymptotic expression to approximate agreement with u on and near II, we cannot be sure that the phase is determined precisely, and a small error in phase would mean the presence of a term in e^{ikw} on and near I. Although such a term, with small coefficient, would not hurt the agreement on and above I, it would spoil the agreement completely below I, where e^{ikw} becomes large. Accordingly, we draw the arrow in (19) pointing from right to left only.

Since, as shown below, Eq. (19) has direct applications of some interest, it might be convenient to call it the third connection formula. This is not justified in the sense of mathematical independence, since the fundamental relation (15) contains just two equations. The conventional presentation of the two formulas, however, as shown in Eqs. (16) and (18), does not lend itself readily to the treatment of cases in which the reality conditions assumed in this presentation do not hold. Thus from the point of view of applications the formula of Eq. (19) is a useful addition to the two standard connection formulas.

An Application

Phase-integral methods have commonly been applied to three types of boundary-value problems, all with $y(z)$ real for real z:

(a) Outgoing waves only for $z\rightarrow+\infty$, no requirement for $z\rightarrow-\infty$. The problem is that of scattering in one dimension, and can be solved for any real value of λ for which $y+\lambda>0$ for $z\rightarrow+\infty$ and for $z\rightarrow-\infty$. The phase-integral method gives useful results only when $y+\lambda<0$ in some part (or parts) of the range $-\infty<z<\infty$; this is the problem of "penetration of a potential barrier."

(b) $u\rightarrow0$ for $z\rightarrow+\infty$, and either $u\rightarrow0$ for $z\rightarrow-\infty$ or else a condition of the form $u(0)+\mu u'(0)=0$, with real μ. The problem can be solved only for certain real characteristic values of λ. Examples are the problems of energy levels of the oscillator and of the radial equation of the central-field problem.

(c) Outgoing wave only for $z\rightarrow+\infty$, and a condition of the form $u(0)+\mu u'(0)=0$. The problem can be solved only for certain characteristic values of λ, and these are in general complex, even for real μ.

Applications of phase-integral methods to problems of types (a) and (b) are well known in the literature of quantum mechanics. We discuss here the applications to certain simple problems of type (c).

The case in which the curve of $-y(z)$, which plays the role of potential energy in quantum mechanics, has a maximum and then approaches zero for $z\rightarrow+\infty$, and $I(\lambda)\ll1$, has been discussed by Gamow[13] in his treatment of radio-active disintegration. The equation

$$y(z)+R(\lambda)=0 \tag{20}$$

has two real zeros, z_1 and z_2; the relations are shown graphically in Fig. 3. Since $\lambda\cong R(\lambda)$, the turning points are very close to z_1 and z_2. For

[13] G. Gamow, Zeits. f. Physik 51, 204 (1928); *Atomic Nuclei and Radioactivity* (Oxford University Press, New York, 1931 and 1937), first edition, pp. 38–50; pp. 87–101, second edition.

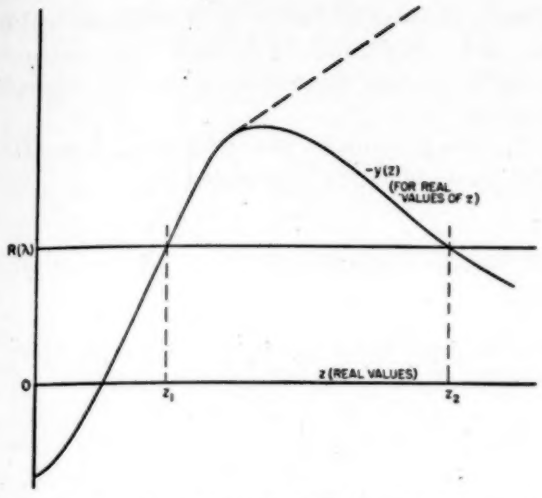

FIG. 3. Curve of $-y(z)$ plotted against real values of z.

the usual case, $\mu=0$, the phase-integral method requires that $R(\lambda)$ be calculated from the condition

$$k\int_0^{z_1}(y+R(\lambda))^{\frac{1}{2}}dz=(m-\tfrac{1}{4})\pi, \qquad (21)$$

where z_1 is the smaller root of Eq. (20) and m is an integer. $I(\lambda)$ is then given by

$$I(\lambda)=\left\{2k\int_0^{z_1}(y+R(\lambda))^{-\frac{1}{2}}dz\right\}^{-1} \cdot \times\exp\left\{-2k\int_{z_1}^{z_2}|y+R(\lambda)|^{\frac{1}{2}}dz\right\}. \qquad (22)$$

Approximate values can be obtained by these formulas for all integer values of m which are small enough so that the exponential factor in Eq. (22) is extremely small. These results can be derived by straightforward application of the boundary conditions and the connection formulas (16) and (18). Because of the fact that the arrows in Eqs. (16) and (18) point only one way, however, such a derivation can be made cogent only at the expense of a certain amount of complication. The more usual procedure is to establish Eq. (21) by considering the problem of type (b) obtained by replacing the outer part of the potential curve by something like the dashed curve in Fig. 3—this is approximately justified, since the "leakage through the barrier" is very small—and then establish Eq. (22) by using the approximate expressions for $u(z)$ in the formula

$$\int_0^z\frac{d}{dz}\left(u^*\frac{du}{dz}-u\frac{du^*}{dz}\right)dz=2ik^2I(\lambda)\int_0^z u^*u\,dz, \qquad (23)$$

which follows from Eq. (1).

The use of a phase-integral method for the solution of problems of type (c) in which $I(\lambda)$ is not small has been developed by Eckersley[14] in papers on the propagation of radio waves. According to Eckersley, the equation from which the complex characteristic values of λ are to be obtained is

$$k\int_0^{z_0}(y+\lambda)^{\frac{1}{2}}dz=(m-\tfrac{1}{4})\pi, \qquad (24)$$

for the case $u=0$. Here m is a positive integer, and z_0 is a function of λ, being a suitably chosen solution of Eq. (2).

This method has been applied successfully in a number of cases, but no readily understandable and convincing argument for its validity has been published; Eckersley's own approach appears to be based essentially on mere analogy with the phase-integral treatment of problems of type (b). The "third connection formula," Eq. (19), provides a means of deriving Eq. (24) directly from the stated boundary conditions. If the time-dependence is taken to be given by a factor $e^{i\omega t}$, the right-hand member of Eq. (19) represents the required outgoing wave. To make the left-hand member vanish for $z=0$, the argument of the cosine, being a negative number, must be set equal to $-(m-\frac{1}{2})\pi$, with m a positive integer. This gives at once Eq. (24).

It is clear that this application of the connection formula can be permissible only if z_0 lies in the lower half-plane. It falls in general in the fourth quadrant of the z plane. It is necessary also that z_0 be a well-isolated turning point. A safe rule for the applicability of Eckersley's method is probably that z_0 be far from all other turning points and also be the only turning point in the fourth quadrant. In the case of a function $-y(z)$, like that of Fig. 3, there is an infinite number of solutions obtainable by Eck-

[14] T. L. Eckersley, Proc. Roy. Soc. **A132**, 83 (1931); **A136**, 499 (1932); **A137**, 158 (1932); T. L. Eckersley and G. Millington, Phil. Trans. Roy. Soc. **A237**, 273 (1938).

ersley's method, with the turning-points well separated, and one lying well below the real axis and in the fourth quadrant; and there may be a finite number of solutions obtainable by Gamow's method, with two turning points, well separated, very near the positive part of the real axis. There may also be one or more solutions which are not obtainable by either phase-integral method, because the turning-points are not well separated.

For the generalized case with $\mu \neq 0$, Eqs. (21), (22), and (24) must be replaced by

$$k\int_0^{x_1}(y+R(\lambda))^{\frac{1}{2}}dz=(m-\tfrac{1}{4})\pi+\tan^{-1}\mu k(y(0)+R(\lambda))^{\frac{1}{2}}, \tag{21'}$$

$$I(\lambda)=\left\{2k\int_0^{x_1}(y+R(\lambda))^{-\frac{1}{2}}dz-2k\mu(y(0)+R(\lambda))^{-\frac{1}{2}}\right.$$

$$\left.\times[1+k^2\mu^2(y(0)+R(\lambda))]^{-1}\right\}^{-1}\exp\left\{-2k\int_{x_1}^{x_2}|y+R(\lambda)|^{\frac{1}{2}}dz\right\}, \tag{22'}$$

and

$$k\int_0^{x_0}(y+\lambda)^{\frac{1}{2}}dz=(m-\tfrac{1}{4})\pi+\tan^{-1}\mu k(y(0)+\lambda)^{\frac{1}{2}}. \tag{24'}$$

The derivations of Eqs. (21') and (24') are obvious; Eq. (22') can be derived by applying to Eq. (23) a modification of the technique illustrated in the following note.

For convenience this discussion has been based throughout on the idea that the time-dependence is given by a factor of the form $e^{i\omega t}$. This seems to be the preferred convention in studies of radio wave propagation. In quantum mechanics, however, the practically universal custom is to write $e^{-i\omega t}$ for the time factor. When this is done, $I(\lambda)$ is, of course, negative instead of positive.

II. NORMALIZATION OF APPROXIMATE WAVE FUNCTIONS OF THE ANHARMONIC OSCILLATOR

Introduction

The phase-integral methods for solving boundary-value problems are based on the approximate solution of differential equations of the type of Eq. (1) in terms of expressions such as that shown in Eq. (3). The solutions so obtained are asymptotic in character, and provide good approximations to actual solutions only in regions remote from turning points. This means that one can expect to obtain good answers for boundary-value problems when the turning points are well separated from each other and from any finite points at which boundary conditions are applied. The meaning of the words "well separated" is that the phase integral between two well separated points is a large number. Accordingly, phase-integral methods should work well in quantum mechanical problems when the quantum number is large, and in problems of classical mathematical physics when one considers high modes of vibration.

The really interesting cases, of course, are almost always those of small quantum numbers or low modes of vibration. The great usefulness of phase-integral methods comes mostly from the fact that in practice they usually give remarkably good results for these cases also. This circumstance suggests the possibility that arguments might be found to justify mathematically the use of the methods in cases of small quantum numbers or low modes of vibration. Such arguments could not be based solely on the general results of Eqs. (3) and (16)–(19), but would have to be of a more special nature.

For the case of the lower energy levels of the anharmonic oscillator two different special arguments for the approximate validity of the phase-integral formula for the energies have been given, one by Birkhoff[15] and the other by Kemble.[11] This case is, accordingly, well understood. In the present note a special argument is used to establish for low quantum numbers the formula for the normalization of the approximate wave functions of the oscillator.

[15] G. D. Birkhoff, Bull. Am. Math. Soc. **39**, 696 (1933).

Derivation of the Formula for the Normalization Constant

The potential-energy[16] function $-y(z)$ is assumed to have a single minimum and no maximum. For convenience we suppose the origin of the z-coordinate and the zero of the energy scale so chosen that

$$y' \gtrless 0, \quad z<0; \quad y'(0)=0; \quad y' \lesseqgtr 0, \quad z>0, \tag{25}$$

$$y(0)=0. \tag{26}$$

Equation (2) has two real roots, one positive and one negative; we denote the negative turning point by z_1, the positive one by z_2.

The characteristic values of λ are given approximately by the roots of the equation

$$k\int_{z_1}^{z_2}(y+\lambda)^{\frac{1}{2}}dz=(n+\tfrac{1}{2})\pi, \quad n=0,1,2,\cdots, \tag{27}$$

which expresses the condition of quantization in the older quantum theory. The arguments of Birkhoff and Kemble show that the approximation is good even for the smaller values of n. Approximate formulas for u are, for values of z not too near to z_1 or z_2:

$$u\cong(-)^n\cdot C|y+\lambda|^{-\frac{1}{4}} \times\exp\left\{-k\int_z^{z_1}|y+\lambda|^{\frac{1}{2}}dz\right\}, \quad z<z_1, \tag{28}$$

$$u\cong(-)^n\cdot 2C(y+\lambda)^{-\frac{1}{4}} \times\cos\left\{k\int_{z_1}^{z}(y+\lambda)^{\frac{1}{2}}dz-\frac{\pi}{4}\right\}, \quad z_1<z<z_2, \tag{29}$$

$$u\cong 2C(y+\lambda)^{-\frac{1}{4}} \times\cos\left\{k\int_{z}^{z_2}(y+\lambda)^{\frac{1}{2}}dz-\frac{\pi}{4}\right\}, \quad z_1<z<z_2, \tag{30}$$

$$u\cong C|y+\lambda|^{-\frac{1}{4}} \times\exp\left\{-k\int_{z_2}^{z}|y+\lambda|^{\frac{1}{2}}dz\right\}, \quad z>z_2. \tag{31}$$

Here all fractional powers are to have real positive values. The combinations (28)–(29) and (30)–(31) represent applications of the first connection formula, Eq. (16). The requirement that the alternative formulas (29) and (30) give the same values for u provides the usual derivation of Eq. (27).

The normalization constant C is to be chosen such that the values given by Eqs. (28)–(31) agree as well as possible with the values of the exact wave function u, which is normalized so that

$$\int_{-\infty}^{\infty}(u(z))^2dz=1. \tag{32}$$

The obvious way to do this is to consider the result of substituting the approximate formulas (28)–(31) into Eq. (32). Since these formulas fail completely near the turning points, such an argument can have meaning only when the contributions to the integral from the regions near the turning points form only a small part of the total. Thus the argument will be valid only for large n, and can be carried out with this in mind. Accordingly, the contributions from the exponential "tails" described by Eqs. (28) and (31) are neglected. Also, since the trigonometric function has numerous nodes, the square of the cosine can be replaced approximately by the mean value $\frac{1}{2}$. This is the usual way[17] of deriving the formula

$$2C^2\int_{z_1}^{z_2}(y+\lambda)^{-\frac{1}{2}}dz\cong 1. \tag{33}$$

The approximate value of C will now be obtained from Eq. (32) by a new method, which makes no use of the formulas (28)–(31) except in the neighborhood of the point $z=0$. Equations (29) and (30) are used to give approximate values of $u(0)$ and $u'(0)$. Taking account of Eqs. (25) and (26) we get from Eq. (29)

$$u(0)\cong(-)^n 2C\lambda^{-\frac{1}{4}}\cos\left\{k\int_{z_1}^{0}(y+\lambda)^{\frac{1}{2}}dz-\frac{\pi}{4}\right\}, \tag{34}$$

$$u'(0)\cong(-)^{n+1}2Ck\lambda^{\frac{1}{4}} \times\sin\left\{k\int_{z_1}^{0}(y+\lambda)^{\frac{1}{2}}dz-\frac{\pi}{4}\right\}; \tag{35}$$

[16] The notation of wave mechanics is obtained from that used here by replacing k^2 by $2m/\hbar^2$, $y(z)$ by $-V(z)$, and λ by E.

[17] Cf., e.g., W. Pauli, *Handbuch der Physik* (Verlagbuchhandlung, Julius Springer, Berlin, or Edwards Bros., Ann Arbor), Vol. 24/1, p. 173.

and from Eq. (30)

$$u(0)\cong 2C\lambda^{-\frac{1}{4}}\cos\left\{k\int_0^{z_2}(y+\lambda)^{\frac{1}{2}}dz-\frac{\pi}{4}\right\}, \quad (36)$$

$$u'(0)\cong 2Ck\lambda^{\frac{1}{4}}\sin\left\{k\int_0^{z_2}(y+\lambda)^{\frac{1}{2}}dz-\frac{\pi}{4}\right\}. \quad (37)$$

Since the phase-integral formulas are used only to give an approximation to the shape of the function u at the point $z=0$, which is ordinarily about as remote from z_1 and z_2 as any part of the classical range of vibration, the result will be established to a fair degree of approximation even for the small values of n.

We proceed with the derivation. The characteristic function $u(z;\lambda)$ satisfies the equation

$$(d^2/dz^2)u(z;\lambda)+k^2(y+\lambda)u(z;\lambda)=0, \quad (38)$$

where λ is a characteristic value, and vanishes at $\pm\infty$. Let $u_1(z;\lambda')$ be the solution of

$$(d^2/dz^2)u_1(z;\lambda')+k^2(y+\lambda')u_1(z;\lambda')=0 \quad (39)$$

which vanishes at $-\infty$ and reduces to $u(z;\lambda)$ for $\lambda'=\lambda$; when λ' is not a characteristic value $u_1(z;\lambda')$ does not vanish at $+\infty$. Similarly, let $u_2(z;\lambda')$ satisfy

$$(d^2/dz^2)u_2(z;\lambda')+k^2(y+\lambda')u_2(z;\lambda')=0, \quad (40)$$

vanish at $+\infty$, and reduce to $u(z;\lambda)$ for $\lambda'=\lambda$. Now multiply Eq. (38) by $u_1(z;\lambda')$ and Eq. (39) by $-u(z;\lambda)$ and add:

$$(d/dz)\{u_1(z;\lambda')u'(z;\lambda)-u_1'(z;\lambda')u(z;\lambda)\}+k^2(\lambda-\lambda')u_1(z;\lambda')u(z;\lambda)=0. \quad (41)$$

We now integrate from $-\infty$ to 0, and insert two terms whose sum is zero:

$$[u_1(0;\lambda')-u_1(0;\lambda)]u'(0;\lambda)-[u_1'(0;\lambda')-u_1'(0;\lambda)]u(0;\lambda)+k^2(\lambda-\lambda')\int_{-\infty}^0 u_1(z;\lambda')u(z;\lambda)dz=0. \quad (42)$$

In writing the added terms use was made of the fact that for $\lambda'=\lambda$, $u_1(z)$ reduces to $u(z)$. Keeping this same fact in mind, we see that on transposing Eq. (42), dividing by $\lambda'-\lambda$, and taking the limit $\lambda'\to\lambda$ we obtain

$$\int_{-\infty}^0[u(z;\lambda)]^2dz=k^{-2}\left\{u_1'\frac{\partial u_1}{\partial\lambda'}-u_1\frac{\partial u_1'}{\partial\lambda'}\right\}_{\substack{z=0\\ \lambda'=\lambda.}} \quad (43)$$

By applying a similar procedure to Eqs. (38) and (40), we find that

$$\int_0^\infty[u(z;\lambda)]^2dz=k^{-2}\left\{u_2\frac{\partial u_2'}{\partial\lambda'}-u_2'\frac{\partial u_2}{\partial\lambda'}\right\}_{\substack{z=0\\ \lambda'=\lambda.}} \quad (44)$$

All that remains to be done is to evaluate the right-hand members of Eqs. (43) and (44) by means of suitable phase-integral approximations, add, and equate to unity. Since $u_1(z;\lambda')$ vanishes at $-\infty$, it is represented by Eqs. (28) and (29), with λ replaced by λ', and for $z=0$ by Eqs. (34) and (35), with λ replaced by λ'. For u_2, on the other hand, Eqs. (36) and (37) must be used. The calculations give

$$\int_{-\infty}^0[u(z;\lambda)]^2dz\cong 2C^2\int_{z_1}^0(y+\lambda)^{-\frac{1}{2}}dz+(C^2/k\lambda)\sin 2\left\{k\int_{z_1}^0(y+\lambda)^{\frac{1}{2}}dz-\frac{\pi}{4}\right\}, \quad (45)$$

$$\int_0^\infty[u(z;\lambda)]^2dz\cong 2C^2\int_0^{z_2}(y+\lambda)^{-\frac{1}{2}}dz+(C^2/k\lambda)\sin 2\left\{k\int_0^{z_2}(y+\lambda)^{\frac{1}{2}}dz-\frac{\pi}{4}\right\}. \quad (46)$$

The last terms in these two equations come from applying the operator $\partial/\partial\lambda$ to the factors $\lambda^{\pm\frac{1}{4}}$ in Eqs. (34)–(37). By Eq. (27), these last terms are equal in magnitude and opposite in sign. Accordingly, Eqs. (32), (45), and (46) yield the result

$$2C^2\int_{z_1}^{z_2}(y+\lambda)^{-\frac{1}{2}}dz\cong 1. \quad (47)$$

This is identical in appearance with the usual formula, Eq. (33). From the manner of its derivation, however, it follows that (47) holds not merely asymptotically, but to the same degree of accuracy to which the phase-integral formulas approximate the shape of the function u in the neighborhood of the point $z=0$.

Comparison of Exact and Approximate Normalized Functions for the Harmonic Oscillator

A numerical comparison of exact and approximate normalized wave functions can most readily

be made in the case of the harmonic oscillator. If the formulas by which the approximate values are computed had, in the general anharmonic case, asymptotic validity only, good agreement for the lower quantum states of the harmonic oscillator would have to be regarded as in all probability fortuitous, and without much significance for anharmonic cases. Since, however, special arguments have now been found for the better-than-asymptotic validity of both the approximate formula for the characteristic values and that for the normalization factors, the results can claim to be roughly representative of the accuracy to be expected in more general cases. There are still, of course, special cases in which the accuracy could be much worse. One is that in which the point at which $y'(z)=0$ is much nearer one turning point than the other, and hence falls in a region in which the phase-integral approximation to u is very poor for the lower quantum states. Another is that in which the slope of the potential-energy curve is very large in the neighborhood of one or both turning points: the complete failure of phase-integral methods for rectangular potential curves is notorious. Apart from such abnormal cases, however, accuracy of the order of that found below for the harmonic case is to be expected.

For convenience in writing formulas we may suppose the units of length and of energy so chosen that for the harmonic oscillator we have

$$k=1, \quad y(z)=-z^2. \tag{48}$$

Both the exact and phase-integral solutions (cf. Eq. (27)) now give for the characteristic values

$$\lambda=2n+1, \quad n=0, 1, 2, \cdots. \tag{49}$$

The exact solutions are

$$u_n(z)=(2^n n!)^{-\frac{1}{2}}\pi^{-\frac{1}{4}}H_n(z)e^{-z^2/2}. \tag{50}$$

From the properties[18] of the Hermite polynomials we get

$$u_n(0)=\begin{cases}(-)^{n/2}(n!/2^n)^{\frac{1}{2}}[(n/2)!]^{-1}\pi^{-\frac{1}{4}}, \\ \qquad\qquad n \text{ even}, \\ 0, \ n \text{ odd};\end{cases} \tag{51}$$

$$u'_n(0)=\begin{cases}0, \ n \text{ even}, \\ (-)^{(n-1)/2}2(n!/2^n)^{\frac{1}{2}} \\ \quad \times[((n-1)/2)!]^{-1}\pi^{-\frac{1}{4}}, \ n \text{ odd};\end{cases} \tag{52}$$

$$u_n(z)=(2^n/n!)^{\frac{1}{2}}\pi^{-\frac{1}{4}}z^n e^{-z^2/2} \times\left\{1-\frac{n(n-1)}{4}z^{-2}+\cdots\right\}, \quad |z|\gg 1. \tag{53}$$

Here the expression in curly brackets is a polynomial.

For the normalization factor of the approximate solutions, Eqs. (47) and (48) give

$$C=(2\pi)^{-\frac{1}{2}}, \tag{54}$$

independent of n. From Eqs. (27), (34)–(37), (48), and (49) we then have

$$u_n(0)\cong u_{n \text{ approx}}(0) =\begin{cases}(-)^{n/2}(2/\pi)^{\frac{1}{2}}(2n+1)^{-\frac{1}{2}}, \ n \text{ even}, \\ 0, \ n \text{ odd};\end{cases} \tag{55}$$

$$u_n'(0)\cong u'_{n \text{ approx}}(0) =\begin{cases}0, \ n \text{ even}, \\ (-)^{(n-1)/2}(2/\pi)^{\frac{1}{2}}(2n+1)^{\frac{1}{2}}, \ n \text{ odd}.\end{cases} \tag{56}$$

From Eqs. (31), (48), (49) we have

$$u_n(z)\cong u_{n \text{ approx}}(z)=(2\pi)^{-\frac{1}{2}} \times(z^2-2n-1)^{-\frac{1}{4}}e^{-W}, \ z>z_1=(2n+1)^{\frac{1}{2}}, \tag{57}$$

where

$$W=\int_{(2n+1)^{\frac{1}{2}}}^{z}(z^2-2n-1)^{\frac{1}{2}}dz. \tag{58}$$

With the notations

$$y=(2n+1)^{-\frac{1}{2}}z=\cosh\xi, \tag{59}$$

we can write

$$\begin{aligned}W&=(n+\tfrac{1}{2})\{y(y^2-1)^{\frac{1}{2}}-\log(y+(y^2-1)^{\frac{1}{2}})\} \\ &=(n+\tfrac{1}{2})\{y(y^2-1)^{\frac{1}{2}}-\cosh^{-1}y\},\end{aligned} \tag{60}$$

or

$$W=\tfrac{1}{4}(2n+1)(\sinh 2\xi-2\xi). \tag{61}$$

By means of expansions in descending powers of z, we can obtain from Eqs. (57)–(60) the result

$$u_{n \text{ approx}}(z)=(2\pi)^{-\frac{1}{2}}[4e/(2n+1)]^{n/2+\frac{1}{4}}z^n e^{-z^2/2} \cdot\left\{1-\frac{(2n+1)(2n-3)}{16}z^{-2}+\cdots\right\}, \quad z>(2n+1)^{\frac{1}{2}}. \tag{62}$$

[18] Courant-Hilbert, *Mathematische Physik* (Verlagsbuchhandlung, Julius Springer, Berlin, or Interscience Publishers, New York), second edition, Vol. I, pp. 78, 79.

The expression in brackets is a power series which converges for $z>(2n+1)^{\frac{1}{2}}$; the convergence is rapid only for $z>2n+1$.

The comparison of exact and approximate values of $u(0)$ and $u'(0)$, as computed from Eqs. (51), (52), (55), and (56) is shown in Table I. The agreement is seen to be surprisingly good even for the smallest values of n, and improves quickly as n increases. The ratios

$$\frac{u_{n\ \mathrm{approx}}(0)}{u_n(0)}=\left(\frac{2}{\pi}\right)^{\frac{1}{2}}\left\{\frac{2\cdot2\cdot4\cdot4\cdots(n-2)\cdot(n-2)\cdot n\cdot n}{1\cdot3\cdot5\cdot5\cdots(n-3)\cdot(n-1)\cdot(n-1)(n+\frac{1}{2})}\right\}^{\frac{1}{2}}\ (n\ \text{even}) \tag{63}$$

and

$$\frac{u'_{n\ \mathrm{approx}}(0)}{u'_n(0)}=\left(\frac{2}{\pi}\right)^{\frac{1}{2}}\left\{\frac{2\cdot2\cdot4\cdot4\cdots(n-1)(n-1)(n+\frac{1}{2})}{1\cdot3\cdot3\cdot5\cdots(n-2)\cdot n\cdot n}\right\}^{\frac{1}{2}}\ (n\ \text{odd}) \tag{64}$$

both converge to unity in virtue of Wallis' infinite product formula,

$$\frac{\pi}{2}=\frac{2}{1}\cdot\frac{2}{3}\cdot\frac{4}{3}\cdot\frac{4}{5}\cdot\frac{6}{5}\cdot\frac{6}{7}\cdots. \tag{65}$$

The convergence is much more rapid than that of Wallis' product, not only because of the fourth root, but especially because the modifications of final factors in Eqs. (63) and (64) are such as to remove the errors of order $1/n$ and leave only those of order $1/n^2$.

For sufficiently large values of z we can compare the exact and approximate solutions by considering the factors outside the curly brackets in Eqs. (53) and (62). This comparison is shown in Table II. Here again the agreement is surprisingly good and improves rapidly with increasing n. The ratio

$$\lim_{z\to\infty}\left(\frac{u_{n\ \mathrm{approx}}(z)}{u_n(z)}\right)=(n!)^{\frac{1}{2}}\{(2\pi)^{\frac{1}{2}}[(n+\tfrac{1}{2})/e]^{n+\frac{1}{2}}\}^{-1} \tag{66}$$

approaches unity as $n\to\infty$, by Stirling's formula.

TABLE I. Comparison of values of $u_n(0)$ and $u_{n\ \mathrm{approx}}(0)$ and their derivatives.

n	$u_n(0)$	$u_{n\ \mathrm{approx}}(0)$	$\frac{u_{\mathrm{approx}}}{u}$	$u'_n(0)$	$u'_{n\ \mathrm{approx}}(0)$	$\frac{u'_{\mathrm{approx}}}{u'}$
0	0.7511	0.7979	1.0623	0	0	—
1	0	0	—	1.0622	1.0501	0.9885
2	0.5311	0.5336	1.0046	0	0	—
3	0	0	—	1.3010	1.2978	0.9976
4	0.4600	0.4607	1.0015	0	0	—

The values of z for which the comparison shown in Table II applies are very large, since the higher terms of the series in curly brackets can be neglected only for $z\gg n^2$. A comparison for smaller values of z is best made by purely numerical calculation from Eqs. (50) and (57). It is interesting to make the comparison at fixed values of the integral W. Equation (61) is easily solved numerically for ξ, once n and W are given, and z is then given by Eq. (59). Values of z for various values of W are given in Table III,[19] and the values of u and u_{approx} are shown in Table IV. The percentage difference between u_{approx} and u is tabulated in Table V.

Inspection of Table V shows that the accuracy of the approximation improves with increasing n only for large values of W. For smaller values of W the amount of error depends principally on the value of W, not that of n. The approximate formulas for u are asymptotic formulas which give the shape of u, as distinct from normalization, for large W. It is interesting, however, to

TABLE II. Comparison of $u_n(z)$ and $u_{n\ \mathrm{approx}}(z)$ for very large values of z.

n	$u_n(z)/(z^n e^{-z^2/2})$	$u_{n\ \mathrm{approx}}(z)/(z^n e^{-z^2/2})$	$\frac{u_{\mathrm{approx}}}{u}$
0	0.7511	0.7244	0.9645
1	1.0622	1.0479	0.9866
2	1.0622	1.0535	0.9918
3	0.8673	0.8622	0.9941
4	0.6133	0.6103	0.9952

[19] Values given are rounded off to three decimal places. In calculating u to the accuracy desired, more accurate values of z are required, particularly for large values of W.

TABLE III. Values of z for various values of W.

n \ W	1	1.5	2	2.5	3	4	6	8	10	15
0	1.957	2.229	2.464	2.676	2.869	3.217	3.811	4.318	4.770	5.738
1	2.560	2.804	3.018	3.212	3.390	3.712	4.269	4.749	5.179	6.110
2	3.005	3.235	3.437	3.621	3.790	4.098	4.632	5.095	5.511	6.415
3	3.379	3.599	3.792	3.968	4.132	4.429	4.946	5.396	5.801	6.686
4	3.705	3.918	4.106	4.276	4.435	4.724	5.228	5.668	6.065	6.932

TABLE IV. Values of u and u_{approx} for various values of W.

n \ W	1		1.5		2		2.5		3	
	u	u_{approx}	u	u_{approx}	u	u_{approx}	u	u_{approx}	u	u_{approx}
0	0.1106	0.1132	0.0627	0.0631	0.0361	0.0360	0.02094	0.02079	0.01225	0.01211
1	0.1026	0.1068	0.0585	0.0599	0.0337	0.0343	0.01965	0.01992	0.01152	0.01164
2	0.0991	0.1043	0.0564	0.0582	0.0327	0.0334	0.01905	0.01940	0.01120	0.01135
3	0.0964	0.1012	0.0550	0.0570	0.0319	0.0328	0.01867	0.01904	0.01096	0.01115
4	0.0949	0.0995	0.0542	0.0561	0.0314	0.0323	0.01837	0.01876	0.01080	0.01099

n \ W	4		6		8		10		15	
	u	u_{approx}	u	u_{approx}	u	u_{approx}	u	u_{approx}	u	u_{approx}
0	0.00426	0.00418	0.0^3528	0.0^3516	0.0^4670	0.0^4653	0.0^5862	0.0^5839	0.0^7531	0.0^7513
1	0.00401	0.00403	0.0^3501	0.0^3501	0.0^4639	0.0^4636	0.0^5824	0.0^5820	0.0^7508	0.0^7504
2	0.00391	0.00394	0.0^3489	0.0^3491	0.0^4625	0.0^4626	0.0^5807	0.0^5807	0.0^7499	0.0^7498
3	0.00383	0.00389	0.0^3481	0.0^3484	0.0^4615	0.0^4617	0.0^5796	0.0^5797	0.0^7493	0.0^7493
4	0.00377	0.00382	0.0^3475	0.0^3478	0.0^4608	0.0^4610	0.0^5787	0.0^5789	0.0^7488	0.0^7488

TABLE V. Percent error, $100(u_{approx}-u)/u$.

n \ W	1	1.5	2	2.5	3	4	6	8	10	15	∞
0	2.4	0.7	−0.1	−0.7	−1.1	−1.8	−2.3	−2.57	−2.74	−3.33	−3.55
1	4.1	2.4	1.8	1.5	1.0	0.4	−0.1	−0.36	−0.55	−0.79	−1.34
2	5.2	3.2	2.3	1.8	1.3	0.9	0.5	0.14	−0.05	−0.28	−0.82
3	5.0	3.6	2.6	2.0	1.7	1.1	0.7	0.37	0.19	−0.04	−0.59
4	4.8	3.5	2.6	2.1	1.8	1.5	0.6	0.46	0.29	0.00	−0.48

note that even for $W=1$ the errors are only a few percent. This illustrates another aspect of the remarkable accuracy of phase-integral methods, namely that they give the shape of the function fairly well, even rather near a turning point. This is a fact of experience, and no clear-cut special argument seems to be available to justify it. In some applications, of course, such as the derivation of Eqs. (21) and (22) by Gamow's method, the calculation depends on the assumption that W is large in other ways besides the approximation of the function u. Very accurate approximation of values of u in the neighborhood of a turning point can be obtained by a modification of the phase-integral treatment given by Langer.[20]

As remarked earlier, the sort of accuracy found here for the case of the harmonic oscillator is also to be expected in more general cases, provided certain exceptional circumstances—extreme asymmetry of the potential curve and/or extreme steepness of potential gradient—are not encountered.

[20] See reference 10. Numerical application of Langer's method is most readily accomplished by means of tables of Airy integrals. Tables for real argument are being published by the British Association Mathematical Tables project. For complex argument, use may be made of *Tables of Modified Hankel Functions and their Derivatives* (Harvard University Press, Cambridge, 1945).

Letters to the Editor

PUBLICATION of brief reports of important discoveries in physics may be secured by addressing them to this department. The closing date for this department is, for the issue of the 1st of the month, the 8th of the preceding month and for the issue of the 15th, the 23rd of the preceding month. No proof will be sent to the authors. The Board of Editors does not hold itself responsible for the opinions expressed by the correspondents. Communications should not exceed 600 words in length.

L-Converted Isomeric Transition*

M. GOLDHABER,** C. O. MUEHLHAUSE, AND S. H. TURKEL
The Argonne National Laboratory, University of Chicago, Chicago, Illinois
February 17, 1947

PRELIMINARY to an investigation of the activation of Ir by resonance neutrons, it seemed of interest to study the radiations associated with the 1.5 min. Ir activity produced by slow neutron capture[1] in Ir. These radiations had been previously believed to be β-rays, and on that basis an atomic activation cross section for thermal neutrons of 2×10^{-24} cm² was ascribed to this activity by Seren, Freidlander, and Turkel.[2] By studying the absorption in Be and Al of the radiations detected with a mica window Geiger counter we found, however, that they were largely x-rays of the L region of Ir. The main L emission lines of $_{77}$Ir and its neighbors, $_{76}$Os and $_{78}$Pt, are shown in Fig. 1, together with the K absorption edges of the elements from Fe–Se. There are three possible ways to account for such L radiation: (1) L electron capture in Ir leading to Os (L radiation of Os). (2) Internally converted isomeric transition in Ir (L radiation of Ir). (3) β-emission from Ir followed by a strongly internally converted γ-ray (L radiation of Pt). Number 3 could be excluded because no β-rays of an energy sufficiently high to be compatible with the short half-life of 1.5 min. could be found. To distinguish experimentally between the theoretically unlikely case number 1, and number 2, critical absorption measurements were made on the x-rays. Because of the wide spread in wave-length of the L radiations, it was important to isolate some of the L components for this work. This was accomplished by using a Zn filter (23.5 mg/cm²) which practically completely removes all but the L III$-M$ V and L III$-M$ IV components of Ir and Os. These components were then shown to be more strongly absorbed in Cu than in Zn, indicating Ir L x-rays arising from the removal of an L III electron. The radiation filtered by 28.2 mg Cu/cm² was shown to be about equally well absorbed by further layers of Cu, Ni, or Fe, which excludes Os L x-rays.

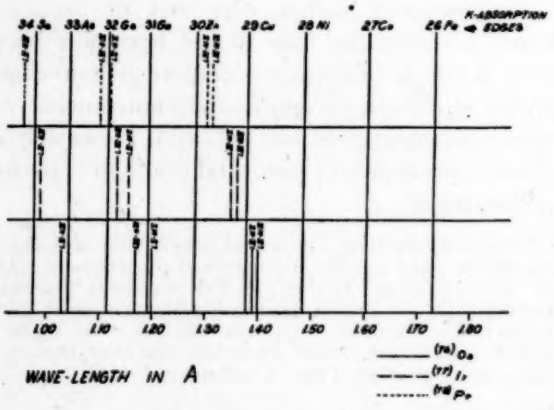

FIG. 1. The L emission lines of Os, Ir, Pt and the K absorption edges of the elements from Fe to Se.

In a few percent of the isomeric transitions unconverted γ-rays are emitted. Absorption in Pb and other elements shows that these are not homogeneous. An approximate energy of 60 Kev was obtained for the highest energy γ-rays present. Internal conversion electrons were detected with an ionization chamber, having a window equivalent to 1.5 mg Al/cm² in stopping power, and their energy compared with those from Co^{60} (10.7 min.).[3] In this manner a value of ~47 Kev was found for the internal conversion electrons of Ir. When the value of the Ir L work function is added, one obtains ~60 Kev as the energy of the isomeric transition, in agreement with the result deduced from Pb absorption for the hardest γ-rays. If we identify the excitation energy of the metastable state with this value it is definitely lower than the work function for a K-electron of Ir (76 Kev). The softer photons found have about one-half of the energy of the hard component. They are possibly due to "two-quantum" transitions.[4]

The atomic activation cross section of Ir (1.5 min.) for thermal neutrons can be estimated to be of the order of 100×10^{-24} cm². Unpublished experiments carried out at the Argonne Laboratory and at the University of Illinois make it probable that the 1.5 min. Ir activity is associated with a metastable state of Ir^{192} (70 d).

* This report is based on work performed under Contract No. W-7401-eng-37 for the Manhattan Project at the Argonne National Laboratory.
** University of Illinois.
[1] E. McMillan, M. Kamen, and S. Ruben, Phys. Rev. **52**, 375 (1937).
[2] L. Seren, H. N. Freidlander, and S. H. Turkel, Bull. Am. Phys. Soc. **22**, 6 (1947).
[3] M. Deutsch and L. G. Elliott, Phys. Rev. **62**, 588 (1942).
[4] See M. Goeppert-Maier, Ann. d. Physik **9**, 273 (1931); R. G. Sachs, Phys. Rev. **57**, 194 (1940).

Magnetic Moment of the Triton

H. L. ANDERSON* AND A. NOVICK
Argonne National Laboratory, Chicago, Illinois
February 15, 1947

WE have measured the ratio of the nuclear g values of the triton and the proton by the method of nuclear induction.[1] Our experimental arrangement was a modification of those which have been used by Bloch, Hansen, and Packard,[1b,d] and by Purcell, Torrey, and Pound.[1a] We were able to observe the nuclear induction peaks of both the triton and the proton simultaneously on the same cathode-ray oscillograph screen while both these substances were in the same magnetic field.

The magnetic field was provided by an electromagnet with 5-inch diameter pole pieces and with a 1-inch gap. The radiofrequency (r-f) fields for the two samples were produced inside of two equal coils about ½ inch in diameter and about ½ inch long. These were symmetrically disposed about the center of the magnetic field and spaced 1 inch apart. The axes of the coils were at right angles to the direction of the magnetic field. The r-f current for the coils was produced by two generators, one crystal controlled (Set *A*), while with the other it was possible to vary the frequency continuously (Set *B*). In each case the coil was in one arm of a "twin *T*" network which was inserted between the generator and a high frequency receiver (National RHO). The network could be adjusted so that no signal would be transmitted to the receiver from the generator. However, a modulated r-f signal of the same frequency developed in the coil would be detected by the receiver and presented as an audio signal on a cathode-ray oscilloscope screen.

To present the nuclear induction peaks on the cathode-ray screen, a small 60-cycle component was superimposed on the main magnetic field by means of a 60-cycle alternating current flowing through an auxiliary winding on the poles of the magnet. In this way, the magnetic field would give the magnetic moments inside the coil a Larmor precession frequency which varied through the frequency of the generator twice each cycle.

To observe the proton peaks, a drop of ordinary distilled water contained in a Pyrex tube was inserted in one of the coils. Following Bloch, Hansen, and Packard,[1] a small amount of $Fe(NO_3)_3$ was added to the water to speed the establishment of thermal equilibrium. Two peaks per cycle were observed when the frequency of the generator was near 23 megacycles and the magnetic field near 5400 gauss, corresponding to each coincidence of the Larmor with the applied frequency.

With a drop of water made from some tritium gas which was available in this laboratory, and conditioned in the same way, we observed identical peaks at the same frequency and field due to the ordinary hydrogen which was present in this water. In addition, however, we observed the same pattern at a *lower* value of the magnetic field, while keeping the frequency of the generator fixed. These second peaks were not present in the ordinary water sample and we, therefore, identified them with the magnetic moment of the triton.

For a precise determination of the ratio of the nuclear *g* values of the triton and the proton, the tritium water was put in one coil while the ordinary water was put in the other. The audio outputs of the two receivers were connected to the same oscilloscope through an electronic switch so that the patterns due to both samples could be observed simultaneously. The frequencies of the two generators were then adjusted so that the peaks due to the triton moments in the one sample coincided with those due to the proton moments in the other. The frequencies of the two generators were measured using a Signal Corps BC-221 AE frequency meter. With the samples interchanged, the ratio of the triton frequency to the proton frequency differed by 0.05 percent, this being the difference in the value of the magnetic field at the positions of the two samples. The geometric mean of these two frequency ratios gives directly the ratio of the nuclear *g* values and cancels any error due to differences in the value of the magnetic field at the two samples. Measurements made at three values of the crystal frequency of Set *A*, 23.0947, 25.4902, and 22.8301 megacycles, gave the same result within 0.01 percent. Our result gives for the ratio of the nuclear *g* value of the triton to that of the proton, 1.06666 ± 0.00010.

The fact that the nuclear *g* value of the triton is larger than that of the proton disagrees with the estimate of Sachs and Schwinger[2] based on the wave function obtained by Gerjuoy and Schwinger.[3] In fact, it shows that the admixture of $^4D_1$ wave functions to the ground state of the triton is not sufficient to account for its magnetic moment.

This work was done under the auspices of the Manhattan District at the Argonne National Laboratory.

* Member of the Institute for Nuclear Studies, University of Chicago.

[1] (a) E. M. Purcell, H. C. Torrey, and R. V. Pound, Phys. Rev. **69**, 37 (1946). (b) F. Bloch, W. W. Hansen, and M. Packard, Phys. Rev. **69**, 127 (1946). (c) F. Bloch, Phys. Rev. **70**, 460 (1946). (d) F. Bloch, W. W. Hansen, and M. Packard, Phys. Rev. **70**, 474 (1946).

[2] R. G. Sachs and J. Schwinger, Phys. Rev. **70**, 41 (1946).

[3] E. Gerjuoy and J. Schwinger, Phys. Rev. **61**, 138 (1942).

Spin and Magnetic Moment of Tritium*

F. Bloch, A. C. Graves, M. Packard, and R. W. Spence
Stanford University, California, and the Los Alamos Scientific Laboratory, Santa Fe, New Mexico

February 17, 1947

NUCLEAR induction[1] has been applied to a small sample containing a 0.3 molar solution of $MnSO_4$ in H_2O, and clearly distinguishable signals have been obtained from both hydrogen isotopes, H_1 (proton), and H_3 (triton) present in the sample. A density determination indicated that about 80 percent of the hydrogen was present in the form of H_3, and about 20 percent in the form of H_1.

A first series of observations was performed by keeping the frequency constant at $\nu = 41.5$ megacycles, and merely varying the magnetic field B_0. The signal originating from H_3 appeared at a field $B_0 = 9160$ gauss, and, except for being about three times larger, had an identical sign and shape as the signal originating from H_1, which appeared at a field $B_0 = 9770$ gauss. It leads to the following conclusions:

(a) The gyromagnetic ratio γ_T of H_3 is about 7 percent larger than γ_P, the gyromagnetic ratio for H_1, as indicated by the ratio of the respective resonance fields B_0.

(b) Within the observational error of about 30 percent, the magnitude of the signals agrees in their ratio with the ratio of the respective amounts of the two isotopes. This shows that the spin of H_3 is the same as that of H_1, which is known to be ½. A spin of ⅜ or more for H_3 would have resulted in a fivefold[2] larger signal relative to that of H_1 than was observed and could therefore be definitely excluded.

(c) With the signals which originate under identical radio frequency conditions from the two isotopes having the same sign, the relative orientation of their magnetic moments and angular momenta is the same. Since H_1 is

known to have a positive magnetic moment, H_3 has therefore likewise a positive moment.

A second series of observations to obtain a more accurate value for γ_T was performed by keeping the current in the electromagnet constant, and observing the induced signals of the two isotopes for different frequencies. The following table gives the results for the resonance frequencies ν_3 and ν_1 of H_3 and H_1, respectively, in megacycles together with the field B_0 in gauss, at which the observation was carried out and the resulting ratio γ_T/γ_P of the gyromagnetic ratios.

TABLE I. Resonance frequencies ν_3 and ν_1 of triton and proton and the resulting value of γ_T/γ_P. The fourth column represents the result of a repetition for tritium to ascertain that the field stayed constant during the run.

B_0	ν_3	ν_1	ν_3	γ_T/γ_P
9770	44.29	41.51	44.28	1.067
9500	43.08	40.37	43.08	1.067

To summarize we can therefore state that the triton has a spin of $\frac{1}{2}$, and that its magnetic moment is positive, and 1.067 ± 0.001 times larger than that of the proton.

* Work done at Stanford University and at the Los Alamos Scientific Laboratory operated by the University of California under U. S. Government contract.

[1] F. Bloch, Phys. Rev. **70**, 460 (1946). F. Bloch, W. W. Hanson, and M. Packard, Phys. Rev. **70**, 474 (1946).

[2] See Eq. (29) of reference 1.

Transition from Classical to Quantum Statistics in Germanium Semiconductors at Low Temperature

VIVIAN A. JOHNSON AND K. LARK-HOROVITZ
Purdue University, Lafayette, Indiana*
February 8, 1947

ANALYSIS[1] of the experimental results[2] obtained with germanium semiconductors in the temperature range from -180°C to about 600°C has shown that one can account for electrical conductivity and thermoelectric power of these impurity semiconductors by assuming that lattice vibrations and scattering by singly charged impurity centers[3] are responsible for the observed resistivity ρ, where $\rho=\rho_L+\rho_I$.

$$\rho_L=DRT^{3/2},$$
$$\rho_I=\frac{9\cdot10^{11}\pi^{3/2}\epsilon^2m^{1/2}}{2^{7/2}e^3(kT)^{3/2}}\cdot\ln\left(1+\frac{36\epsilon^2k^2T^2d^2}{e^4}\right),$$

where $R\sim1/n$ is the Hall constant, n the number of conduction electrons per cc, m the electronic mass, ϵ the dielectric constant, $d=0.28n^{-1/3}$=one-half the average distance between impurity centers D determined from experiments.

In both cases it has been assumed that classical statistics can be applied. This is justified in most cases since the number of electrons, as determined from Hall effect measurements, is small.

If the number of electrons is nearly independent of temperature one may apply the well-known criterion for degeneracy and define a degeneracy temperature

$$T_d=\frac{h^2}{8mk}\left(\frac{3n}{\pi}\right)^{2/3}=4.2\times10^{-11}n^{2/3}\ ^\circ\text{K}.$$

Since n varies from sample to sample, one finds that degeneracy temperatures vary from a fraction of a degree K to about 150°K in the germanium samples studied at Purdue. Therefore, at low temperatures, the behavior of these semiconductors should vary widely, depending upon the number of electrons and the activation energy.

Measurements of such semiconductors down to about 10°K have been reported recently.[4] The observations show that three kinds of samples exist:

(1) Very pure samples with a resistance increasing so sharply with decreasing temperature that the material becomes almost non-conducting (Estermann's "pure" germanium and silicon samples).

(2) Samples for which the resistivity increases with decreasing temperature and in some cases seems to reach a "saturation" value.

(3) Samples with constant resistivity from liquid air temperature to liquid hydrogen temperature. All of the samples of type (3) have degeneracy temperatures of about 100°K or higher; calculations using classical statistics, such as have been used at medium temperatures, are not justified for such samples at low temperatures.

We have, therefore, carried out calculations assuming Fermi statistics instead of classical statistics and can summarize our results as follows:

(*a*) Lattice scattering.[5]

above T_d, $\rho_L=DRT^{3/2}$,
below T_d, $\rho_L=D'RTG(\Theta/T)\rightarrow D'RT^5$ at 25°K.

These expressions, calculated for germanium samples, show a smoothly decreasing resistivity with decreasing temperature and, therefore, contribute little to the observed resistivity at low temperatures.

(*b*) Impurity scattering. By calculating the scattering of electrons by randomly distributed, singly-charged impurity centers, one obtains:

$$\frac{1}{\rho_I}=\sigma_I=\frac{32}{3}\frac{\epsilon^2mk^3T^3}{ne^2h^3}\int_0^\infty\frac{x^3\exp(x-\mu^*)dx}{[\exp(x-\mu^*)+1]^2\ln Y},$$

$$Y=1+\frac{4\epsilon^2k^2T^2d^2x^2}{e^4},\quad x=\frac{mv^2}{2kT},\quad \mu^*=\frac{\mu}{kT}$$

TABLE I.

Sample	Measured by Estermann	Measured at Purdue	Calculated
26 *Z*	0.0051	0.0044	0.0040
11 *R*	0.0040	0.0034	0.0037
26 *E*	0.0037	0.0033	0.0034
27 *L*	0.0034	0.0029	0.0033

(All of the above values represent constant low temperature resistivities measured in ohm-cm.)

Thus the transition from classical to quantum statistics leads to a constant residual resistance due to impurity scattering in degenerate samples in agreement with experiment.

where μ is the chemical potential. As T approaches 0, Y can be developed and the integral evaluated, giving finally:[6]

$$\rho_I = (3\pi^2 n)^{1/3} d^2 h/e^2 \text{ e.s.u.}$$
$$= 6270\, b^{-1/3} \text{ ohm-cm.}$$

A detailed theory has to be based on a knowledge of both the Hall constant and the resistivity throughout the temperature range, but comparison of our calculations with Estermann's resistivity values indicates good agreement between theory and experiment. See Table I.

* This work has been carried out under contract No. #-36-039-sc-32020 between the Purdue Research Foundation and the Signal Corps.
[1] K. Lark-Horovitz and V. A. Johnson, Phys. Rev. 69, 258, 259 (1946).
[2] K. Lark-Horovitz, A. E. Middleton, E. P. Miller, and I. Walerstein, Phys. Rev. 69, 258 (1946). K. Lark-Horovitz, A. E. Middleton, E. P. Miller, W. W. Scanlon, and I. Walerstein, Phys. Rev. 69, 259 (1946).
[3] E. Conwell and V. F. Weisskopf, Phys. Rev. 69, 258 (1946).
[4] G. L. Pearson and W. Shockley, Bull. Am. Phys. Soc. 21, 9 (1946). I. Estermann, A. Foner, and J. A. Randall, Bull. Am. Phys. Soc. 22, 31 (1947).
[5] $G(\Theta/T)$ is the Gruneisen function; Mott and Jones, *Properties of Metals and Alloys*, p. 261.
[6] It can be seen that ρ_I is of this form at low temperatures by developing the classical formula for ρ_I and setting $kT = (3n/\pi)^{\frac{1}{3}} h^2/8m$.

Possible Use of Thermal Noise for Low Temperature Thermometry*

EDWARD GERJUOY AND A. THEODORE FORRESTER
University of Southern California, Los Angeles, California
January 31, 1947

FOLLOWING the suggestion of Lawson and Long[1] that the thermal agitation of a quartz crystal be used to establish a law temperature thermodynamic scale, a quantitative investigation of the problem was undertaken. It appeared to be simpler to consider the problem from the circuit point of view[2] than from the detailed analysis of the crystal mechanism. If the complex impedance of the low temperature resonant circuit (crystal or ordinary parallel resonant combination) is given by $R(f)+iX(f)$, then the noise voltage appearing across the element, *on open circuit*, in the range f to $f+df$, is given by the Nyquist formula

$$d\langle e^2\rangle_{Av} = 4kTR(f)df.$$

In practice the resonant circuit is always paralleled by the input capacity, indicated by C_2 in Fig. 1. Associated with this capacity are losses represented by the resistance r_2. The noise voltage appearing across this parallel combination can be obtained from the formula[3]

$$\langle e^2\rangle_{Av} = \langle e_a^2\rangle_{Av}\left|\frac{Z_b}{Z_a+Z_b}\right|^2 + \langle e_b^2\rangle_{Av}\left|\frac{Z_a}{Z_a+Z_b}\right|^2,$$

where e is the fluctuating voltage appearing across the parallel combination of an impedance Z_a in series with a generator e_a and an impedance Z_b in series with a generator e_b. Imposing the condition that the noise appearing across the parallel combination of the resonant circuit and the input capacity be characteristic of the low temperature T_a rather than room temperature T_b, one obtains the necessary inequality.

$$C_1 \gg \frac{Q_0}{Q_2} C_2 \frac{T_b}{T_a}, \tag{1}$$

where C_1, which is in parallel with C_2, is the capacity in the

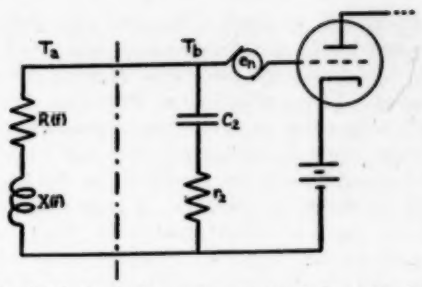

FIG. 1. Simplified circuit for measurement of thermal agitation at low temperature.

low temperature resonant circuit, Q_0 is the Q of this part of the circuit, and Q_2 is the Q of the capacity C_2.

Another condition which must be met is that the low temperature noise be large compared to the tube noise, represented in Fig. 1 by e_n, and which is given approximately by[4,5]

$$d\langle e_n^2\rangle_{Av} = 4kT\left(\frac{3r_p}{\mu} + 19.3 I_g |Z_g|^2\right)df,$$

where the first term on the right is the term caused by shot noise in the plate circuit, referred to a generator placed on the grid, and the second term is the shot noise due to the grid current I_g in the tube. These two terms result in the inequalities

$$C_1 \ll \frac{\pi}{2}\frac{1}{(3r_p/\mu)\Delta\omega}\frac{T_a}{T_b}, \tag{2}$$

and

$$C_1 \gg 20 I_g \frac{Q_0}{\omega_0}\frac{T_b}{T_a}. \tag{3}$$

In these inequalities ω_0 is the angular frequency at resonance and $\Delta\omega$ is the band width of the amplifier. The minimum value of this band width which will include 99 percent of the energy of the resonant circuit is

$$\Delta\omega = \frac{200}{\pi}\frac{\omega_0}{Q_0}. \tag{4}$$

Equations (1)–(4) lead to estimates of the lowest measurable temperature T_a for any desired accuracy, this accuracy determining the amount by which the left-hand sides of inequalities (1), (2), and (3) must differ from the right. If it is assumed that the background noise voltage cannot be measured or balanced out more accurately than to one percent, the $\gg$ symbols must be replaced by $>$ 4 times, in order to measure T_a to about 2 percent. Assuming $C_2 = 30\mu\mu f$, $Q_2 = 10^5$ (a value which seems generous if one either extrapolates from known Q's of air condensers, or calculates roughly on the basis of the power factors of glass and other material which might surround the input lead), and $\Delta\omega > 1$ cycle per second (a practical minimum), the lowest T_a is readily calculable.

The lowest temperatures can be attained with electrometer tubes, for which, due to low grid currents, the right-hand side of (3) is less than the right-hand side of (1) so that (1) and (2) can be used to determine the minimum T_a. For a favorable tube such as the Western Electric D-96475, the minimum measurable temperature, under the

conditions stated, is about 2°K, and then only if the parallel capacity C_1 of the resonant circuit can be made precisely 0.02μf and the associated network components are designed to give a resonance at 1600 c/s.

It may be possible to reduce the measurable T_a below 2°K. A tube might be designed around Eqs. (1), (2), and (3) which would have better properties for this application than the D-96475; furthermore, if this tube could be inserted in the low temperature bath along with the resonant circuit (R, X in Fig. 1), C_2 might be lowered to 6$\mu\mu$f; perhaps also the background could be measured or balanced out to better than one percent. A scrutiny of these possibilities leads, however, to the conclusion that the ultimate attainable temperature will almost certainly be greater than 0.1°K. It must be noted, however, that these calculations depend on the assumption that the noise arising in the portion of the circuit at temperature T_b can be accurately determined or balanced out. If this is not possible, the minimum temperature measurable by this method may be very much higher.

* Bulletin of the American Physical Society **21**, 6 (1946).
[1] A. W. Lawson and E. A. Long, Phys. Rev. **70**, 220 (1946).
[2] This conclusion was arrived at independently by J. B. Brown and D. K. C. MacDonald, Phys. Rev. **70**, 976 (1946).
[3] F. B. Llewellyn, Proc. I.R.E. **18**, 243 (1930).
[4] D. O. North, RCA Review **4**, 441 (1946).
[5] F. E. Terman, *Radio Engineers' Handbook*, first edition, p. 316.

On Bringing the Beam out of a Betatron

ROLF WIDERÖE
Giesshübelstrasse 14, Zurich, Switzerland
February 18, 1947

COURANT and Bethe[1] have given a brief discussion of their theoretical considerations on bringing the electron beam out of a betatron. I should like to mention that in the autumn of 1944 I made similar considerations and came to the same conclusion that the deflection electrodes for bringing out the beam should be located quite near the point where Br is a maximum. If the simplifying assumption is made that Br follows a parabolic law, for instance $Br=(Br)_{max}(1-\alpha\rho^2)$, with ρ indicating the distance from the point r_m where Br is a maximum, while the magnetic guiding field must vary (relative to the induction field) with the time constant T (for example, as $B_{\Delta t}=B_0(1-\Delta t/T)$, then as a first approximation the following differential equation for the electron orbits is obtained.

$$\frac{\partial^2\rho}{\partial t^2}=\frac{V^2}{r_m}\left(\alpha\rho^2+\frac{\Delta t}{T}\right)$$

where V is the tangential velocity of the electrons at the radius r_m.

This corresponds to the so-called Painlevé differential equation $y''=y^2+x$, which cannot be solved by known functions. Figure 1 shows a solution of this differential equation, the initial conditions being so selected that the electrons do not execute any superposed oscillations. It will be seen that the curve for y' (which also corresponds to the separation of the single orbits) rises very steeply when the radius r_m is exceeded (about proportionality to y^3). In order therefore that the divergence of the emerging

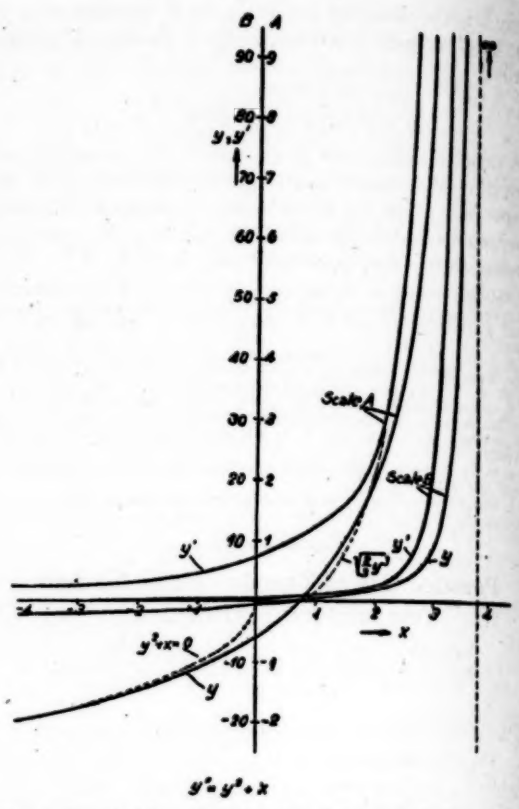

FIG. 1. Graphical form of the solution of the equation $y''=y^2+x$.

electrodes should not become too large, the deflecting electrodes must not be located too far outside the circle r_m. On the other hand, in order that too many electrons do not fall on the edge of the deflecting plate, this latter must not be placed too far inwards.

These two conditions result in an optimum position for the deflecting plates which, in conjunction with a particular construction of the deflecting field (preliminary deflection by means of a special very thin deflecting electrode), has formed the subject matter of a patent application filed by me in December, 1944. In this patent application also the refocusing of the emerging beam by means of an auxiliary magnetic field has been provided.

[1] E. D. Courant and H. Bethe, Phys. Rev. **70**, 798 (1946).

On the Dissociation Energy of CO

H. D. HAGSTRUM
Bell Telephone Laboratories, Inc., Murray Hill, New Jersey
February 17, 1947

THREE proposed interpretations of the band spectrum of CO lead to $D(CO)=6.92$ ev,[1] 9.14 ev,[2] and 11.11 ev,[3] respectively. Electron collision experiments in CO give the unique value, $D(CO)=9.6$ ev.[4] Clearly a reconciliation of these conflicting positions is demanded.

$D(CO)=9.6$ ev from electron impact rests upon the appearance potentials of four ionization and dissociation

processes studied by a retarding potential method[3] and the mass spectrometer[4] with excellent numerical agreement. Similar studies in H_2, N_2, NO, and O_2 with the same apparatus are in excellent agreement with well-established results from the band spectrum. It is contended that to demand a discrepancy of 0.5 ev in the single case of CO, as is required by any of the present interpretations of the band spectrum, does considerable violence to an otherwise consistent and well-established body of data.

The spectroscopic determinations of $D(CO)$ are based on interpretations of a number of intensity weakenings or breakoffs in the rotational structure of emission bands. These occur 9.61 ev above $X\,^1\Sigma^+$ in $v'=7$, 8, and 9 of $A\,^1\Pi$; 11.11 ev above $X^1\Sigma^+$ in $v'=0$, 1 of $B\,^1\Sigma^+$ and $v'=0$, 1 of $b\,^3\Sigma^+$; and 11.58 ev above $X\,^1\Sigma^+$ in $v'=0$ of $C\,^1\Sigma^+$. An interpretation of these data is proposed here which is consistent with $D(CO)=9.6$ ev and which, it would appear, is at least as credible as any of the present interpretations.

If $D(CO)=9.6$ ev, there are dissociation limits of the molecule corresponding to the products $C(^3P)+O(^3P)$ at 9.6 ev, $C(^1D)+O(^3P)$ at 10.86 ev, $C(^3P)+O(^1D)$ at 11.58 ev, etc. Thus the effects in the spectrum at both 9.61 and 11.58 ev could be genuine predissociations at the corresponding dissociation limits. The effect at 11.11 ev, however, cannot occur at a dissociation limit.

It is suggested that $B\,^1\Sigma^+$ and $b\,^3\Sigma^+$ are predissociated by $a'\,^3\Sigma^+$ [Case I(b)], as has been supposed, but that $a'\,^3\Sigma^+$ has a potential curve with maximum, the maximum occurring at the predissociation in $B\,^1\Sigma^+$ and $b\,^3\Sigma^+$ and the convergence of the vibrational levels of $a'\,^3\Sigma^+$ at 11.11 ev. The dissociation limit of the state would in all probability be $C(^1D)+O(^3P)$ at 10.86 ev, requiring the maximum to be 0.25 ev high.

It is known that a criterion for a potential curve with maximum is the form of the so-called limiting curve of dissociation which must be a straight line of slope predicting a reasonable value for the internuclear distance (r_m) at which the maximum occurs.[6] If one accepts all the intensity changes reported[7] in the $B\,^1\Sigma^+$ and $b\,^3\Sigma^+$ states as predissociation by $a'\,^3\Sigma^+$ one can draw a straight line through the data but of slope giving $r_m=3.8$A, an impossibly high value. However, it is to be observed that the four data on which this curve is based are by no means of equal credibility. The breakoffs in $v'=0$ of $B\,^1\Sigma^+$ and $v'=1$ of $b\,^3\Sigma^+$ are observed in the P, Q, and R branches and can hardly be questioned. That in $v'=1$ of $B\,^1\Sigma^+$, on the other hand, is observed only in the P branch of the (1, 0) and the Q branch of the (1, 1) angström bands in which considerable superposition by CO_2 bands occurs. Considering these to result from a perturbation and not predissociation by $a'\,^3\Sigma^+$, one can obtain $r_m=2.9$A, a quite reasonable value. It should be remarked that since $D(a'\,^3\Sigma^+)>4$ ev a maximum only 0.25 ev high would be expected to lie at quite large internuclear separation.

Attributing the breakoffs in $v'=1$ of $B\,^1\Sigma^+$ to a perturbation or perhaps another predissociation is certainly no less tenable than attributing the breakoffs in the three levels $v'=7$, 8, 9 of $A\,^1\Pi$ at 9.61 ev to accidental predissociation or a perturbation as is now required by $D(CO)=9.14$ or 11.11 ev. If, in addition, it should be found that the failure of Dieke and Mauchly[8] to follow the structure of bands with $v'=0$ of $b\,^3\Sigma^+$ to $K>55$ is the result of something other than a predissociation by $a'\,^3\Sigma^+$ as is now supposed,[9] it would be possible to draw a straight-line limiting curve through the two remaining and most trustworthy sets of points having a slope which gives r_m as small as 2.1A. This may not be necessary to the interpretation, however.

[1] R. Schmid and L. Gerö, Zeits. f. physik. Chemie **B36**, 105 (1937), a general review.
[2] G. Herzberg, Chem. Rev. **20**, 145 (1937), a general review.
[3] A. G. Gaydon and W. G. Penney, Proc. Roy. Soc. **A183**, 374 (1945).
[4] H. D. Hagstrum and J. T. Tate, Phys. Rev. **59**, 354 (1941).
[5] W. W. Lozier, Phys. Rev. **46**, 268 (1934).
[6] See G. Herzberg, *Molecular Spectra and Molecular Structure* (Prentice Hall, New York, 1939), pp. 444–459.
[7] See summary by L. Gerö, Zeits. f. Physik **100**, 374 (1936).
[8] G. H. Dieke and J. W. Mauchly, Phys. Rev. **43**, 12 (1933).
[9] F. Brons, Nature **135**, 873 (1935); L. Gerö, Zeits. f. Physik **95**, 747 (1935).

A Mass Spectroscopic Analysis of the Polyatomic Gases in a Fast Counter

S. S. FRIEDLAND
New York University, University Heights, and Memorial Hospital, New York, New York
February 13, 1947

THE function of the polyatomic gas in a fast counter as proposed by S. A. Korff and R. D. Present[1] has a twofold purpose: (1) to quench the ultraviolet photons that are emitted by the excited states of the inert gas (argon) and (2) to quench secondary emission by positive ions reaching the cathode. The authors point out that the characteristic property of a polyatomic molecule which is of importance in the counter is the large probability of predissociation from excited electronic states. They claim that the quenching of ultraviolet photons in the initial avalanche occurs through the photo-decomposition of the polyatomic gas, and the electron transfer probability ensures that the positive ion sheath, when it reaches the cathode, is composed entirely of polyatomic ions. These are neutralized at about 10^{-7} cm from the wall and the excited neutral molecules predissociate in 10^{-13} sec. before they can liberate a secondary electron by an ineslastic collision with the wall or by recombination radiation. The authors point out that since no supply of secondary electrons is available the discharge terminates.

Korff and Present suggest that the primary decomposition products of the polyatomic molecules are free radicals which combine to form a miscellaneous assortment of organic molecules. They claim that some of these decomposition products will be quenching gases; however, with continued use of the counter all of the larger vapor molecules will be broken up and the end products of the decomposition are a non-quenching gas of much smaller molecular weight.

Partly to verify this theory two argon-ethyl acetate counters (argon pressure 8 cm, ethyl acetate pressure 1.2 cm) were prepared simultaneously on a Geiger counter filling system. One counter was kept unused and the other was run for 10^{10} counts, when it no longer acted as a self-

quenching counter. The two counters were prepared with break-off seals and their vapors were examined by a mass spectrometer. Table I indicates the results obtained:

TABLE I. Relative abundance as a function of mass number in used and unused counters. R = Peak height for mass number M/peak height for A^{40}.

Mass Number	R for unused counter	R for used counter
88	0.13×10^{-2}	0.00×10^{-2}
87	1.76×10^{-2}	0.00×10^{-2}
86	0.10×10^{-2}	0.00×10^{-2}
73	1.57×10^{-2}	0.00×10^{-2}
70	3.37×10^{-2}	0.00×10^{-2}
62	0.17×10^{-2}	0.00×10^{-2}
61	5.24×10^{-2}	0.00×10
46	0.18×10^{-2}	0.09×10^{-2}
45	5.49×10^{-2}	0.54×10^{-2}
44	2.52×10^{-2}	34.80×10^{-2}
43	35.30×10^{-2}	2.08×10^{-2}
42	1.79×10^{-2}	0.29×10^{-2}
40	1	1
39	0.08×10^{-2}	0.21×10^{-2}
36	0.34×10^{-2}	0.36×10^{-2}
32	4.84×10^{-2}	0.07×10^{-2}
31	0.43×10^{-2}	0.30×10^{-2}
29	5.35×10^{-2}	1.95×10^{-2}
28	32.00×10^{-2}	63.40×10^{-2}
27	2.47×10^{-2}	0.93×10^{-2}
26	0.69×10^{-2}	1.59×10^{-2}
25	0.08×10^{-2}	0.22×10^{-2}
22	0.03×10^{-2}	0.22×10^{-2}
20	10.70×10^{-2}	15.37×10^{-2}
18	0.90×10^{-2}	3.51×10^{-2}
16	0.23×10^{-2}	5.74×10^{-2}
15	2.25×10^{-2}	4.47×10^{-2}
14	1.54×10^{-2}	1.93×10^{-2}

The complete disappearance of mass numbers above 46 and the increases at smaller mass numbers for the used counter is in agreement with the theory. The large peaks that appear at mass numbers 44, 28, and 16, would indicate that the final vapors present in the counter after use are carbon dioxide, carbon monoxide, and some methane. In this test, the spectrometer was not operated below mass 14.

A further study of various gases and a determination of disintegration as a function of the number of counts is now in progress.

The writer wishes to express his thanks to Drs. J. A. Hipple and R. E. Fox of the Westinghouse Research Laboratories for their cooperation in making the gas analysis, and to Dr. S. A. Korff for helpful suggestions.

[1] S. A. Korff and R. D. Present, Phys. Rev. 65, 274 (1944).

Evidence[1] for a $\gamma-p$ Reaction in Be^9

WM. OGLE, LEON BROWN, AND RICHARD CONKLIN[2]
University of California, Los Alamos Scientific Laboratories, Santa Fe, New Mexico

February 17, 1947

SEVERAL activities have been observed in elements irradiated by 20-Mev gamma-rays from the betatron that could be explained by $\gamma-p$ process. However, the γ-rays from the betatron have associated with them an appreciable number of fast neutrons, so that it is not clear whether these activities were the results of a $\gamma-p$ or an $n-p$ process. Accordingly, a search was made for an element such that a fast neutron reaction would cause no confusion.

Be^9 seemed to be such a substance. A $\gamma-n$ process produces Be^8 which decays to two alpha-particles immediately. An $n-\gamma$ process produces Be^{10} which has a half-life at 10^6 years, and hence would cause no confusion. An $n-p$ reaction, producing Li^9, is not known. The $\gamma-p$ process would produce Li^8 which decays with the emission of betas with a maximum energy of 12 Mev, and a half-life of 0.88 sec. The only confusing process is a $n-\alpha$ on Be^9 producing He^6 which decays with the emission of betas of maximum energy of 3.7 Mev, and a half-life of 0.88 sec.

Irradiation of Be^9 with 20-Mev gammas produced a beta-activity of half-life 0.88 ± 0.03 sec., indicating the formation of either Li^8 or He^6. A simple absorption experiment showed the presence of betas of energies up to 12 Mev, and a recheck of the half-life with $\frac{3}{32}$ inch of aluminum between the beryllium and the counter tube, again indicated a half-life of about 0.9 sec. $\frac{3}{32}$ inch of aluminum should remove all betas of energy less than 3.9 Mev, thus eliminating the possibility of the observed half-life being caused by the decay of He^6. Thus it seems clear that Li^8 is formed.

A rough threshold experiment was run, again with $\frac{9}{32}$ inch of aluminum between the beryllium and the counter tube, which indicated that the $\gamma-p$ process has an energy threshold of 18 ± 1 Mev. A similar experiment with no absorber shows some activity remaining when the gamma-rays have an energy as low as 7 Mev, which would indicate that He^6 is also formed, since the threshold for this process is expected to be 2.6 Mev, i.e., 1.6 Mev for the $\gamma-n$ process in Be^9, and 1 Mev for the $n-\alpha$ process. Mass values taken from Segrè's isotope chart of May 1945 indicate a $\gamma-p$ threshold of 16.8 Mev, where no account is taken of the Coulomb barrier seen by the proton.

[1] This paper is based on work performed under Contract No. W-7405-Eng-36 with the Manhattan Project at the Los Alamos Scientific Laboratory of the University of California.
[2] Now at the University of Illinois, Urbana, Illinois.

Nuclear Properties of U^{233}: A New Fissionable Isotope of Uranium*

G. T. SEABORG, J. W. GOFMAN, AND R. W. STOUGHTON
Department of Chemistry and Radiation Laboratory, University of California, Berkeley, California

April 13, 1942
(Received February 11, 1947)

THE bombardment of thorium with slow neutrons produces Th^{233} (by the reaction $Th^{232}(n,\gamma)Th^{233}$), which emits beta-particles and has a half-life of 23.5 minutes. The daughter of Th^{233} is the 27.4-day beta-emitting Pa^{233} which in turn decays to U^{233}. We have measured the radioactive and the fission properties of U^{233}. Our measurements on a sample of U^{233} weighing 3.8 micrograms show that this isotope undergoes fission with neutrons. The same result was obtained in a check experiment with another sample of U^{233} weighing 0.8 microgram.

* This paper was mailed from Berkeley, California, to the "Uranium Committee" in Washington, D. C. on April 14, 1942. The experimental work was done during 1941 and the early part of 1942. It is being published in the open literature now for historical purposes, with the original text somewhat changed, by omissions, in order to conform to present declassification standards. The information covered in this document will appear in Division IV of the MPTS, as part of a contribution of the University of California.

A Classical Model for the Nucleus

J. G. WINANS
University of Wisconsin, Madison, Wisconsin
December 26, 1946

WHEN the cube root of the mass number is plotted against the square root of the atomic number for the most abundant or longest lived isotope of the elements, there is obtained a very nearly straight line extending from the neutron to curium. Hydrogen and helium are the only elements appreciably off of the line. The equation is $M^{\frac{1}{3}}-1.15=0.528Z^{\frac{1}{2}}$. To show this more accurately, $(M^{\frac{1}{3}}-1.15)^2$ is plotted against the atomic number in Fig. 1.

Assuming nuclei spherical, made of protons and neutrons each of radius r_0, with the protons confined to the outside giving a constant surface charge density at a depth xr_0 below the surface, we have:

$$4\pi(r-xr_0)^2=K_1Z\pi r_0^2 \quad \text{and} \quad 4/3\pi r^3=K_2M4/3\pi r_0^3,$$

where M is the mass number and Z is the atomic number. Combining gives

$$M^{\frac{1}{3}}-\frac{x}{K_2^{\frac{1}{3}}}=\frac{K_1^{\frac{1}{2}}}{2K_2^{\frac{1}{3}}}Z^{\frac{1}{2}}.$$

Use of $K_2=1.35$ as for spherical close packing gives $x=1.28$, and $K_1=1.36$. The correction factor for K_1 to get a value of K_1 corresponding to the middle of the surface particles, depends on M and Z. For holmium, for example, $M=165$, $Z=67$, and the surface $K_1=1.66$. If the surface contained equal numbers of protons and deuterons in hexagonal close pack the surface constant would be 1.65. This surface with each neutron surrounded by six protons, and each proton surrounded by three neutrons and three protons, we will call the surface pattern for stability.

The model of the nucleus to fit these observations is that of a positively charged chunk of solid hydrogen.

This model provides an explanation for many of the observations of nuclear physics, and leads to the prediction of new effects.

According to this model, α-particle emission could result from union of two surface deuterons to produce an α-particle with the 24-Mev reaction energy going into melting the nucleus, and setting it into pulsations. These pulsations could increase the surface, concentrating charge at the ends to eject the α-particle. The distortion needed to free the α-particle would determine its energy and the lifetime of its parent.

The model of a neutron to fit this picture is a sub-nuclear proton, with electron and neutrino rotating about it. If the neutron is radioactive, the maximum mass of the neutrino would be 0.00080 atomic units. The exact mass should be determinable by photo-ionization of neutrons.

β^--emission could result when a neutron disintegrates either spontaneously, or through photon-absorption, with ejection of β^{-1} and neutrino in the same direction. The freezing of the nucleus could transfer energy to vibration of a proton to give the photon for β^--emission. γ-radiation could be associated with rotation of a distorted non-rigid nucleus following $\alpha-$emission, or of a rigid nucleus following β^--emission. Guggenheimer showed that γ-rays were like radiation of a rigid rotator.[1]

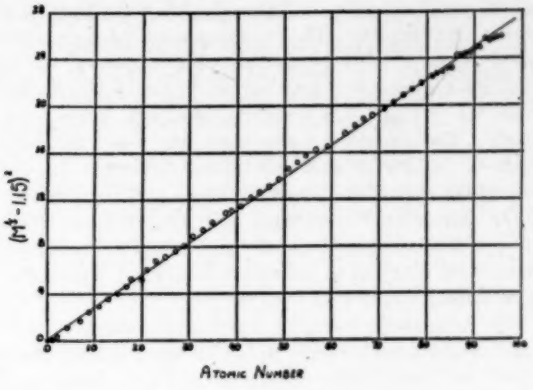

FIG. 1. Atomic number.

According to this model, the packing fraction of heavy nuclei could be high because of mutual repulsion of protons. Fission could result from splitting a near-perfect crystalline nucleus by a neutron. Heavy nuclei should serve as crystals for diffraction of high energy photons. Nuclei bombarded by high energy electrons should give electronic γ-ray spectra.

The concept of nuclear particles as close packed spheres leads to a model for light nuclei as flat, with thickness $2r_0$. According to this model the primary constituents of the nucleus are protons, deuterons, and neutrons. Double neutrons, corresponding to H_2 molecules, should be observable. Heavy atoms bombarded by deuterons, might form stable, heavier atoms. Very heavy nuclei could exist.

If this model of the nucleus is correct the properties of isotopes should be predictable from models treating the nucleus as a rigid rotator and as a polyatomic molecule.

[1] K. M. Guggenheimer, Proc. Roy. Soc. **A181**, 169 (1942–43).

Cosmic-Ray Bursts in an Unshielded Chamber and Under One Inch of Lead at Different Altitudes*

HERBERT BRIDGE AND BRUNO ROSSI
Laboratory for Nuclear Science and Engineering, Massachusetts Institute of Technology, Cambridge, Massachusetts
February 13, 1947

THE original purpose of this experiment was an investigation of the altitude dependence of *high energy* electrons and photons in cosmic rays. Such an investigation provides a much more critical test for the various hypotheses on the origin of the electron-photon component than a study of the *total intensity* of this component.

The instrument used was a cylindrical ionization chamber three inches in diameter, twenty inches in length, filled with pure argon at 4.7 atmospheric pressure. The axis of the chamber was kept horizontal. The chamber was connected to a fast pulse amplifier, and the pulses were analyzed by means of a four-channel electronic discriminator. A weak polonium source of α-particles (5.3 Mev) was placed in the chamber for the purpose of calibration.

Measurements were taken both with, and without a lead

shield, one inch thick, in the shape of half a cylinder placed above the chamber. The measurements at high altitude were made in a B-29 aircraft. The biases of the four-channel discriminator were adjusted to record pulses larger than 1.1, 1.5, 2.0, 2.5 times the α-particle pulses, respectively. The observed burst-rates are listed in Table I (figures in parenthesis are actual numbers of bursts recorded). At all elevations the burst-rate with lead is 1.5 to 2 times as large as without lead. The variation of burst-rate with atmospheric depth can be represented approximately by function of the type $\exp(-x/L)$, where x is the atmospheric depth and $L=150$ g/cm^2.

We tentatively interpret the bursts observed without lead as produced partially by air showers, but for the most part by cosmic-ray induced nuclear disintegrations ("stars").[1] The increase in burst-rate caused by the lead is attributed to shower production in the lead by high energy electrons and photons. As an indication of the energies involved, we may mention that an electron of 10 Bev produces, on the average, in one inch of lead, a shower of 140 electrons which, by traversing the chamber in a direction perpendicular to the axis, give rise to a pulse of an average rise twice that of an α-particle. Since it seems that one inch of lead does not appreciably change the burst-rate from stars,[1] the variation with height of the "lead difference" (burst-rate with lead minus burst rate without lead) is representative of the variation with height of the number of high energy electrons and photons. This is true even if an appreciable fraction of the bursts observed under lead are produced by air showers because, in a qualitative sense at least, it is immaterial whether the showers recorded originate from single electrons or photons striking the lead or have partially developed in air before reaching the lead.

The large increase in the number of high energy electrons and photons, shown by the results in Table I, provides crucial evidence against the hypothesis that all cosmic-ray electrons and photons arise from the decay of ordinary mesons. Since the number of mesons in the range above 10 Bev does not change substantially from sea level to 35,000 feet, the intensity of their decay products should only increase inversely proportional to the air density; i.e., by about a factor of four.

Besides the disintegration of ordinary mesons, two other possible sources of electrons and photons have been considered at various times, namely (a) the existence of an electron and/or photon component in the primary radiation, and (b) the disintegration of short-lived mesons. From both hypotheses one predicts a rapid variation with height of the electron-photon intensity in the lower part of the atmosphere. According to hypothesis (a), however, the intensity should keep on increasing up to the top of the atmosphere *provided one only considers electrons and photons of energy larger than the geomagnetic cut-off*. According to hypothesis (b), instead, the intensity should go through a maximum and drop to zero at the top of the atmosphere. It is hoped that experiments at higher elevation than the present ones will make a decision between hypothesis (a) and (b) possible.

If our analysis is correct, Table I shows that the intensities of the "star producing radiation" and of the electron-photon component vary approximately by the same factor from 0 to 35,000 feet. Since this can hardly be an accident and since stars do not seem to be produced by electrons or photons,[1] one is led to the conclusion that the star producing radiation and the electron-photon component are both in equilibrium with a common parent radiation, a result which can be brought into agreement more easily with hypothesis (b) than with hypothesis (a).

TABLE I. Dependence of burst rates on altitude.

Altitude (feet) Atmospheric depth (g/cm^2)	Lead	Burst-rates (per hour) $>1.1\alpha$	$<1.5\alpha$	$<2.0\alpha$	$<2.5\alpha$
0 (1030)	On	4.0 (209)	1.7 (112)	1.32 (70)	0.67 (44)
	Off	*	*	*	*
14,000 (610)	On	51 (152)	30 (90)	20 (61)	14 (42)
	Off	36 (132)	20 (74)	13 (47)	6.3 (23)
25,000 (388)	On	286 (476)	149 (375)	93.8 (236)	57.3 (144)
	Off	141 (242)	87.8 (262)	54.6 (163)	32.2 (96)
30,000 (310)	On		289 (231)	156 (125)	97.5 (78)
	Off		158 (213)	90 (122)	63 (85)
35,000 (248)	On	786 (800)	453 (461)	267 (271)	175 (178)
	Off	420 (406)	238 (230)	133 (129)	81.6 (79)

* The ratio of bursts per hour with lead on to those with lead off was determined as 2.1 for this range of pulse heights with slightly different equipment.

* The research described in this letter was supported partially by Contract N5 ORI-78, U. S. Navy Department, Office of Naval Research. The B-29 used for the measurements at high altitude was provided by the U. S. Army Air Force. The authors wish to express their gratitude to the pilot, Lt. C. C. Davis and the crew of the B-29 for their cooperation.

[1] This view is supported by the preliminary results of experiments by R. W. Williams at 11,000 feet altitude, which are now in progress. See also D. Skobeltzyn, Phys. Rev. **70**, 441 (1946).

A Metastable State of Half-Life about 10^{-6} Second in Re^{187}

S. DE BENEDETTI AND F. K. MCGOWAN
Clinton Laboratories, Oak Ridge, Tennessee
February 17, 1947

USING sources of W^{187} (24 hrs.) and an experimental arrangement similar to that described in a previous letter,[1] we were able to detect delayed coincidences whose number as a function of time is shown in Fig. 1. It appears from this curve that the disintegration of W^{187} leads to a metastable state Re^{187*}, which in turn decays to the ground state with a half-life of about one microsecond (only statistical errors are indicated on the figure; errors involved in the calibration of the time-scale may be considerably larger).

In order to increase the counting rate by eliminating absorption in the counter windows, the two G-M counters

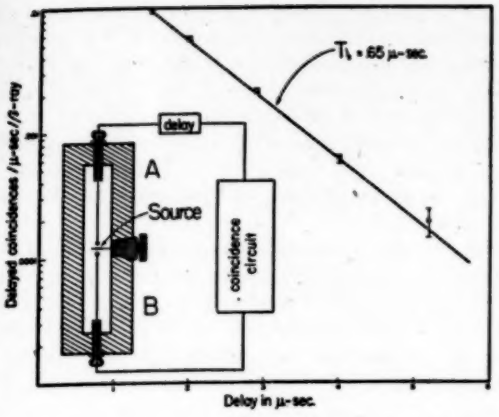

FIG. 1. Delayed coincidences vs. delay time from the disintegration of W^{187}.

and the source (deposited on a thin aluminum foil) were located within the same envelope (Fig. 1). Since the minimum delay used was 1.5μ sec. it was necessary to prove that the recorded coincidences were not due to simultaneous rays (immediate internal conversion, or radiation scattered from one to the other counter) which gave delayed pulses because of the time lag of the counters. To test this point β-rays from RaE were sent through both counters, and it was found that these did not give any delayed coincidences despite the large number of immediate coincidences recorded.

Absorption measurements were performed under the geometrical conditions described in the previous letter[1] by use of two mica window G-M counters. The absorption curve of the disintegration electrons followed by a delayed ray proved that the metastable state follows the softer part of the β-spectrum[2] of W^{187}. Some γ-radiation also seems to precede the metastable state. From absorption measurements on the delayed electrons it appears that the energy of the delayed γ-rays may correspond to any one of the three soft lines (0.086, 0.101, or 0.130 Mev) previously observed in the spectrum of W^{187}. However, it seems probable that the metastable state is associated with the 0.130-Mev transition since this has been observed with a β-spectrometer to be strongly converted.[3]

The disintegration of the metastable state is accompanied by a soft electromagnetic radiation (less than 100 kev) which could be either the unconverted γ-ray from the metastable state (which in this case should be attributed to the 86-kev transition), or a γ-ray following it, or the atomic x-radiation from Re. The number of delayed electrons per disintegration of W^{187} was evaluated as 0.1. Since not all β-rays of W^{187} lead to the metastable state, the internal conversion coefficient must be larger than this value.

This work was done under the auspices of the Manhattan District.

[1] S. De Benedetti and F. K. McGowan, Phys. Rev. **70**, 569 (1946).
[2] W. H. Sullivan, Phys. Rev. **68**, 277 (1945).
[3] We are indebted to L. C. Miller and L. F. Curtiss for the communication of this result.

Metastable Ion Transitions in the Mass Spectra of the Monochloropropenes

VERNON H. DIBELER, C. EDWARD WISE, JR., AND FRED L. MOHLER
National Bureau of Standards, Washington, D. C.
February 13, 1947

RECENTLY Hipple and Condon,[1] and Hipple, Condon, and Fox,[2] have called attention to the occurrence and origin of metastable ions which dissociate soon after traversing the electric field in a mass spectrometer. The authors have found an instance of this type of dissociation in the monochloropropenes in which the chlorine atom is lost from the ionized molecule after traversing the accelerating field. In this case the characteristic isotope ratio of about three to one for Cl^{35} to Cl^{37}, labels the metastable peaks and confirms the mass assignment. According to the theory of Hipple *et al.*, the effective mass, m^*, of the dissociating ion is given by the relation $m^* = m^2/m_0$, where m_0 and m are, respectively, the masses before and after dissociation. For monochloropropene, $m_0 = 76$ and 78, and in both cases, $m = 41$. Therefore, $m^* = 22.1$ and 21.6 for the metastable dissociation of Cl^{35} and Cl^{37}, respectively. The metastable peaks observed in monochloropropene are at the predicted positions, and the peak heights are in the ratio of 3 to 1 as expected. They are differentiated from normal peaks by being wider and more diffuse, and are roughly triangular in shape with a base 0.7 of a mass unit wide, compared with a normal peak width of 0.2 mass units.

The allyl chloride was obtained from Eastman Kodak Company and was used without further purification. The other monochloropropenes were obtained from Columbia Organic Chemicals Company as a cis-trans mixture of 1-chloro-1-propene, containing some 2-chloropropene as an impurity. The identity of the components was confirmed by combined data from the mass spectrometer and the fractional distillation curves. The original was fractionated at reduced pressure to obtain the separate isomers but because only a small sample was available an independent check on the purity of each fraction was impossible. At about 304 mm the boiling points of the 2-chloropropene, cis-1-chloro-1-propene, and trans-1-chloro-1-propene were -2°C, $+6$°C, and $+12$°C, respectively.

Table I lists the relative peak heights for the isomers of the monochloropropenes at the mass peaks in question. In view of the possible incomplete fractionation, the results indicate that the metastable transition may be completely absent in 1-chloro-1-propene. This offers an analytical aid

TABLE I. Some mass peaks of the monochloropropenes.

		Fraction containing			
m/e	Ion	2-Chloro-propene	(Cis)1-chloro-1-propene	(Trans)1-chloro-1-propene	3-Chloro-1-propene
21.6	$[Cl^{37}C_3H_5^+] \rightarrow C_3H_4^+ + Cl^{37}$	0.42	0.05	0.02	0.56
22.1	$[Cl^{35}C_3H_5^+] \rightarrow C_3H_4^+ + Cl^{35}$	1.3	0.15	0.05	1.7
35	Cl^+	5.9	5.3	4.2	7.0
41	$C_3H_5^+$	200.	232.	226.	300.
76	$Cl^{35}C_3H_5^+$	100.	100.	100.	100.
78	$Cl^{37}C_3H_5^+$	31.8	31.7	31.7	31.7

for distinguishing 1-chloro-1-propene from its isomers. The direct dissociation into an ion of mass 41 is by far the most probable result of electron collision, and the delayed dissociation a comparatively rare event. However, the relative peak height is not a direct measure of the abundance of metastable ions but depends in a complicated manner on the geometry of the instrument, and other factors.

It is hoped that this research will be continued with larger samples of higher purity.

[1] J. A. Hipple and E. U. Condon, Phys. Rev. **68**, 54 (1945).
[2] J. A. Hipple, R. E. Fox, and E. U. Condon, Phys. Rev. **69**, 347 (1946).

Disintegration by Consecutive Orbital Electron Captures $_{56}Ba^{131} \rightarrow {}_{55}Cs^{131} \rightarrow {}_{54}Xe^{131}$

FU-CHUN YU, DONALD GIDEON, AND J. D. KURBATOV
The Ohio State University, Columbus, Ohio
February 23, 1947

THE radiations emitted by two radioactive species in consecutive electron capture disintegrations have been studied. The mass number of the radioactive species is assumed to be 131 since $_{56}Ba^{131}$ of half-life 11.7±0.3 days was obtained by (n,γ) reaction of barium[1] with strong intensity of radiation after activation in a pile and by (d,p) reaction with weak intensity of radiation after several hours bombardment in a cyclotron. The $_{55}Cs^{131}$ formed by chain reaction was separated from barium, and the latter was chemically freed from other radioactive species. Sufficient time was allowed for disintegration of known short periods in barium.

Three gamma-rays of energies 220±10 kev, 500±15 kev, and 1.7±0.1 Mev were found to be present in barium. The most intense radiation was associated with the 500-kev gamma-rays while those of the 1.7-Mev gamma-rays were weak. Since the sources of Ba^{131} used for determination of energy of 1.7-Mev gamma-rays were of the order of 10 mc, the secondary radiations produced by absorbers were filtered off. Half-lives of barium measured for the three gamma-rays separately showed that the 220- and 500-kev gamma-rays belong to the 11.7-day barium. No information so far has been obtained that the 1.7-Mev gamma-rays do not correspond to the same period. Evidence of x-rays emitted by the barium fraction was obtained, but the x-rays were masked by the intense gamma-radiation especially by the 220-kev gamma-rays.

By cloud-chamber observations the particles emitted by the barium fraction were identified as electrons. For energies of more than 100 kev no positrons could be found. The electron spectrum of Ba^{131} and the full account of cloud-chamber observations will be published later.

By absorption measurements electrons of energy less than 500 kev were established. In addition, the shape of the absorption curve showed that electrons of less than 200 kev were very abundant.

The cesium fractions separated from activated barium immediately after activation and after 20-days accumulation were purified. The $_{55}Cs^{131}$ decays with a period of 10±0.3 days, emitting highly converted gamma-rays of 145±10 kev energy. Conversion was calculated to be about 97 percent. In addition, x-rays of 0.412A were found to be present. Very intense radiation of electrons with energy of 112 kev were observed in $_{55}Cs^{131}$ and identified as conversion electrons of 145-kev gamma-rays.

Thus, the transition, after orbital electron capture in mass number 131, from even to odd Z, considerably exceeds in gamma-energy emitted, the transition from odd to even Z.

It is a pleasure to express our appreciation to the Clinton Laboratories and its Isotopes Branch, Research Division, for activation of barium. The grant given by the Ohio State University Development Fund for construction of research instruments is gratefully acknowledged by the authors.

[1] Manhattan Project Announcement, Science **103**, 697 (1946).

On the New Fission Processes of Uranium Nuclei

TSIEN SAN-TSIANG, HO ZAH-WEI, R. CHASTEL, AND L. VIGNERON
Laboratoire de Chimie Nucléaire du Collège de France, Paris, France
February 13, 1947

THE phenomenon of uranium fission has been known since 1939. It consists in the splitting of the uranium nucleus into two lighter nuclei, excited either by capture of a neutron, or by bombardment of charged particles or photons. The maximum energy liberated in this phenomenon is about 200 Mev, 150–160 Mev of which is used to project the two resulting nuclei in opposite directions, and the rest for the internal excitation of the fission fragments and the energy carried by the neutrons emitted during the fission. This well-known fission process is also called binary fission.

The possibility of fission into three charged nuclei has been pointed out by theoretical physicists,[1] predicting a liberation of maximum energy of 210–220 Mev, even 10–20 Mev higher than that of binary fission. But until now, definite experimental proof has not been published.

In order to search for the existence of fission into more than two charged fragments, experiments have been made with the *Ilford Nuclear Research* photographic emulsion, manufactured under the direction of Dr. Powell of the University of Bristol.[2] The plate was soaked in a 10 percent solution of uranyl nitrate, dried, and bombarded by slow neutrons produced near the Be target of the cyclotron of the Collège de France. With a suitable technique of development, the plate shows numerous thick fission tracks clearly distinguished from thin, natural α-ray tracks. The major part of the fission tracks are straight lines, representing two nuclei projected in opposite directions, no determination of the origin of the fission fragments being possible. Occasionally, near the ends of the track, there are collisions between the fission fragments and the nuclei contained in the emulsion (branches and bendings).[3]

(*A*) *Ternary fission.* Certain fission tracks show a peculiar aspect: three tracks originate from a common point, usually two heavy tracks and one long lighter track (Figs.

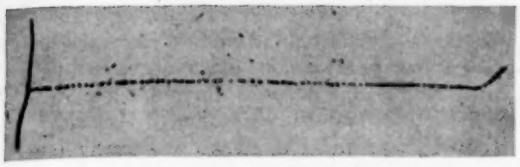

FIG. 1. Ternary fission: third fragment—mass≈9, range=17 cm air equivalent.

FIG. 2. Ternary fission: third fragment—mass≈6, range=44 cm air equivalent. The two branches on one of the heavy fragments are caused by nuclear collisions.

1 and 2). Precise analysis, based on the conservation of momentum, shows that it is impossible to describe all of them as branches caused by a collision of the fission fragment at the beginning of its range, with a known nucleus contained in the emulsion (such as H, C, N, O, Br, and Ag). It seems more plausible to conclude that these are fissions of uranium into three charged fragments (ternary fission).

Taking account of the measured angles and ranges, and of the velocity-range relation of heavy ions,[4] and requiring conservation of momentum, we can determine the mass and energy of each fragment. The distribution of masses of the three fragments is shown in Fig. 3: the two heavy fragments have average masses of 99 and 131, respectively, the third fragment seems to have two probable values, one about 5 or 6, the other about 9.[5] The average total kinetic energy of ternary fission is 165 Mev, slightly higher than that of binary fission. If the total internal excitation energy is about the same for binary and ternary fission fragments, the agreement between the observed kinetic energy and the theoretical value may be regarded as satisfactory.

The ratio of ternary fission to binary fission is 0.003 ±0.001. This value may be regarded as the lower limit, because certain cases with a heavier third fragment are discounted from the statistics owing to the possibility of attributing them to nuclear collisions.

(*B*) *Quaternary fission.* Besides those of ternary fissions, we have observed some cases which cannot be explained otherwise than by fission into four charged fragments (quaternary fission). One of these has already been described in detail (Fig. 4).[6] It seems interesting to indicate that the observed ternary fissions are almost all of the same type, i.e., two heavy, and one light; whereas the

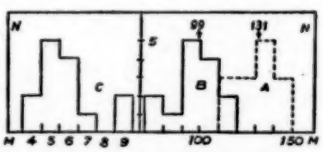

FIG. 3. Distribution of masses of ternary fission fragments.

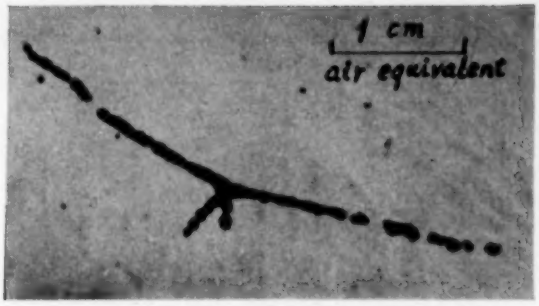

FIG. 4. Quaternary fission.

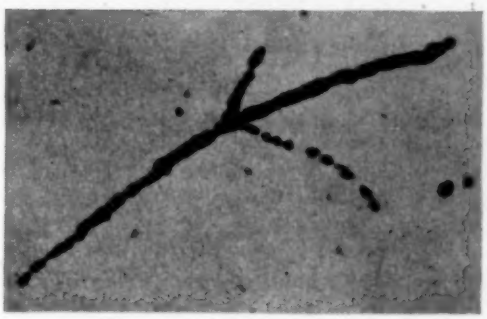

FIG. 5. Quaternary fission. (In same scale as Fig. 4.)

quaternary fissions may occur in various fashions: (1) two heavy, and two relatively light (Fig. 4), (2) three heavy, and one light (Fig. 5). If the total internal excitation energy is about the same for binary and quaternary fission fragments, the mean observed kinetic energy for the latter, about 110 Mev, is in good agreement with that estimated by Bohr and Wheeler.[1,6] The ratio of quaternary fission to binary fission is 0.0003±0.0002.

The detailed report of this work will be published shortly in *Journal de Physique et le Radium.*

[1] N. Bohr and J. A. Wheeler, Phys. Rev. **56**, 426 (1939). R. D. Present, Phys. Rev. **59**, 466 (1941).
[2] C. F. Powell, C. P. S. Occialini, D. L. Livesey, and L. V. Chilton, J. Sci. Inst. **23**, 102 (1946).
[3] Tsien San-Tsiang, R. Chastel, Ho Zah-Wei, and L. Vigneron, Comptes rendus **223**, 986 (1946).
[4] J. K. Bøggild, K. J. Brostrøm, and T. Lauristen, Kgl. Danska Vid. Sels. Math.-Fys. Medd **18**, 1 (1940). O. J. Knipp and E. Teller, Phys. Rev. **59**, 659 (1941). F. Joliot, Comptes rendus **218**, 488 (1944).
[5] Tsien San-Tsiang, Ho Zah-Wei, R. Chastel, and L. Vigneron, Comptes rendus **224**, 272 (1947).
[6] Ho Zah-Wei, Tsien San-Tsiang, L. Vigneron, and R. Chastel, Comptes rendus **223**, 1119 (1946). In the table of this article, the data under the columns M_3 and M_4 should be exchanged. Similarly, those under E_3 and E_4 should also be exchanged.

Microwave Absorption Frequencies of $N^{14}H_3$ and $N^{15}H_3$

W. E. GOOD AND D. K. COLES
Westinghouse Research Laboratories, East Pittsburgh, Pennsylvania
February 19, 1947

FIFTY microwave absorption lines of $N^{14}H_3$ and $N^{15}H_3$ have been observed in the region between 19,000 and 26,000 mc/s.[1–5] We have now remeasured the frequencies of all of these lines with a precision of better than one part

TABLE I. Microwave absorption frequencies in ammonia.

J	K	$N^{14}H_3$	$N^{15}H_3$
1	1	23,694.49 mc/s	22,624.96 mc/s
2	2	23,722.63	22,649.85
2	1	23,098.79	22,044.28
3	3	23,870.13	22,789.41
3	2	22,834.17	21,783.98
3	1	22,234.53	21,202.30
4	4	24,139.41	23,046.10
4	3	22,688.29	21,637.91
4	2	21,703.36	20,682.87
4	1	21,134.29	—
5	5	24,532.98	23,421.99
5	4	22,653.00	21,597.86
5	3	21,285.27	20,272.04
5	2	20,371.46	—
6	6	25,056.02	23,922.32
6	5	22,732.43	21,667.93
6	4	20,994.61	—
6	3	19,757.57	—
7	7	25,715.17	24,553.42
7	6	22,924.94	21,846.41
7	5	20,804.83	—
8	8	—	25,323.51
8	7	23,232.24	22,134.89
8	6	20,719.21	—
9	8	23,657.48	22,536.26
9	7	20,735.44	—
10	9	24,205.29	23,054.97
10	8	20,852.51	—
11	10	24,881.90	—
11	9	21,070.70	—
12	11	25,695.23	—

in a million. The standard frequency transmissions of the National Bureau of Standards Station, WWV, were used as the basis of these measurements in order to obtain the necessary precision. These absorption lines should now provide excellent secondary frequency standards in the region mentioned.

Harmonics, from a 240 mc/s crystal controlled oscillator, falling in the above region were used as frequency markers. Interpolation between the markers was done with a calibrated communication receiver. It is estimated that the values in Table I are accurate to ± 0.02 mc/s.

[1] B. Bleaney and R. P. Penrose, Nature **157**, 339 (1946).
[2] W. E. Good, Phys. Rev. **70**, 213–218 (1946).
[3] C. H. Townes, Phys. Rev. **70**, 665 (1946).
[4] D. K. Coles and W. E. Good, Phys. Rev. **70**, 979 (1946).
[5] Dailey, Kyhl, Strandberg, Van Vleck, and Wilson, Phys. Rev. **70**, 984 (1946).

Proton-Proton Scattering at 10 Mev

ROBERT R. WILSON*
Harvard University, Cambridge, Massachusetts
February 23, 1947

THE 10-Mev protons available from the sixty-inch cyclotron at the Radiation Laboratory of the University of California have been used for studying the scattering of protons by protons. Coincidences between the scattered and recoil protons were measured as a function of the angle of the scattered protons utilizing the same method and equipment which had been developed at Princeton University[1] for use with 8-Mev protons.

A scattering foil of Nylon $(C_{12}H_{22}N_2O)_x$ about 2×10^{-4} cm thick was placed at the center of the scattering chamber such that the normal to the plane of the scattering foil made an angle of 30° with the direction of the incident proton beam which was 2.0 mm in diameter. The scattered protons were counted with a proportional counter, the "defining counter," which had a circular aperture of 1.65 mm diameter 7.8 cm from the center of the scattering foil. Another proportional counter, the "monitor counter," was mounted such that it received the recoil protons at 90° with respect to the defining counter. It had an oval aperture $\frac{3}{16}$" wide and $\frac{3}{8}$" high and was only 3.7 cm from the scattering foil. Coincidences between the defining counter and the monitor counter were registered. The solid angle of the monitor counter was large to insure that the recoils of all protons entering the defining counter would also enter the monitor counter.

The proton integrator consisted of a 2.10 mf condenser which was connected between the Faraday collector cup and ground. The charge collected on the condenser during a ten-minute run was measured at the end of each run using a ballistic galvanometer.[2] The system was not accurately calibrated since all the measurements were relative. It was not convenient to vary the magnetic field or frequency of the sixty-inch cyclotron, which customarily accelerates deuterons of α-particles, so molecular hydrogen ions of unit charge were accelerated to 20 Mev, thus giving the equivalent of 10-Mev protons. This energy was determined by accurate range measurements made on the scattered protons. Thus the protons scattered at 30.5° had a mean range of 0.097 mg/cm² in aluminum, corresponding to an energy of 7.35 Mev or 9.9[4] Mev for the incident protons.

At each angle of scattering a counting plateau was established by measuring the number of coincidences per incident proton as a function of the discriminator biases. Good plateaus were found for all angles except 12° where it was necessary to extrapolate to zero bias, thereby introducing a correction of 9 percent. The accidental

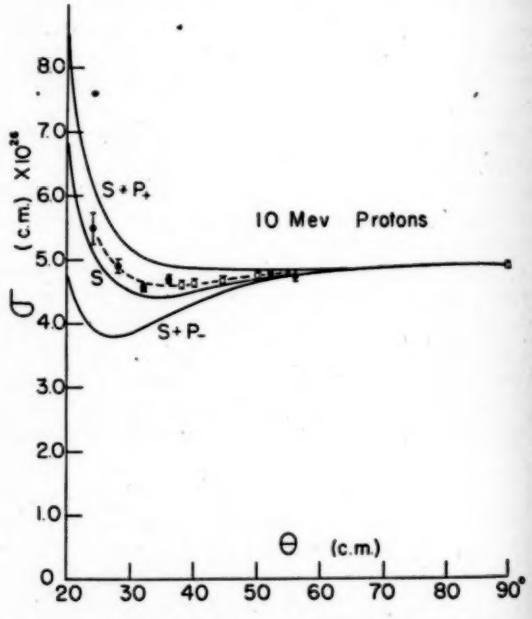

FIG. 1. The cross section per unit solid angle in the center of mass system as a function of the scattering angle in the center of mass system. All the data are relative.

coincidence rate was always kept to less than 0.5 percent of the true coincidence rate. At 12° a geometrical correction of 3 percent was also applied because at that angle not all the scattered and recoil protons could enter both counters.

The results are given in Fig. 1 in which the cross section per unit solid angle is plotted as a function of the scattering angle; both coordinates are in the center of mass system. The open circled points are adjusted to 4.90×10^{-26} at 90° (center of mass). The other points were taken later with a different scattering foil and have been adjusted to the open circled points in the neighborhood of 50° (center of mass). The vertical lines represent the mean square error as determined experimentally from the consistency of the data.

The solid curves were calculated by L. B. Eisenbud and L. L. Foldy on the assumption of a square well of depth 10.5 Mev and width (e^2/mc^2). The central curve is for S wave scattering only; the upper curve is for S plus P wave scattering with the potential for the P wave repulsive; and the bottom curve shows the P wave effects for an attractive interaction. The data are clearly inconsistent with any attractive P wave effects. They indicate, and are consistent with, the dotted curve which could correspond to a small admixture of repulsive P wave effects—perhaps one-third the full effect—or to pure S wave scattering but using a different potential well.

It is a pleasure to thank Professor E. O. Lawrence and Dr. J. G. Hamilton for their hospitality and help in making the facilities of the Crocker Laboratory at Berkeley available to me. I am also indebted to the crew of the sixty-inch cyclotron for their cheerful help and interest in the experiment.

* Now at Cornell University, Ithaca, New York.
[1] R. R. Wilson and E. C. Creutz, Phys. Rev. 71, 339 (1947).
[2] Equivalent but more refined electronic circuits were borrowed from the Los Alamos Laboratory for use in the Berkeley experiments.

Range, Straggling, and Multiple Scattering of Fast Protons

ROBERT R. WILSON
Harvard University, Cambridge, Massachusetts
February 1, 1947

THE following is a short report on the details of calculations used in a paper[1] considering the radiological properties of fast protons, i.e., 10 to 200 Mev.

The rate of loss of energy per cm of path of charged particle is given by Bethe's expression[2] which can be written

$$-\frac{dW}{dx}=\frac{2\pi e^4z^2}{mc^2E_0W}NZ\ln\left(\frac{4mc^2W}{I}\right), \tag{1}$$

where W is the ratio of the kinetic energy of the particle to its rest energy E_0, N and Z are, respectively, the number of nuclei per cm³ and the atomic number of the stopping material, which has an average excitation energy I; ez is the charge of the ion, and mc^2 is the rest energy of the electron. Bloch[3] has shown that I is proportional to Z for atoms heavier than air; the constant of proportionality has been determined[4] to be 11.5 ev. It can be observed that

$$\ln\left(\frac{4mc^2W}{11.5Z}\right)\approx2.2W^{0.2}\ln(3.6\times10^3/Z) \tag{2}$$

in the interval $0.01<W<0.2$. Hence the range R is

$$R=\int_0^W\frac{dW}{|dW/dx|}=\frac{10^{24}E_0W^{1.8}}{NZz^2\ln(3.6\times10^3/Z)} \tag{3}$$

where E_0 is now in Mev.

Because of the unknown effects of the L and M electrons, Eq. (3) is not expected to hold accurately for heavy elements with $Z>50$. The approximation Eq. (2) is not too good for light elements with $Z<5$; in any case a value $Z'=I/11.5$ should be used in Eq. (3) for such light elements. For protons in air, Eq. (3) agrees to within a few percent with the Cornell range curve[5] down to a few Mev, and with Smith's recent range calculations[6] up to 200 Mev. A more convenient formula for the range of protons in air in meters is $R_m=(E/9.3)^{1.8}$ where E is in Mev.[6]

Livingston and Bethe[2] give an expression for straggling which for high particle energy reduces approximately to

$$\delta R^2=(4\pi e^4z^2NZ/E_0^2)\int_0^W dW/|dW/dx|^3, \tag{4}$$

where δR^2 is the mean square fluctuation of the range. Substituting Eqs. (1) and (2) into (4), integrating then eliminating W, using Eq. (3), and neglecting the variation of the one-half power of the log term in Z times $Z^{0.055}$, we get

$$\delta R/R\approx4.5E_0^{-\frac{1}{2}}(NZz^2R/E_0)^{-0.055} \tag{5}$$

$$\approx0.24W^{-0.1}E_0^{-\frac{1}{2}}, \tag{6}$$

where $\delta R=(\delta R^2)^{\frac{1}{2}}$. This is in excellent agreement with the values calculated for air by Livingston and Bethe for the highest energies that they consider, which are about 15 Mev.

Williams[7] has given a formula for multiple scattering which can be written

$$(\theta^2)_{Av}=\frac{\pi}{E_0^2}\left(\frac{Zze^2}{W}\right)^2Nx\ln\left(\frac{Z^{4/3}Nxh^2}{4m^2c^2W}\right) \tag{7}$$

where $(\theta^2)_{Av}$ is the mean square angle of deflection a particle receives in passing through a thickness x of stopping material. One can calculate the root mean square angle of deflection of a particle of range R which has passed through a thickness x of stopping material by putting Eq. (6) in the differential form, eliminating W using Eq. (3), then integrating, ignoring the variation of the log terms, and taking the square root to get

$$\theta_{rms}=[(\theta^2)_{Av}]^{\frac{1}{2}}\approx18.5\left(\frac{Z}{E_0}\right)^{\frac{1}{2}}\left(\frac{NZR_z^2}{E_0}\right)^{-0.055}\times\left[\left(1-\frac{x}{R}\right)^{-0.11}-1\right]^{\frac{1}{2}}. \tag{8}$$

The log terms have been evaluated for 50-Mev protons in air but the errors so introduced are not greater than 5

percent for protons varying from 10 to 200 Mev. Now make the rough approximation that the root mean square displacement y_{rms} perpendicular to the initial direction follows θ_{ms}, i.e.,

$$y_{rms}=\int_0^R \theta_{rms}dx.$$

On substituting Eq. (7) and graphically evaluating the definite integral

$$\int_0^1\left[\left(1-\frac{x}{R}\right)^{-0.11}-1\right]\frac{dx}{R}=0.305,$$

we get

$$y_{rms}/R\approx 5.7(Z/E_0)^{\frac{1}{2}}(NZz^2R/E_0)^{-0.055}, \quad (9)$$

or

$$\approx 0.3(Z/E_0)^{\frac{1}{2}}W^{-0.1}. \quad (10)$$

A photograph of the 40-Mev α-particle beam from the 60" Crocker cyclotron at the Radiation Laboratory in Berkeley shows a total spread of about 4.5 cm at the end of the 115-cm range. This is in fair agreement with the calculated *spread* ($2y_{rms}$) of 4.8 cm given by Eq. (10).

The above formulae show that the range of 150 Mev protons in tissue is about 16 cm, that the range straggling ($2\delta R$) is 0.3 cm, and the transverse spread ($2y_{rms}$) is 0.6 cm. It is evident that such protons have radiological applications[1] since it is possible to treat a volume as small as one cm³ anywhere within the body, and give to that volume several times the dose of any of the neighboring tissue. Thus 10^9 protons per cm² will produce more than 1000 r.e.d.[8] in the last half cm of range, but the skin dose will be less than 100 r.e.d.

One cannot emphasize too strongly the danger of working near the modern high energy accelerators. Something like one billion protons per cm² ($\sim 10^{-10}$ amp./cm² for one second) could have lethal effects. When one remembers that the range of 150-Mev protons in air is 150 meters, it is apparent that even a small scattering by air could make any point within a moderately large room lethally dangerous if a current of the order of microamperes is free in the air.

[1] R. R. Wilson, Radiology **47**, 487 (1946).
[2] M. S. Livingston and H. A. Bethe, Rev. Mod. Phys. **9**, 263 (1937).
[3] F. Bloch, Zeits. f. Physik **81**, 363 (1933).
[4] R. R. Wilson, Phys. Rev. **60**, 749 (1941).
[5] J. H. Smith, Phys. Rev. **71**, 32 (1947).
[6] W. M. Brobeck first noticed this relationship.
[7] E. J. Williams, Proc. Roy. Soc. **169**, 531 (1939).
[8] Roentgen equivalent dose, 83 ergs absorbed per gram of tissue.